NRC FORM 699 (9-2003) U.S. NUCLEAR REGULATORY COMMISSION

CONVERSATION RECORD

DATE: 10/03/2007

TIME: 1:30pm

NAME OF PERSON(S) CONTACTED OR IN CONTACT WITH YOU: Donis Shaw

TELEPHONE NO.:

ORGANIZATION: Transnuclear, Inc.

TYPE OF CONVERSATION: ☐ VISIT ☐ CONFERENCE ☑ TELEPHONE ☐ INCOMING ☐ OUTGOING

SUBJECT

Summary of 10/3/07 phone call with Transnuclear, Inc. to discuss requests for additional information associated with the Standardized NUHOMS Amendment 10 review.

SUMMARY *(Continue on Page 2)*

On 10/3/07 staff from the Division of Spent Fuel Storage and Transportation held a phone call with Transnuclear, Inc. to discuss requests for additional information (RAIs) associated with Amendment 10 to the Standardized NUHOMS design. The participants in the call were:

Transnuclear: Robert Grubb, Jayant Bondre, Peter Shih, Don Shaw, Miguel Manrique, Raheel Haroon,
Structural Integrity: Stan Tang, Dave Harris, George Licina
NRC: Bob Tripathi, Geoff Hornseth, Joe Sebrosky

The phone call was a followon to discussion that the staff had with TN in a September 19, 2007, meeting (see ADAMS accession number ML072780244 for a summary of the meeting). Subsequent to the September 19, 2007, meeting the staff sent the following information associated with RAI 3-12 and RAI 3-6 for the Amendment 10 application. The information was provided from the perspective of one of the NRC's technical reviewers.

RAI 3-12

There are two issues here; 1) Kic value, and 2) crack size. A Kic value of 16.36 ksi in((1/2 power) was used. This appears to be in line with the EPRI report so this value should be okay as long as the reevaluation of the K1 using a reasonable crack size does not approach the Kic value. If the reevaluated Ki value is near Kic then TN would have to evaluate the EPRI report to determine the uncertainty on Kic and account for the uncertainty in their evaluation. While the uncertainty in the Kic value is important for storage it is crucial for transportation if TN persists to use a fracture mechanics approach.

TN provided brief summaries of a number of studies looking at breaches that developed in fuel rods under a number of conditions. Some were irrelevant to high burnup fuel. They drew the conclusions that cracks that formed in high burnup fuel were most likely to be long axial cracks. This is probably the case for fuel under normal reactor operating conditions.

Continue on Page 2

ACTION REQUIRED

NAME OF PERSON DOCUMENTING CONVERSATION	SIGNATURE	DATE
Joseph M. Sebrosky		10/05/2007

ACTION TAKEN

TITLE OF PERSON TAKING ACTION	SIGNATURE OF PERSON TAKING ACTION	DATE

CONVERSATION RECORD (Continued)

SUMMARY *(Continue on Page 3)*

These cracks are most likely due to propagation of the most prevalent current failure mechanism, i.e. debris fretting. (TN's conclusions dealing with rods tested under LOCA conditions are irrelevant since under this situation in a reactor, many rods would break leading to a multitude of damage fuel similar to TMI).

The problem comes with TNs designation of a crack length in the analysis #1. All the data relevant to high burnup fuel (ref 3.39, 3.42, and 3.444, which TN should supply to the NRC as complete documents for us to check) indicate an axial or long axial crack. TN used a crack length of 0.22 inches, hardly a long axial crack. They then say this is conservative compared to a 0.039 inch crack in ref 3.36, but this is for low burnup fuel. For the other cask under this Amendment, i.e. 32PTH1 the crack length they have used is even smaller which is 0.166 inches as shown on page U.3.6-44. TN should provide the references above and also choose a crack length that they can justify for high burnup fuel.

RAI 3-6

I do not know which plots from Geelhood and Beyer (G&B) that TN used to justify saying there was a lot of data. Geelhood and Beyer have a number of plots:

1.Fig 10 - UTS vs. fluence does show many data up to 1.2 E26 n/m2 but the data is irrespective of hydrogen content. G&H says that there is a slight overprediction when H2 > 600 ppm (sec G&B Sec 3.1)
2.yield as a function of hydrogen but all fluences
3.Fig 2 - yield as a function of fluence but all hydrogen contents.

None of these are really appropriate for high burnup fuel, i.e. high fluence and high hydrogen content. Since TN is concerned about BWR fuel, the data to use is in G&B sec 3.6 Fig 25 for fully recrystallized fuel. Almost all the data are below 2 E25 n/m2. There are three points at 9 e E25 n/m2 and these points are 1-75 MPa below the predicted value, i.e. predicted < measured. Using Fig 26, one can determine that the high fluence data in Fig 25 were probably low hydrogen. There is really no data on high fluence, high hydrogen fuel; just predictions. Then there is the question of uncertainty. TN calculates a stress only 80 psi below the yield yet based on G&B the uncertainty in the yield may be as large as 15 ksi. I would say best they are at yield.

Prior to the phone call TN provided the attached information for the staff to refer to during the phone call. The information that TN included was a draft non-proprietary response to RAIs 3-14, 3-16, and 3-12. TN also provided references associated with the RAI responses. Regarding RAI 3-12, TN indicated the it intends to use a Kic value of 16.36 ksi in its response. TN indicated that its response will rely on long axial crack length response and not rely on a LOCA type break in its evaluation. TN indicated that the 0.22 in 0.039 inch and 0.166 in reference in the staff's RAI 3-12 insights above are for circumferential cracks and not longitudal cracks. TN indicated that the longitudal crack length assumed in the analysis was on the order of 10 inches. Using these values in the analysis result in a large margin of safety and TN refered the staff to a discussion on page T.3.6-28 3rd paragraph. The staff indicated that TN's response to RAI 3-12 should include the discussion above because the information is not apparent in the Amendment 10 application.

Regarding RAI 3-6 TN wanted to know the basis for the 15ksi uncertainty in the yield that the staff refers to in its observations above. TN indicated that it did not believe that at high burnups there is a 15 ksi penality. TN then referred the staff to page 3 of its proposed response. TN indicated based on these results that they believe they have a minimum of a 10, 000 psi margin. The staff took the following action:
- review the draft response to RAI 3-6 and consider if additional feedback to TN is needed in this area.

The staff questioned TN's reference to the following paper: "H. C. Chu, S. K. Wu, K. F. Chien and R. C. Kuo, "Effect of radial hydrides on the axial and hoop mechanical properties of Zircaloy-4 Cladding," Journal of Nuclear Materials, Vol. 362, 2007". The staff wanted to know if there was a version of this paper in 2006. Subsequent to the phone call TN referred the staff to the cover page for the reference. At the top of the reference it has a date of 2007, after the title for the reference it states Received 27 June 2006, accepted 13 November 2006. Although there are multiple dates on the cover page TN believes that it referred to the reference correctly.

The staff and TN took the following joint action:
- arrange a separate phone call to discuss TN's draft response to RAI 3-4.

Continue on Page 3

October 3, 2007

Draft Responses for Telephone Discussions

RAI Question 3-4:

Information Withheld

Information Withheld

The following references are included in this draft response for information.

"H. C. Chu, S. K. Wu, K. F. Chien and R. C. Kuo, "Effect of radial hydrides on the axial and hoop mechanical properties of Zircaloy-4 Cladding," Journal of Nuclear Materials, Vol. 362, 2007".

"J. Y. R. Rashid and A. J. Machiels, "Assessment of Data Availability and Data Needs for Spent Fuel Transportation," ANS Winter Meeting, Washington, D. C. 2005".

RAI Question 3-6:

This question has two parts. Part 1 is regarding small margin of the calculated cladding stress vs. cladding yield strength. Part 2 is to justify the yield strength used for high burnup cladding.

Response to Part 1:

The margin to yield stress in the original side drop analysis was calculated to be 79 psi, 2,333 psi, and 6,783 psi for the 9x9-72/1 (Siemens QFA), 9x9-74/2 (GE11 and GE13) and the 10x10-91/1 (Atrium 10) fuel assemblies respectively. Due to the uncertainty in material data for Zircaloy-4 more margin is required. Additional margin is achieved by refining the internal pressure calculation using actual plenum volumes specific for each fuel assembly type and the amount of end fitting weight carried by each fuel rod.

Using actual internal pressure for each fuel assembly type

The original calculations for internal pressure used very conservative values for fuel rod plenum volumes
. The internal pressure was recalculated for all fuel assemblies based on plenum volumes specific for each fuel assembly type. The calculated internal pressures and fuel cladding stresses for the three different types of fuel rods are listed in the following table for information:

Fuel Assembly		9x9 72/1	9x9 74/2	10x10 91/1
		Siemens QFA	GE11, GE13	Atrium-10
Original Analysis	Internal Pressure (psig)	3,838	5,656	3,222
	Stress due to internal pressure (psi)	16,499	22,876	14,024
Updated Analysis	Internal Pressure (psig)	2,448	2,396	2,330
	Stress due to internal pressure (psi)	10,524	9,691	10,142
Additional margin obtained using realistic pressure (psi)		5,975	13,185	3,882

Using realistic end fitting load

The original calculations conservatively assumed that the weights of the end fittings are completely carried by the fuel rods. However, the stiffness of the water rods in the lateral and rotational directions are approximately 25 times greater than the stiffness of the fuel rods. Since the water rods will carry a big portion of the end fittings weights, it was assumed that total weight of the end fittings will be averaged over the number of rods possible in the fuel assembly. For example a 9x9 fuel assembly can have a total of 81 rods, thus the weight carried by a single rod is Weight of end fitting / 81.

The calculated fuel cladding stresses based on more realistic end fitting loads for the three different types of fuel rods are listed in the following table for information:

Fuel Assembly		9x9 72/1	9x9 74/2	10x10 91/1
		Siemens QFA	GE11, GE13	Atrium-10
Original Analysis	Max Bending Stress, S_b (psi)	77256	68625	73027
Updated Analysis	Max Bending Stress, S_b (psi)	73184	62888	67565
Additional margin obtained using realistic end fitting load (psi)		4,072	5,737	5,462

The following table summarizes the stresses and margins for the three most critical cases in the original 61BTH side drop analysis.

Fuel Assembly		9x9 72/1	9x9 74/2	10x10 91/1
		Siemens QFA	GE11, GE13	Atrium-10
Original Analysis	Combined Stress (psi)	93,755	91,501	87,051
Updated Analysis	Combined Stress (psi)	83,708	72,579	77,707
Yield Stress (psi)		93,834	93,834	93,834
Margin based on updated analysis (psi)		10,126	21,255	16,127

Response to Part 2:

Information Withheld

Information Withheld

Information Withheld

Conclusion:

[redacted] And after recalculating the fuel cladding stresses using the more realistic internal pressures and end fitting load distributions, the lowest stress margin is approximately 10,000 psi, this margin is expected to off set any potential uncertainty of the Beyer's model.

In addition, based on reference 12, the maximum oxide thickness is less than 30 μm. However, 120 μm is conservatively used for reducing the cladding thickness for cladding stress calculation. The margin can be improved if actual oxidation thickness is used.

Please note that the stress is conservatively calculated based on 75g hypothetical accident loads, the actual g load calculated during the side drop (From LS-DYNA) is much less than the g load (75g) used for the stress calculations.

RAI Question 3-7 and 3-12:

These two questions have three parts.

Part 1: Kic values for high burnup fuel cladding
Part 2: Failure modes for high burnup fuel cladding
Part 3: Fracture toughness evaluations

Response to Part 1: [redacted]

Response to Part 2: [redacted]

Information Withheld

Response to Part 3:

Information Withheld

Stress Intensity Factor for a Through-wall Axial Crack in Cylinder

Information Withheld

References:

1. H. C. Chu, S. K. Wu, K. F. Chien and R. C. Kuo, "Effect of radial hydrides on the axial and hoop mechanical properties of Zircaloy-4 Cladding," Journal of Nuclear Materials, Vol. 362, 2007.
2. Interim Staff Guidance – 11, Spent Fuel Project Office, Revision 3, November 2003.
3. J. Y. R. Rashid and A. J. Machiels, "Assessment of Data Availability and Data Needs for Spent Fuel Transportation," ANS Winter Meeting, Washington, D. C. 2005.
4. A. Machiels, "Spent Fuel Transportation Applications: Longitudinal Tearing Resulting from Transportation Accidents – A probabilistic Treatment," EPRI Report 1013448, December 2006.
5. K. J. Geelhood and C. E. Beyer, "PNNL Stress/Strain Correlation for Zircaloy," March 2005.
6. Osawa, M., Takahashi, T., Homma, T., and Goto, K., "Behavior of Irradiated Zircaloy-4 Fuel Cladding Under Simulated LOCA Conditions," Zirconium in the Nuclear Industry: Twelfth International Symposium, ASTM STP 1354, G. P. Sabol and G. D. Moan, Eds., ASTM, West Conshohocken, PA, 2000.
7. Garde, A. M., "Effect of Irradiation and Hydriding on the Mechanical Properties of Zircaloy-4 at High Fluence," Zirconium in the Nuclear Industry: Eigth International Symposium, ASTM STP 1023, L. F. P. Van Swan and C. M. Eucken, Eds., ASTM, Philadelphia, 1989.
8. F. H. Huang and W. J. Mills, "Fracture and Tensile Properties of Irradiated Zircaloy-2 Pressure Tubes," Nuclear Technology, Vol. 102, June 1993.
9. EPRI Report 1003128, (Proprietary Licensed Material).
10. S. Shimada, E. Etoh, H. Hayashi, and Y. Tukuta, "A Metallographic and Fractographic Study of Outside-in Cracking Caused by Power Ramp Tests," Journal of Nuclear Materials, Vol. 327, 2004.
11. Barsoum, R. S., "On the Use of Isoparametric Finite Elements in Linear Elastic Fracture Mechanics," International Journal for Numerical Methods in Engineering, Vol. 10, 1976.
12. EPRI Report 1000214, "Limerick 1 EOC7 GE11 Poolside Examination (52 GWd/MTU).

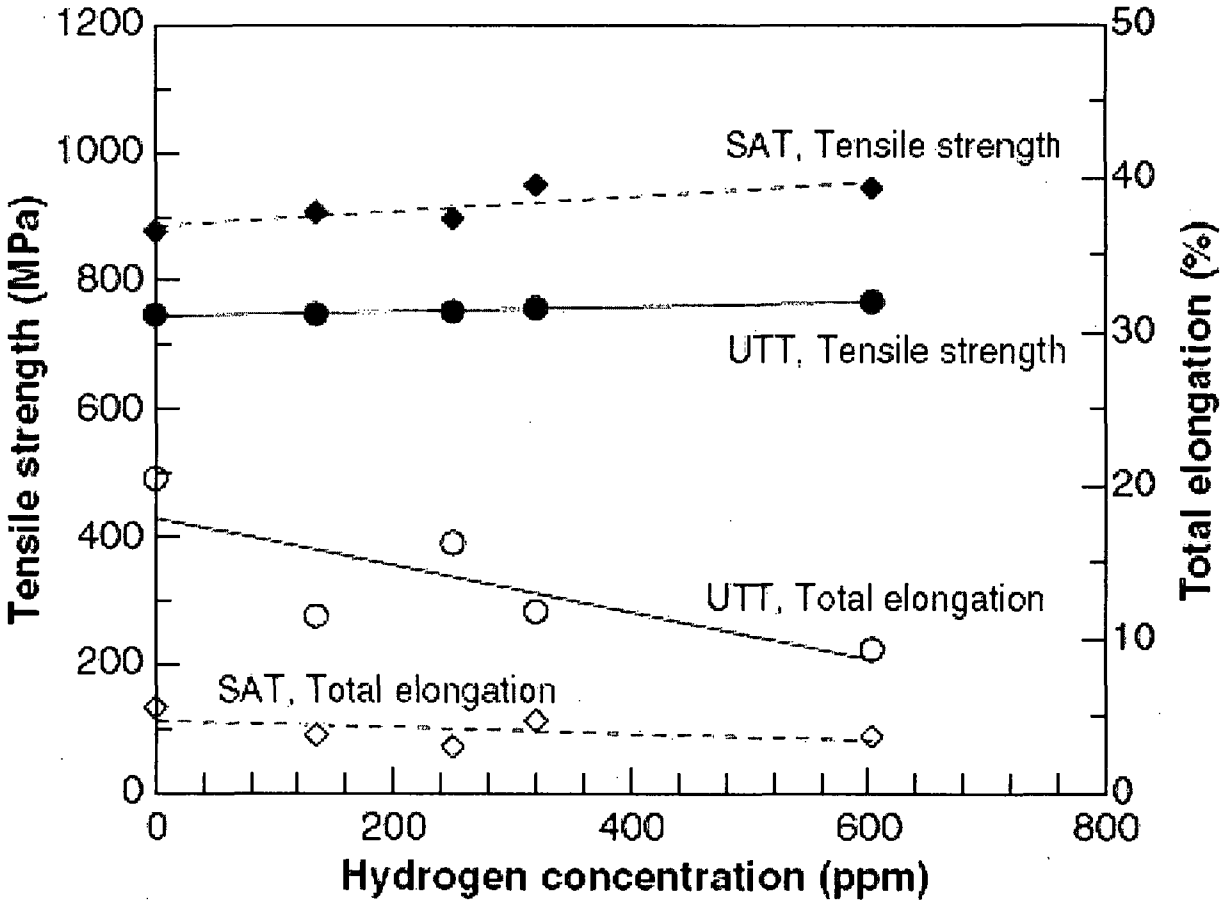

Figure 1. Effect of hydrogen concentration on the mechanical properties of SRA fuel cladding specimens tested under uniaxial tension and slotted arc tension; all hydrides in specimens were circumferentially aligned, [1]

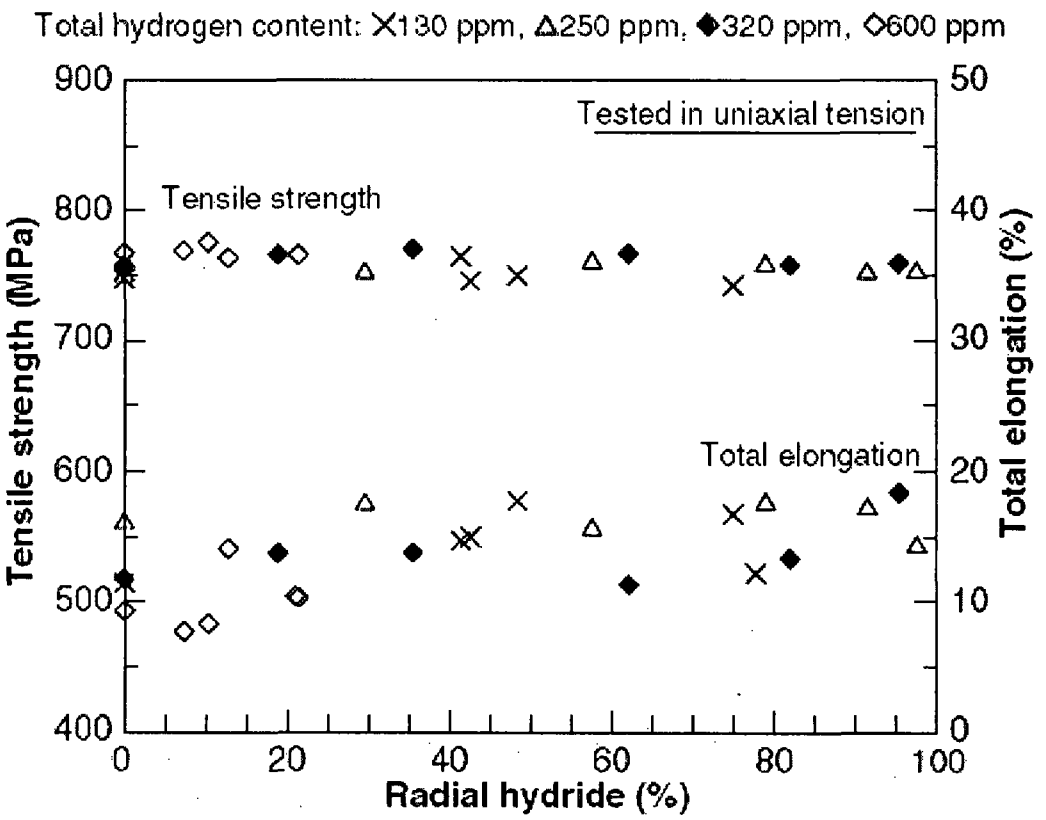

Figure 2. Effect of radial hydrides on the mechanical properties of SRA fuel cladding specimens tested under uniaxial tension at room temperature, [1]

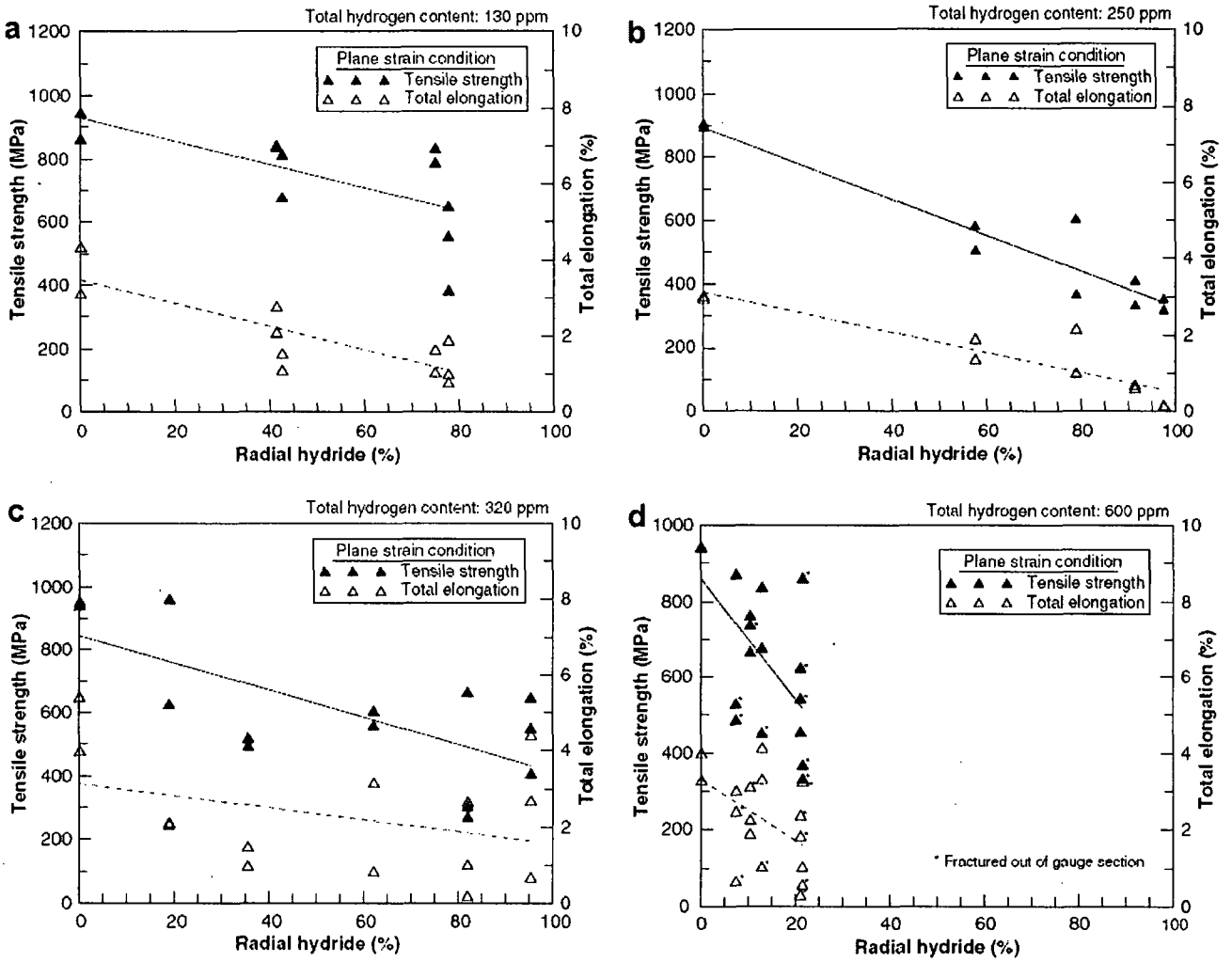

Figure 3. Effect of radial hydrides on the mechanical properties of cladding specimens with various hydrogen content levels tested under slotted arc tension at room temperature: (a) 130 wt ppm, (b) 250 wt ppm, (c) 320 wt ppm, and (d) 600 wt ppm.

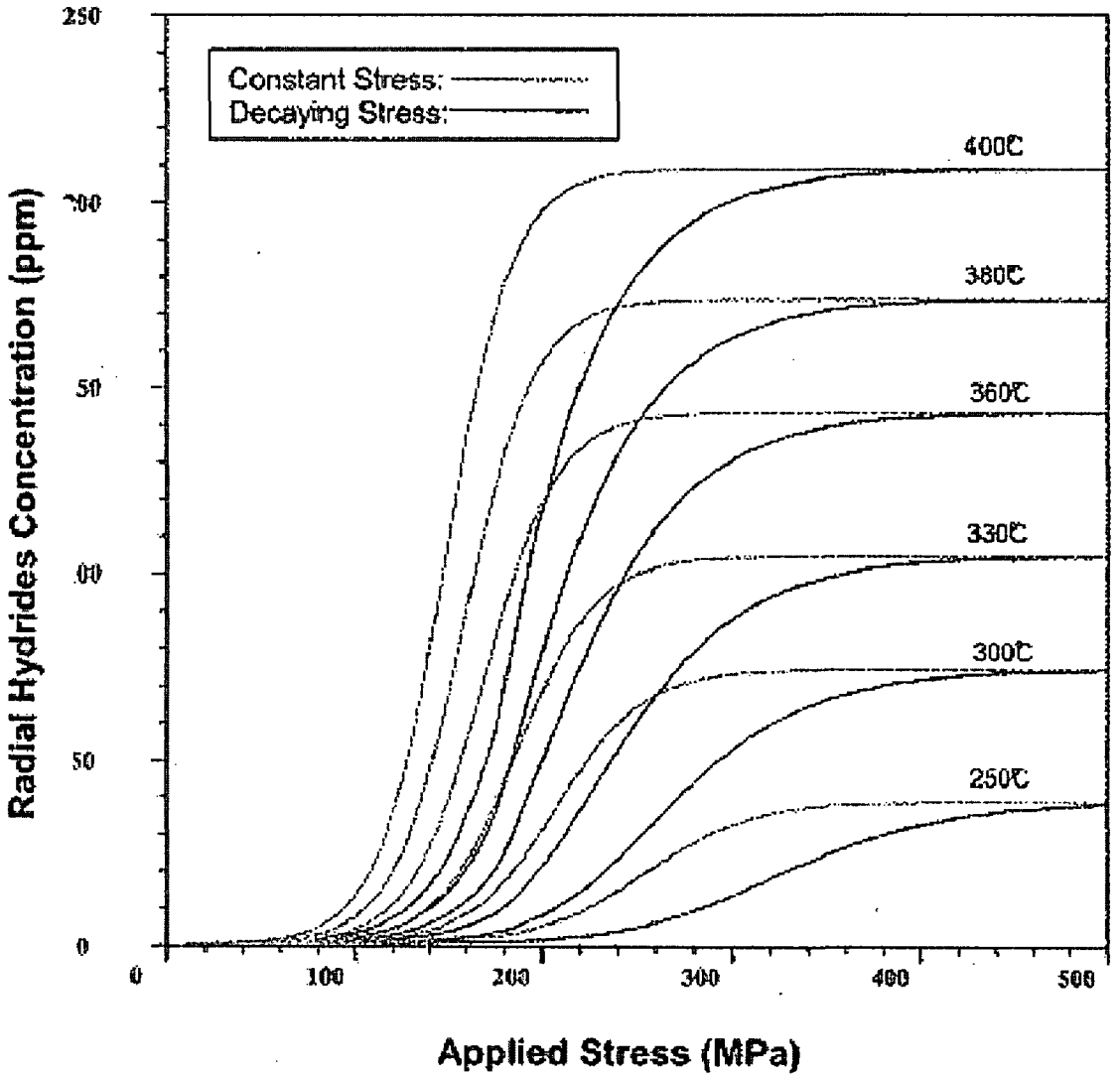

Figure 4. Model Prediction of Radial Hydrides Precipitation for Cooling to 20 C under Decaying Stress Compared to Constant Stress

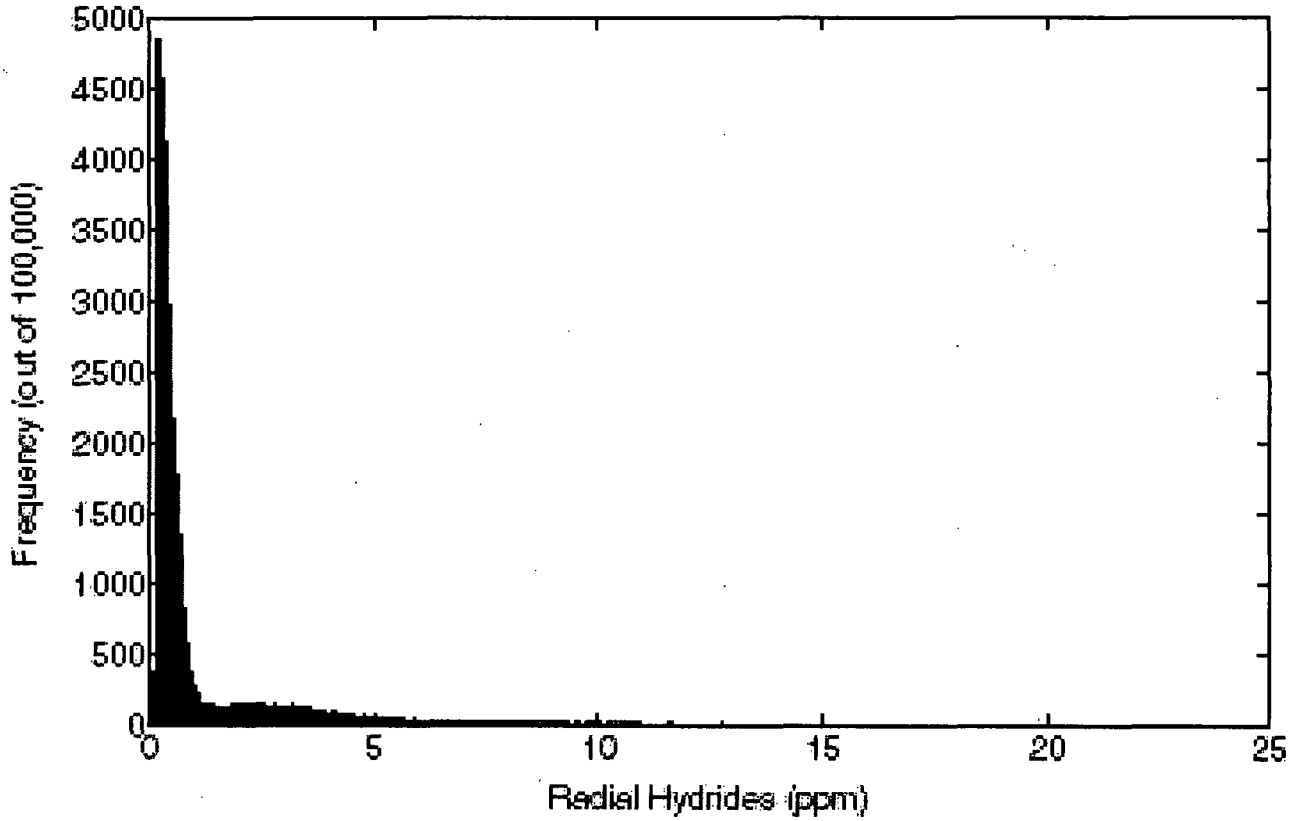

Figure 5. Monte Carlo Frequency Distribution of Radial Hydride Concentration

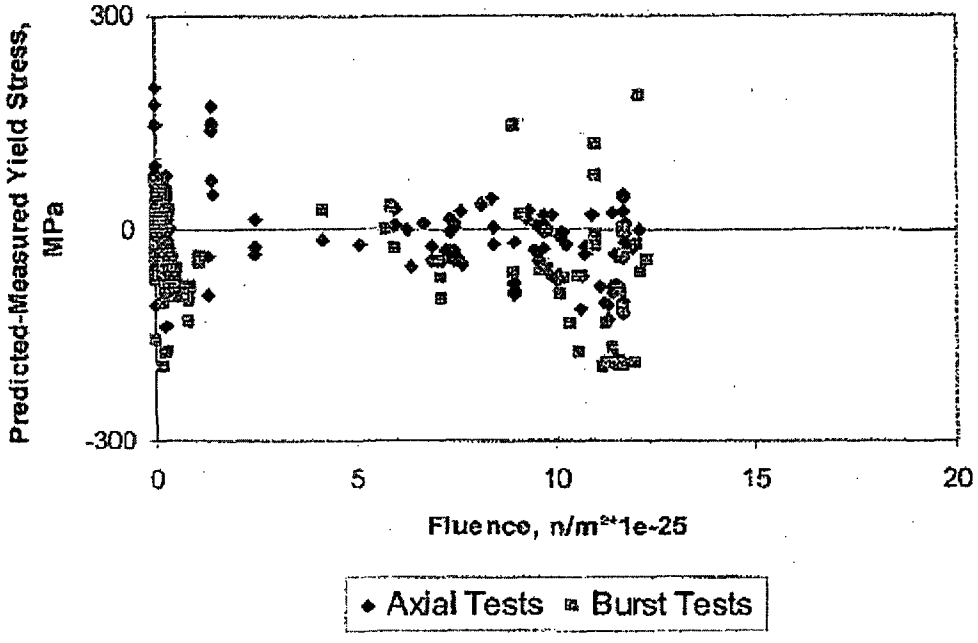

Figure 6. Predicted minus measures yield stress from the PNNL database as a function of fluence

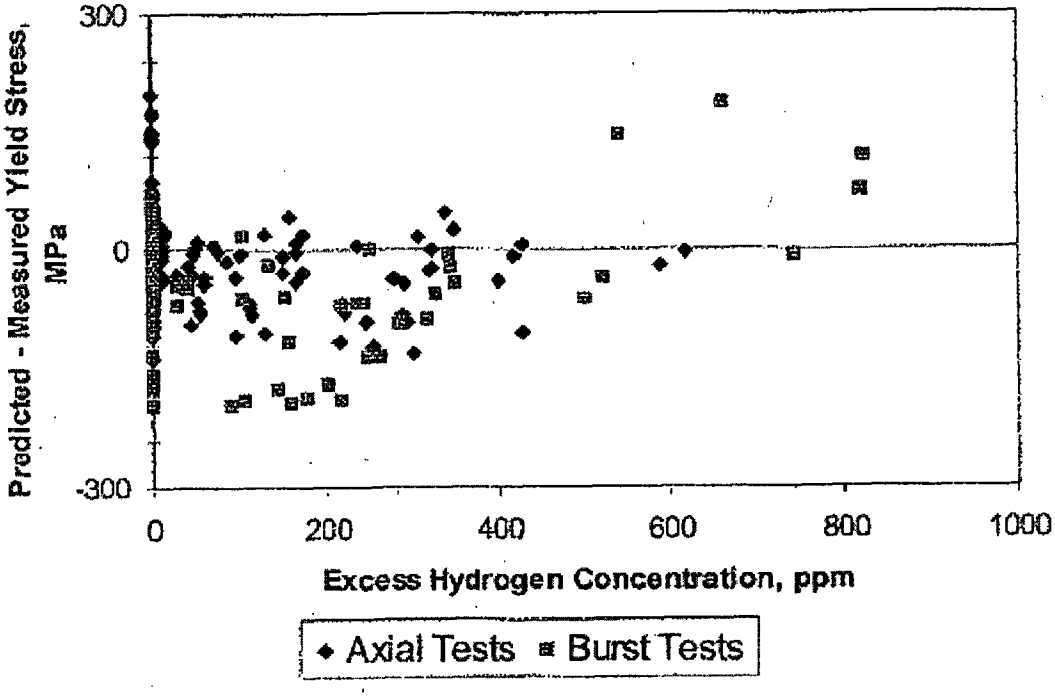

Figure 7. Predicted minus measured yield stress from the PNNL database as a function of excess hydrogen

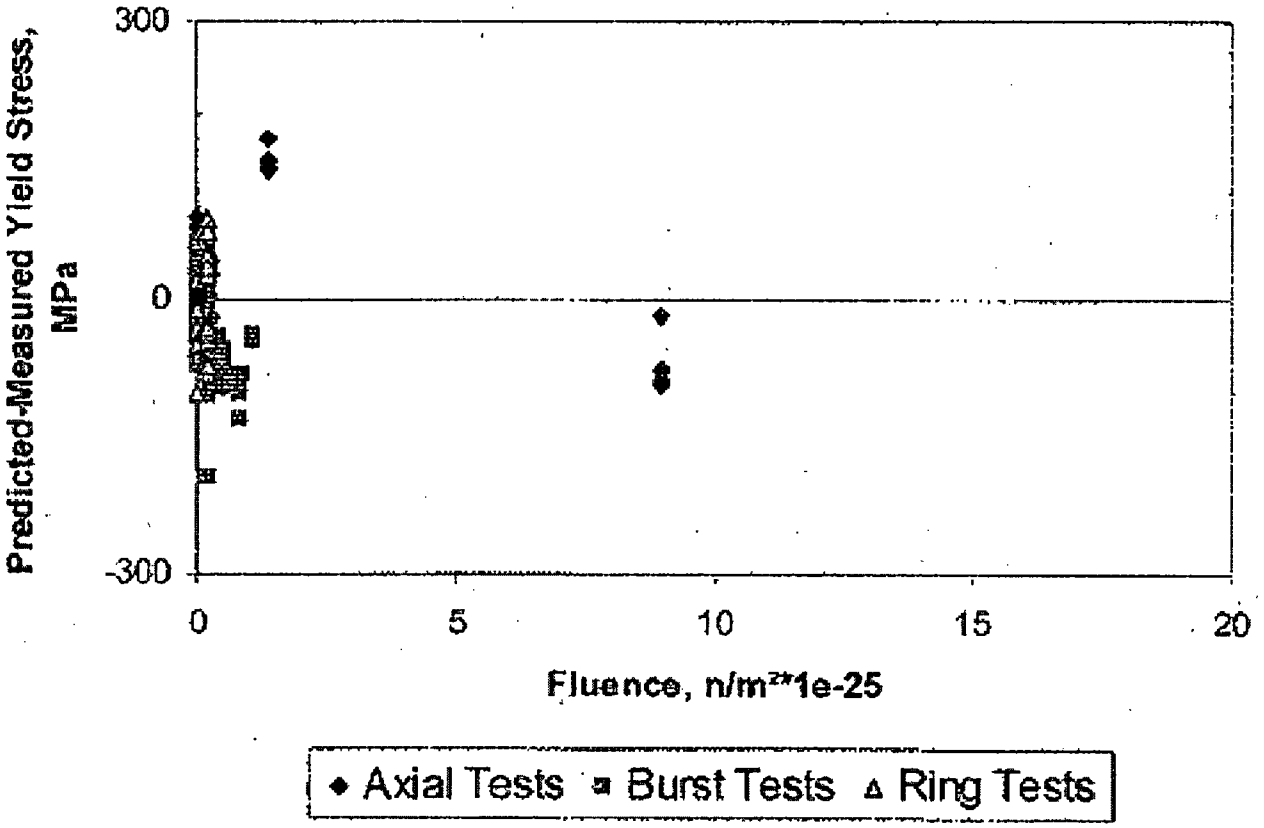

Figure 8. Predicted minus measured yield stress from RXA cladding as a function of fluence.

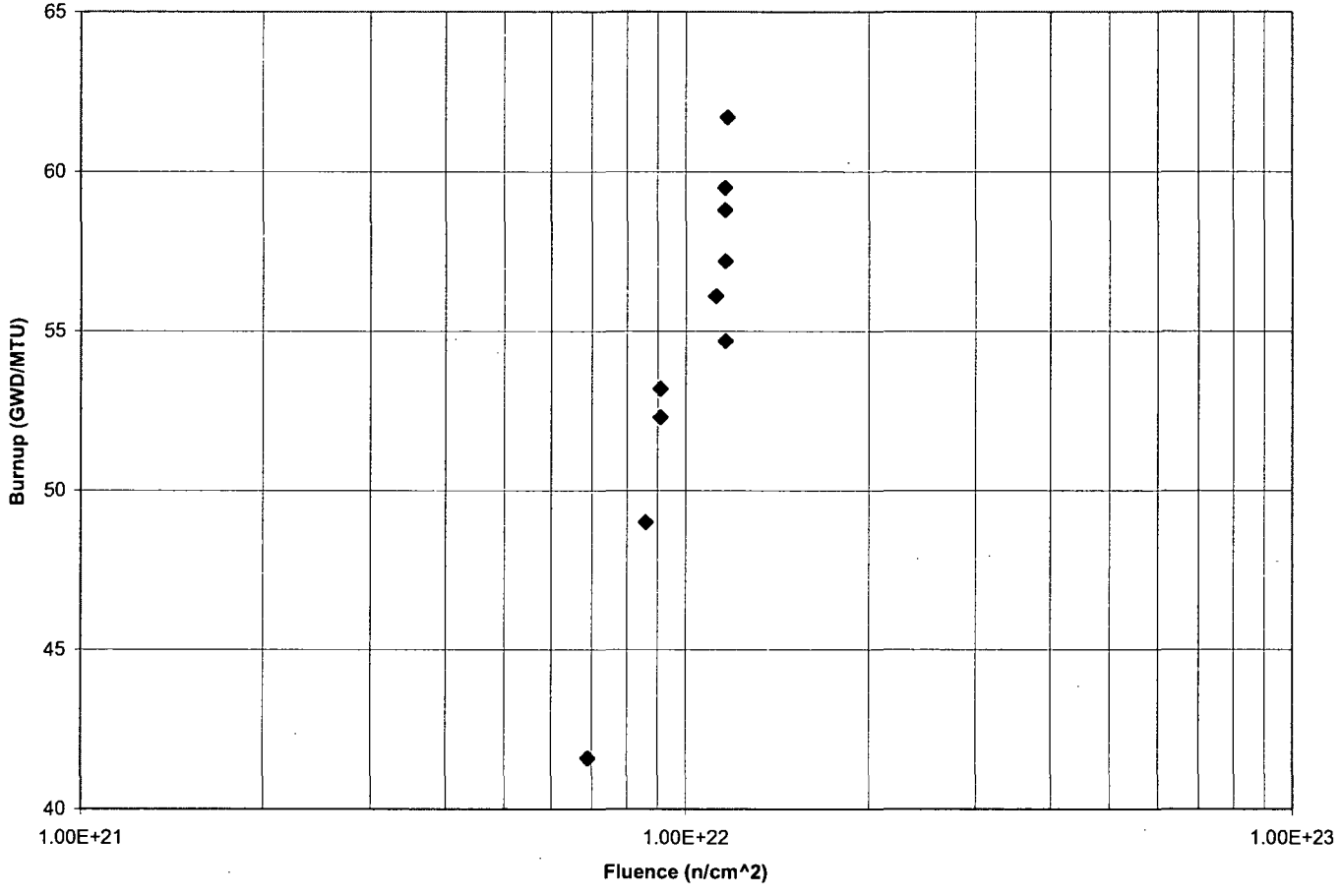

Figure 9. Burnup as a Function of Fluence [7, 8]

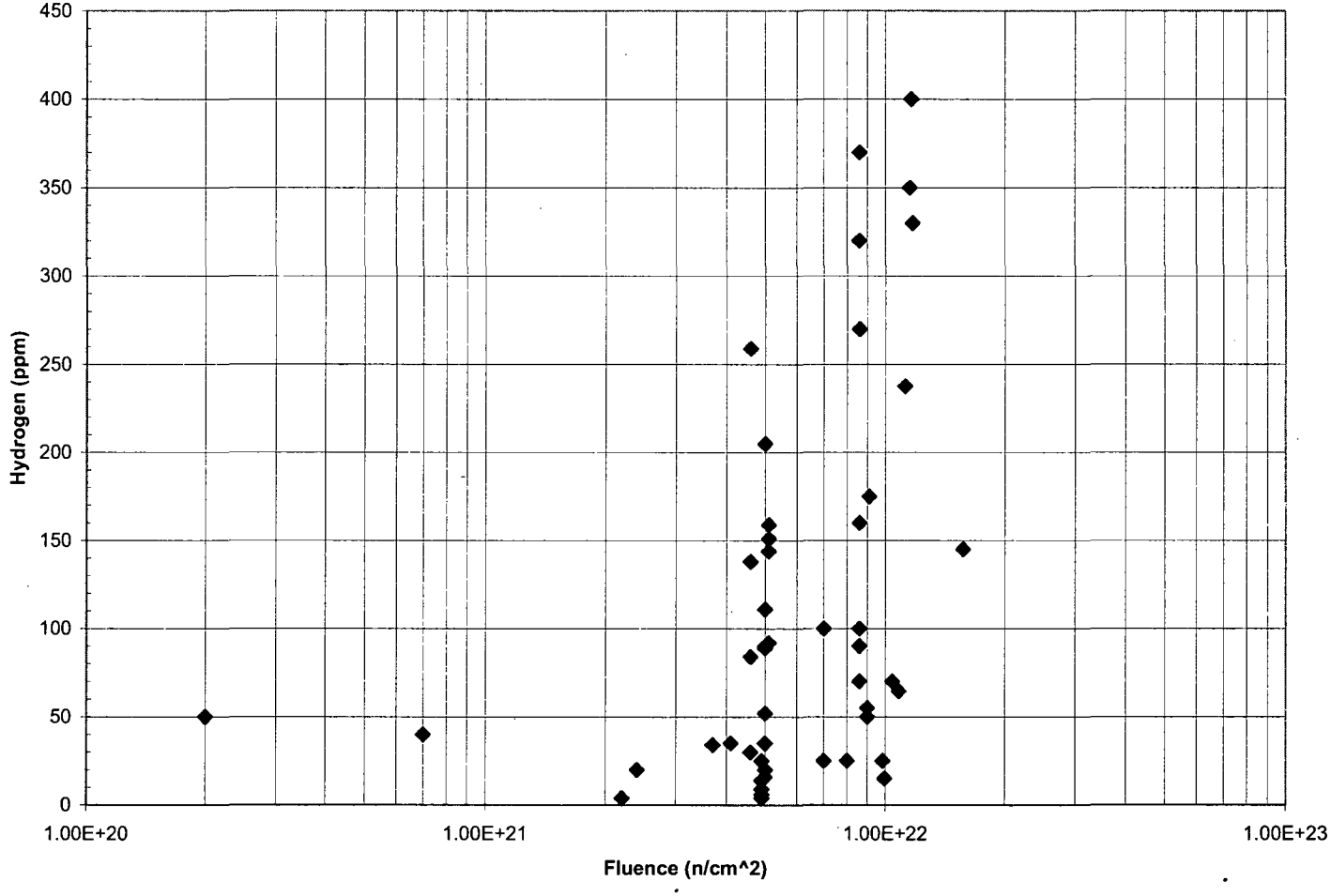

Figure 10. Hydrogen as Function of Fluence

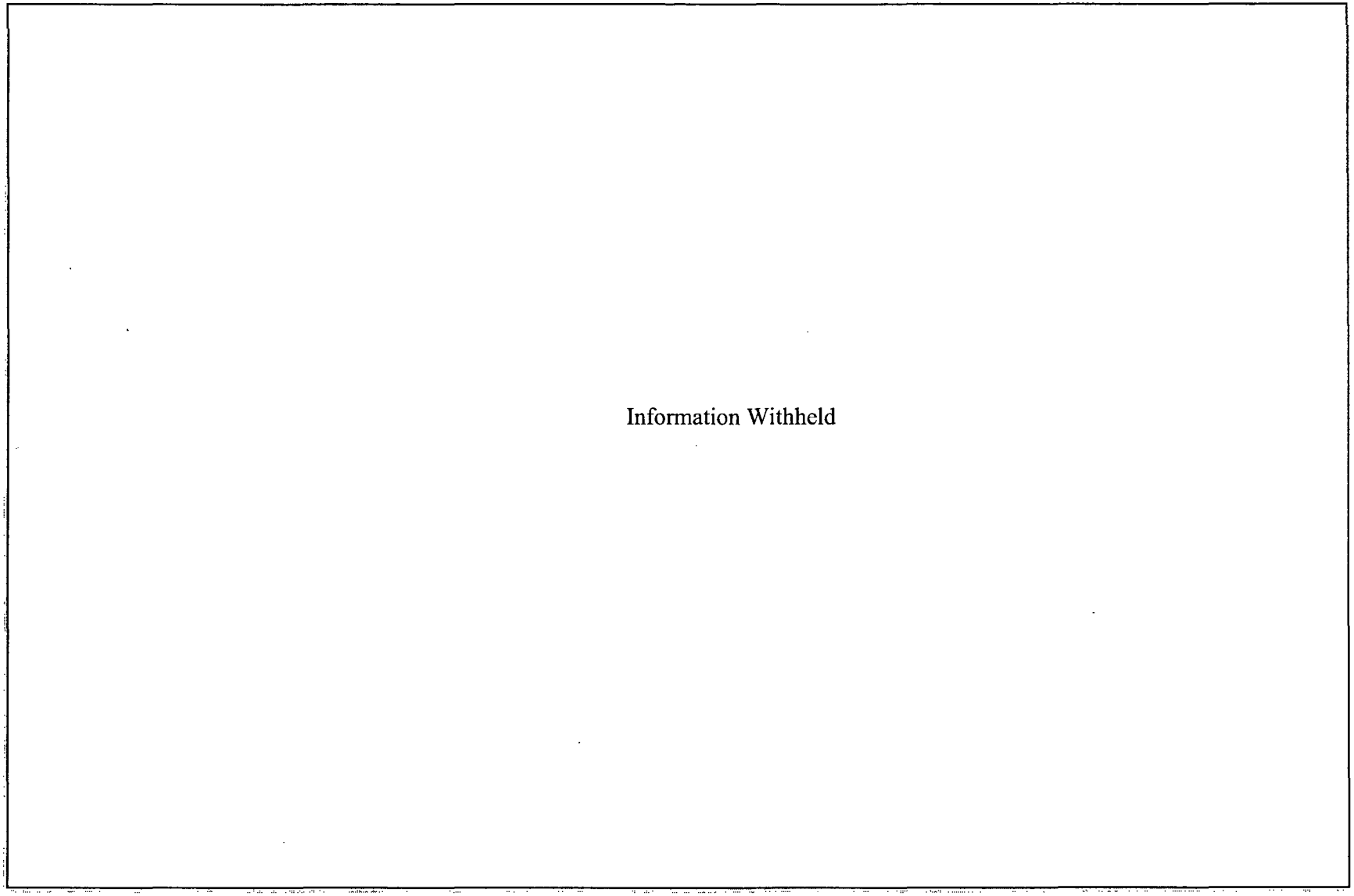

Figure 11. Hydrogen Content versus Burnup

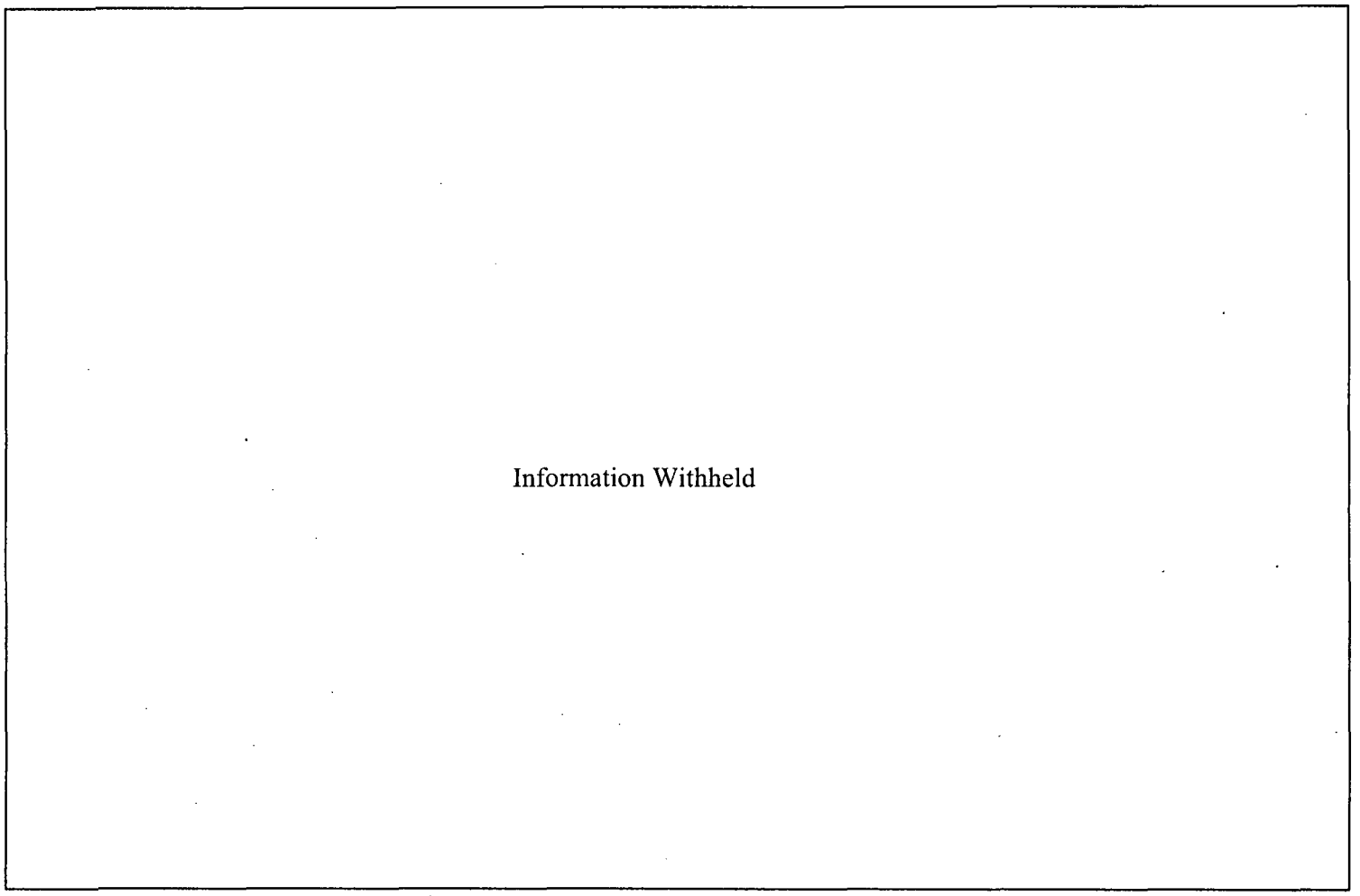

Figure 12. Statistically –Derived Maximum Wall Thickness Average (MWTA) Hydrogen Content in Zicaloy-4 Cladding – Selected Post-Irradiation Examination Measurement Shown for Comparison

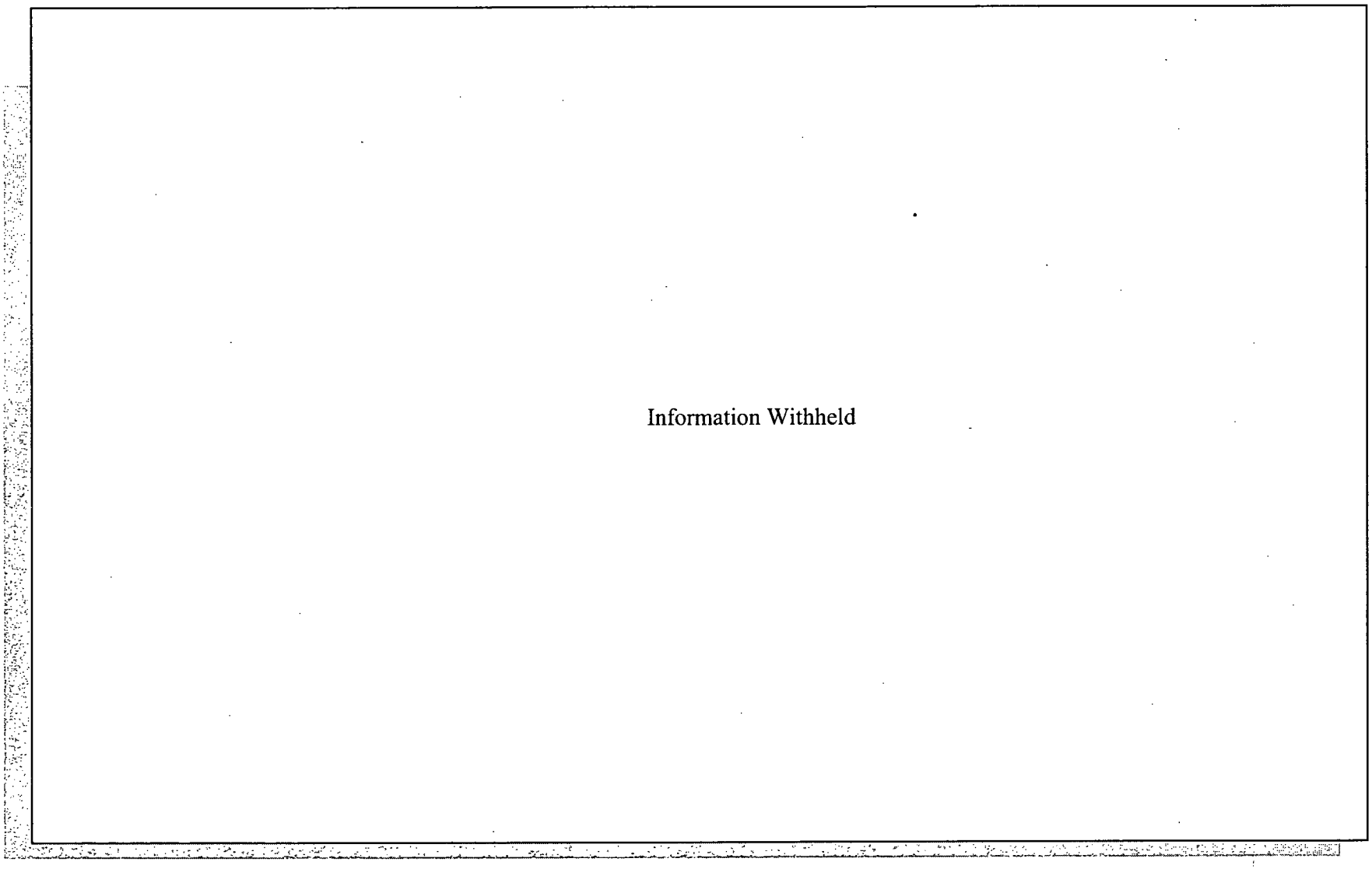

Figure 13. Yield Strength versus Hydrogen Content, EPRI Proprietary Data

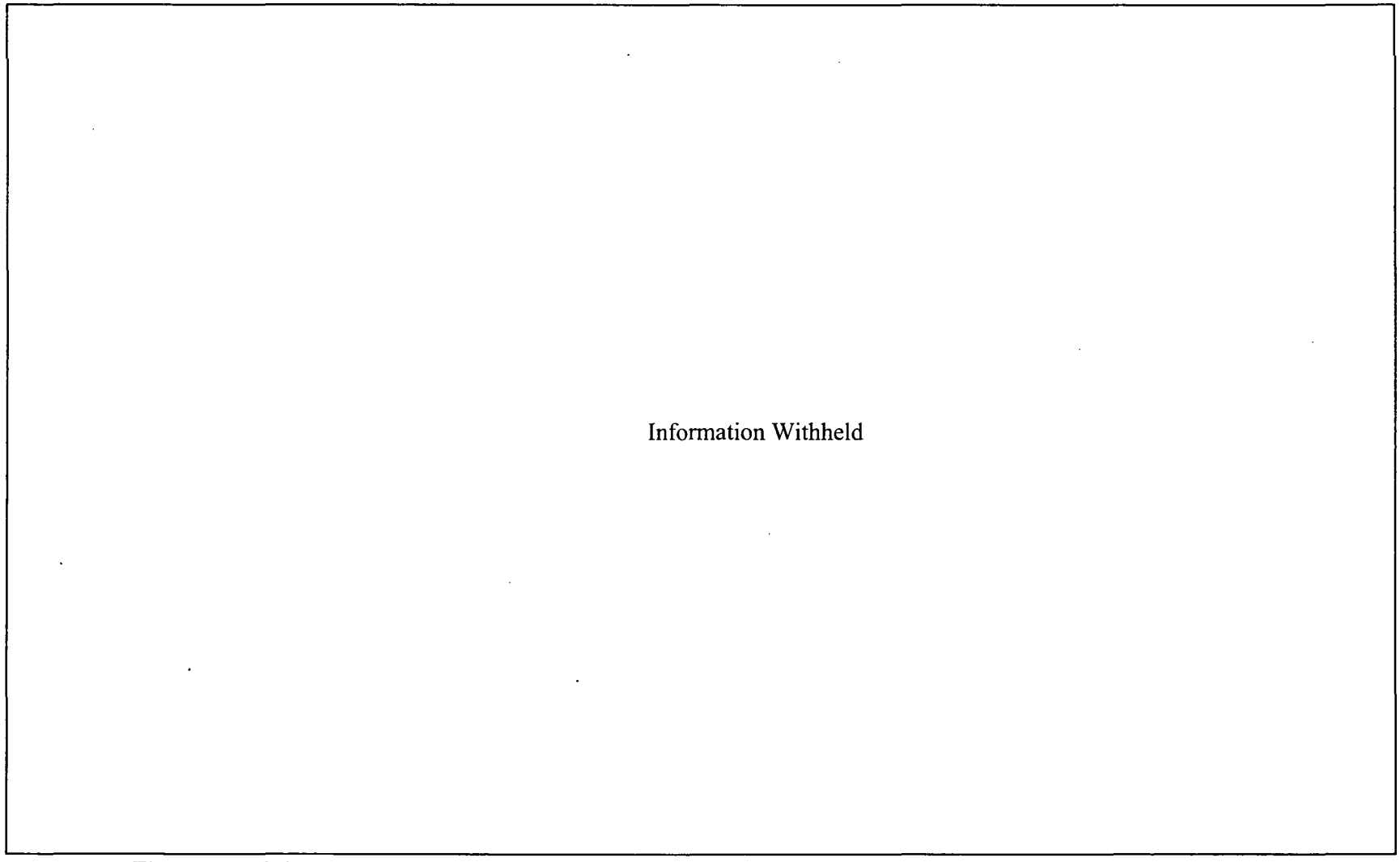

Figure 14: Finite Element Model for Through-wall Axial Crack in Cylinder under Bending or Axial Load

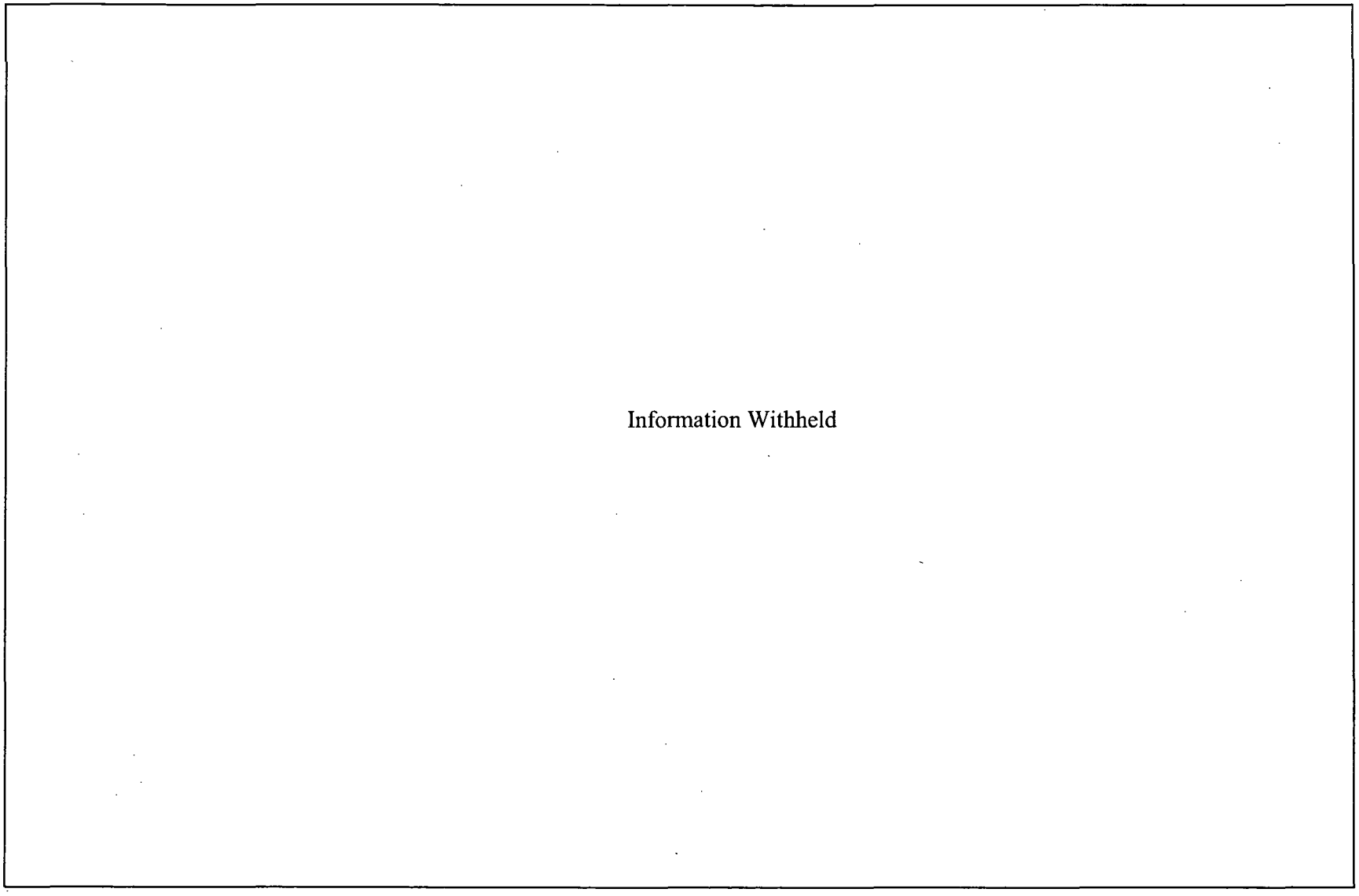

Figure 15: Bending Stress in Tube with Through Wall Axial Crack

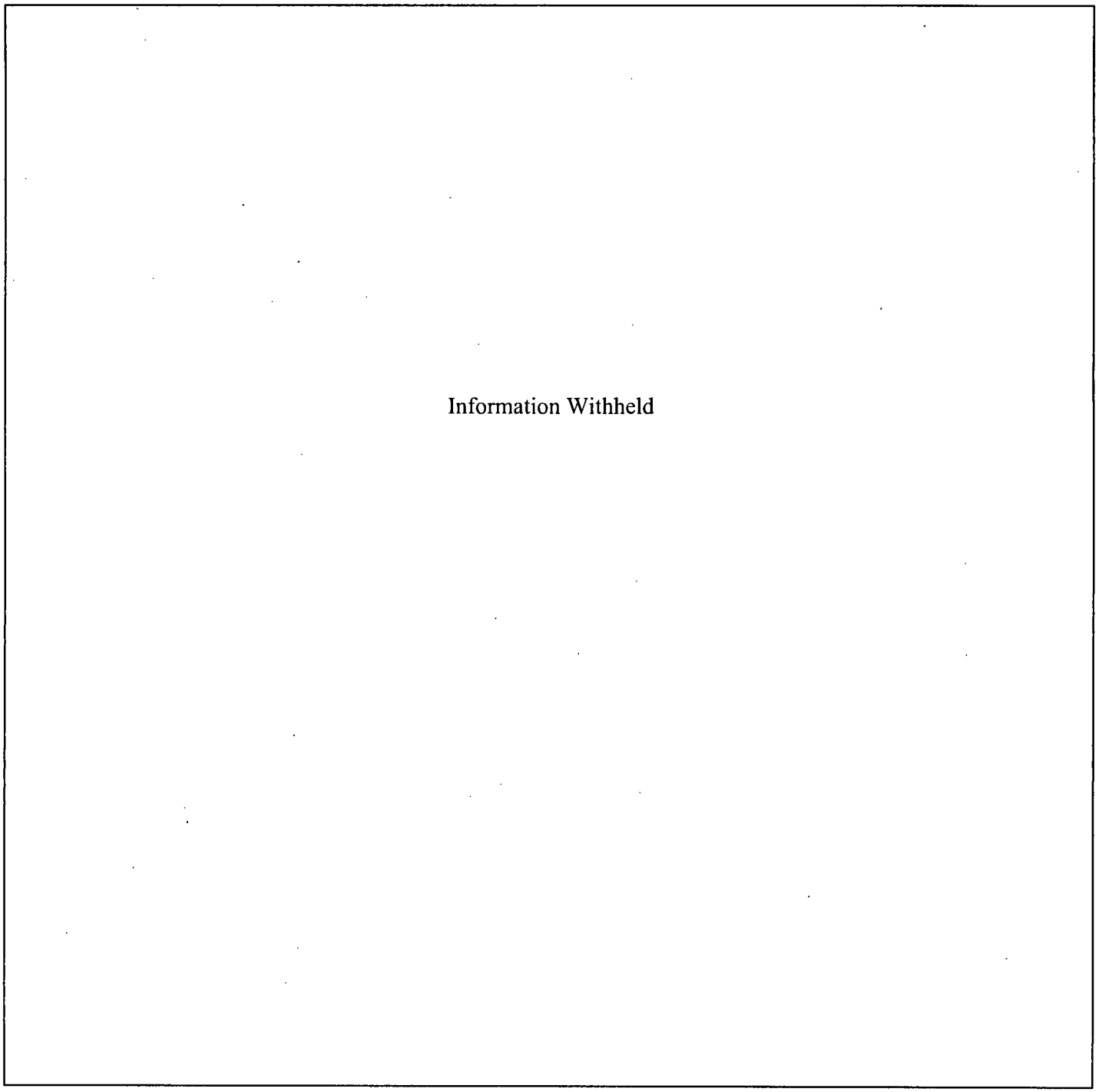

Figure 16. Visaul Appearance of Failed Segment Rods

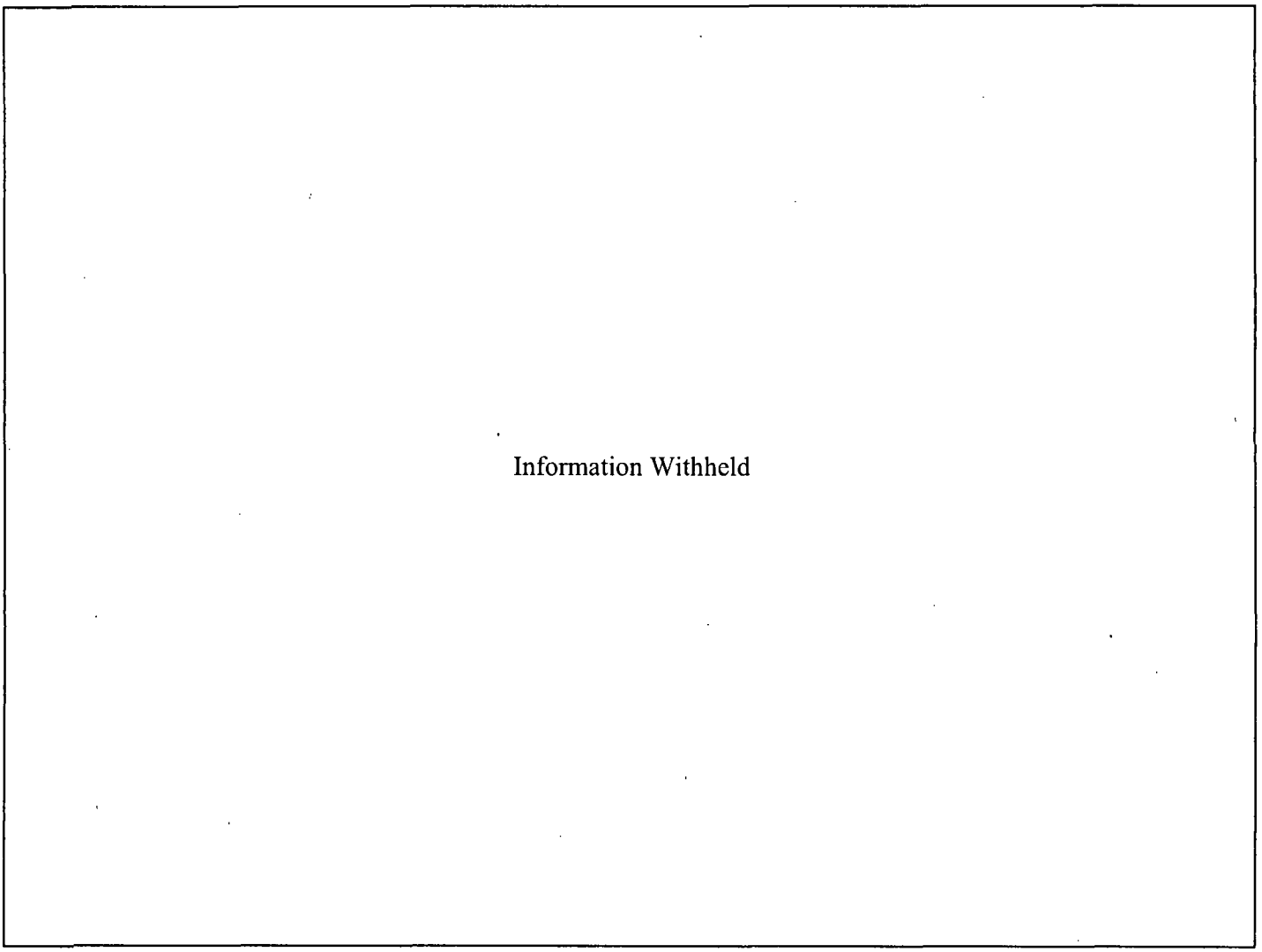

Figure 17
Fracture Analysis #1 - Through-Wall Circumferential Crack under Bending

Available online at www.sciencedirect.com
ScienceDirect
Journal of Nuclear Materials 362 (2007) 93–103
journal of nuclear materials
www.elsevier.com/locate/jnucmat

Effect of radial hydrides on the axial and hoop mechanical properties of Zircaloy-4 cladding

H.C. Chu [a,b,*], S.K. Wu [a], K.F. Chien [b], R.C. Kuo [b]

[a] Department of Materials Science and Engineering, National Taiwan University, Taipei 10617, Taiwan, ROC
[b] Institute of Nuclear Energy Research, P.O. Box 3-14, Longtan, Taoyuan 32546, Taiwan, ROC

Received 27 June 2006; accepted 13 November 2006

Abstract

The effect of radial hydrides on the mechanical properties of stress-relief annealed Zircaloy-4 cladding was studied. Specimens were firstly hydrided to different target hydrogen levels between 100 and 600 wt ppm and then thermally cycled in an autoclave under a constant hoop stress to form radial hydrides by a hydride reorientation process. The effect of radial hydrides on the axial properties of the cladding was insignificant. On the other hand, the cladding ductility measurements decreased as its radial hydride content increased when the specimen was tested in plane strain tension. A reference hydrogen concentration for radial hydrides in the cladding was defined for assessing the fuel cladding integrity based on a criterion of the tensile strength 600 MPa. The reference hydrogen concentration increased with the specimen (bulk) hydrogen concentration to a maximum of ~90 wt ppm at the bulk concentration ~300 wt ppm H and then decreased towards higher concentrations.

PACS: 62.20.Fe

1. Introduction

The mechanical properties of Zircaloy fuel cladding can be adversely affected by the presence of hydrides, especially when they are oriented towards the radial direction of the tubing (i.e. radial hydride). Marshall and Louthan, Jr., demonstrated that Zircaloy-2 tube containing radial hydrides of more than 50 ppm hydrogen exhibited no macroscopic ductility [1], whereas specimens with circumferentially oriented hydrides at the same hydrogen levels showed better ductility [2,3]. In order to retain sufficient ductility to keep its integrity during reactor service, Zircaloy fuel cladding tube is manufactured to ensure that only circumferential hydride platelets are developed due to the hydrogen pickup from the waterside corrosion reaction. However, radial hydrides can be formed when a specimen is cooled down under stress from temperatures at which a fraction of hydrides is dissolved [4–6]. As a result of the larger hoop stress and higher hydrogen concentration attendant with fuel cladding at

* Corresponding author. Address: Department of Materials Science and Engineering, National Taiwan University, Taipei 10617, Taiwan, ROC. Tel.: +886 3 4711400x6694; fax: +886 3 4711409.
E-mail address: hcchu@iner.gov.tw (H.C. Chu).

0022-3115/$ - see front matter © 2006 Elsevier B.V. All rights reserved.
doi:10.1016/j.jnucmat.2006.11.008

higher burnups, the stress reorientation of hydrides is very likely to happen under some conditions during spent fuel dry storage or reactor operation [7–9].

To assure the cladding integrity, Interim Staff Guidance-11, Revision 3 (ISG-11) is used by the US NRC staff when reviewing analyses of the potential for spent fuel reconfiguration during storage conditions. It contains some limitations on the peak cladding temperature, cladding hoop stress and repeated thermal cycling [10]. These acceptance criteria are applicable for all commercial spent fuel burnup levels less than 45 GW d/MTU, and are proposed on the basis of the reduction in cladding ductility associated with the formation of radial hydrides. For spent fuel with higher burnups (exceeding 45 GW d/MTU), the analyses will be reviewed on a case-by-case basis because the current technical information is still insufficient. Therefore, a proper understanding of the mechanism responsible for the stress reorientation of hydrides in the high-burnup fuel cladding is helpful to license application for spent fuel dry storage and transportation. However, the studies of radial hydrides and relevant influences on cladding tube with higher hydrogen levels are limited. In this work, the hydride reorientation behavior and its effects on mechanical properties of the Zircaloy-4 cladding with hydrogen contents up to 600 wt ppm were investigated. Specimens were firstly hydrided to different target hydrogen levels and followed by thermal cycling under a constant hoop stress to form radial hydrides. Then these specimens with a mixture of circumferential and radial hydrides were tested at room temperature. The effect of radial hydride on the mechanical properties is discussed in this paper.

2. Experimental

2.1. Material and hydriding process

Stress-relief annealed (SRA) Zircaloy-4 cladding with an outside diameter of 9.5 mm and wall thickness of 0.58 mm was used in this study. Its chemical composition is given in Table 1. Cladding tube, cut into 13-cm lengths, was first uniformly hydrogen-charged by a thermal cycling process. The specimen was encapsulated with a pre-determined amount of pure hydrogen in a Pyrex capsule of sufficient volume such that a low hydrogen partial pressure could be obtained to avert the formation of hydride layers. The encapsulated cladding specimen was then thermally cycled between ~200 °C and 300 °C for a certain number of cycles, depending on the target hydrogen concentration level. The heating and cooling rates were at 3 °C/min and 2 °C/min, respectively. The target hydrogen levels ranged from 100 to 600 wt ppm. Typically, hydrides were oriented in the circumferential direction and homogeneously distributed across the cross-section of the cladding specimen.

Table 1
Chemical compositions of Zircaloy-4 cladding tube (weight %)

Sn	Fe	Cr	O	N	C	H	Zr
1.26	0.22	0.12	0.13	0.0029	0.01	0.0007	Balance

2.2. Hydride reorientation experiment

In order to obtain radial hydrides, the as-hydrided specimen was further subjected to thermal cycling in an autoclave under a constant hoop stress by regulating the differential pressure between its internal and external pressures with a constant differential pressure control system, as schematically shown in Fig. 1. Prior to the hydride reorientation run, the autoclave was evacuated and then filled with helium gas of ~2 MPa and the cladding specimen was internally pressurized with water at room temperature. Then the tube was heated at a rate of 3 °C/min to 400 °C under a constant differential pressure of 20.7 MPa that was equivalent to a hoop stress of

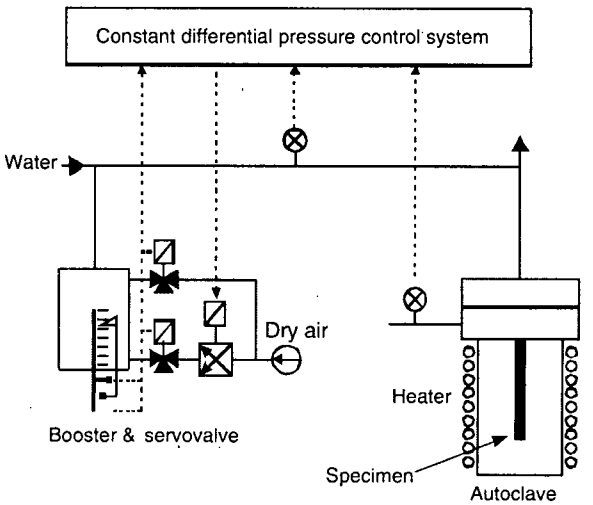

Fig. 1. Schematic diagram of the constant differential pressure control system.

160 MPa being applied on the tubing wall. After solution annealed at 400 °C for 2 h, the specimen was slowly cooled down at a cooling rate of 1 °C/min to 170 °C to make up one thermal cycle. Another thermal cycle started once the tube was cooled down to 170 °C. Upon completion of the thermal cycle treatment, the cladding tube was furnace cooled from 170 °C to room temperature. The pressure fluctuations due to thermal expansion of water and helium gas were regulated and minimized by the constant differential pressure controller, the maximum variation in differential pressure was less than 0.1 MPa. During thermal cycling, a fraction of hydride precipitates dissolved at higher temperatures. With the aid of the hoop stress, zirconium hydrides would re-precipitate out with their precipitate planes oriented in the radial direction of Zirclaoy cladding, when the specimen was cooled down. In this work, cladding tubes were treated under the same thermal parameter and differential pressure but different cycling numbers, i.e. 1, 2, 4, 8 and 12 cycles, to obtain specimens with various fractions of radial hydride precipitates.

Transverse sections of tubing specimens before and after thermal cycling were examined by optical microscopy to reveal the hydride morphology and orientation. The etchant used for metallographic examination was composed of HF, HNO_3, H_2SO_4, and H_2O in a volume ratio of 1:10:10:10. Hydrogen concentrations of Zircaloy-4 cladding specimens were determined by an inert-gas fusion method using a LECO RH-404 hydrogen determinator. The sample for optical metallographic examination was cut from the same piece for hydrogen analysis.

2.3. Mechanical test

Following the reorientation process, the cladding tubes were subsequently cut in two pieces and machined into mechanical test specimens. Two types of test configuration were used: uniaxial tension test (UTT) for axial loading and slotted arc tension (SAT) test for circumferential loading. Detailed dimensions of these two specimens are given in Fig. 2.

2.3.1. Uniaxial tension test

UTT tests were conducted on an Instron model 5582 mechanical testing machine at a nominal strain rate of $\sim 1 \times 10^{-4}\ s^{-1}$. A gripping device was designed to provide suitable mate surfaces for the specimen curvature and lateral support to minimize

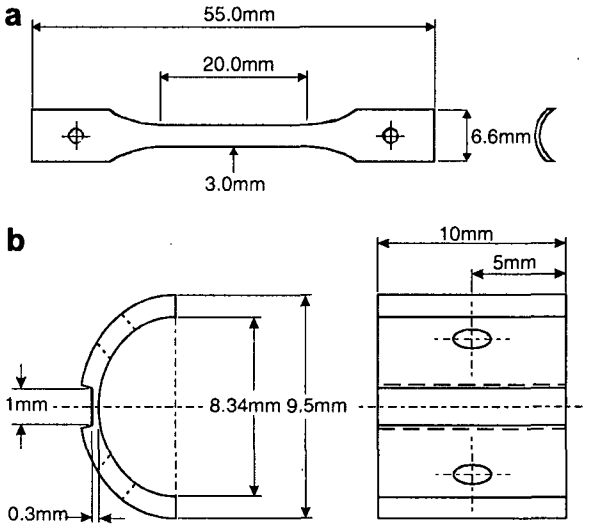

Fig. 2. Dimensions of (a) uniaxial tension specimen and (b) slotted arc tension specimen.

specimen bending that would result from the specimen curvature and fillet arc. The specimen elongation was measured by an LVDT extensometer over the mid-gauge section of 16 mm. The accuracy of the LVDT extensometer is ±0.2% of reading.

2.3.2. Slotted arc tension test

To simulate the loading conditions prevailing on fuel cladding in service, the SAT test was developed to determine the mechanical properties of Zircaloy-4 tubing material. Specimens were also tested on Instron mechanical testing machine at a nominal strain rate of $\sim 1 \times 10^{-4}\ s^{-1}$. An anti-bending mechanism was added to the specimen grip with trough-shaped guides positioned on opposite ends of the slot, as depicted in Fig. 3. A dual-head optical extensometer was employed to take the strain measurements of an SAT specimen from both sides of its gauge section concurrently during testing. Then the strains were averaged to nullify the counteracting bending effects on both sides of the specimen section. The strain measurements taken by the optical extensometer were verified and calibrated by the strain gauge. The resolution of the extensometer is about 4 μm.

2.4. Analysis of hydride orientation

Since hydride platelets were inclined to precipitate in the form of long stringers and always linked together, the general orientation of hydride stringers

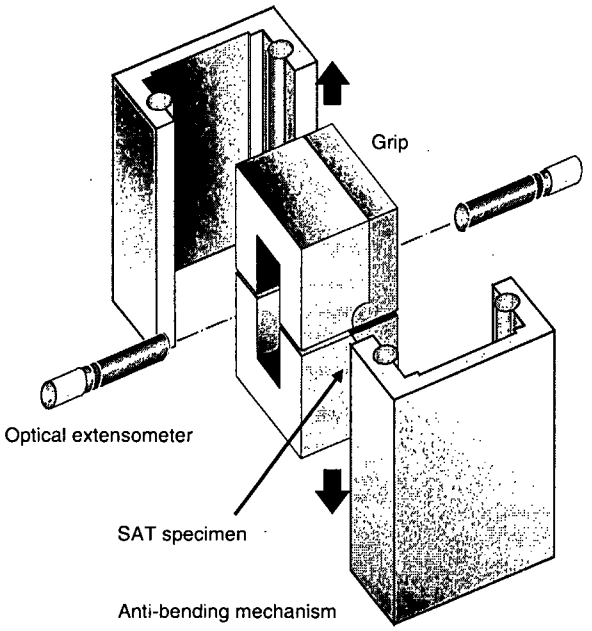

Fig. 3. A sketch of the arrangement of a tension test on a slotted arc tension specimen.

was thus selected to assess the hydride orientation rather than the specific orientation of individual platelets. The majority of hydride traces observed was either along the specimen hoop direction or perpendicular to it, so it was convenient to classify the hydride stringers into two groups: circumferential and radial hydrides. The former was defined as the clusters with their precipitate planes oriented within 0–40° to the reference (circumferential) axis; the clusters within 50–90° to the reference axis were recognized as radial hydrides. The small clusters within 40–50° to the reference axis were classified into neither of the two groups, and not counted into the total amount of hydrides.

The percentage of radial hydrides was determined by calculating the areal fraction of radial strings on a photomicrograph. To provide a high-resolution digital image for this analysis, a digital camera with a CCD array of 2048×2048 pixels was mounted on a microscope to project the hydride traces onto a screen. A magnification of 200 was selected. The orientation of hydride trace was recorded as each pixel in the image was scanned, the fraction of total pixel of hydrides in each category was then determined. On a photomicrograph, the hydride orientation analysis was conducted at two locations in the middle of the cladding wall. From the measurements, the average fraction of radial hydrides was then calculated. Because both radial and circumferential hydride precipitate planes were predominantly parallel to the axial direction of cladding tube, all hydride reorientation data were measured on the transverse cross-section.

3. Results and discussion

3.1. Effect of thermal cycling on hydride reorientation

An example of the reorientation of hydride precipitates in Zircaloy fuel cladding is given in

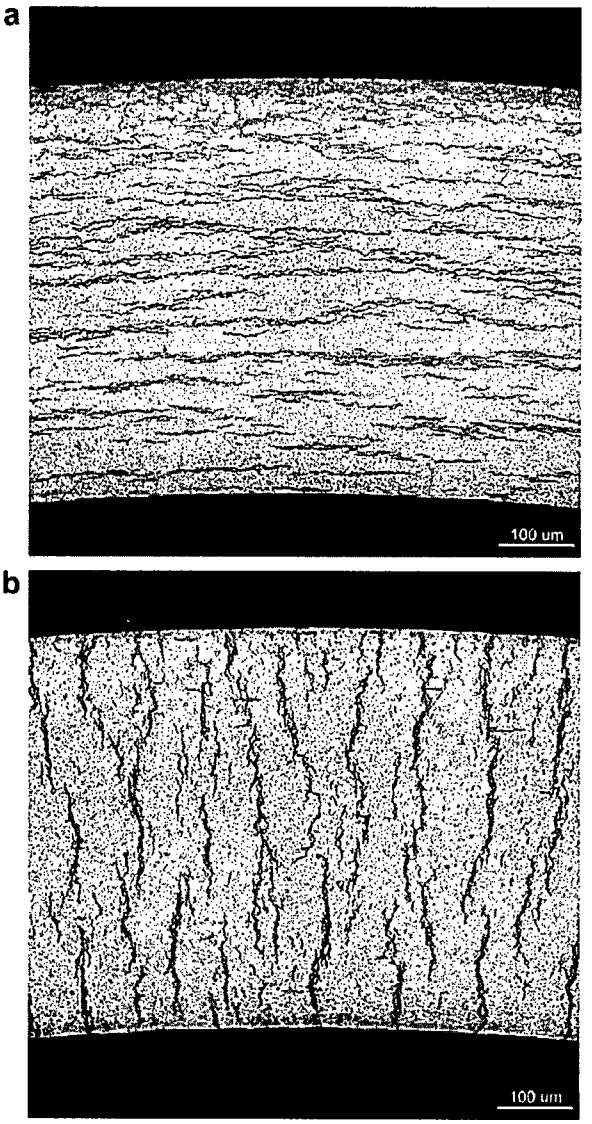

Fig. 4. Micrographs showing reorientation of hydrides in Zircaloy-4 cladding: (a) as-hydrided, (b) after 8 cycles of thermal treatment (~230 wt ppm).

Fig. 4. Most hydrides were circumferentially aligned and uniformly distributed across the as-hydrided cladding wall. The majority of the hydride traces was thick and long; there existed a minor amount of fine hydrides. In general, both the coarse and fine hydrides had the same orientation. With increasing the number of thermal cycles, the proportion of these fine hydrides decreased and the reorientation of hydrides from circumferential to radial direction became more noticeable. The slow cooling rate of 1 °C/min provided sufficient time for hydrogen atoms to diffuse and precipitate at their preferable sites.

The effect of the thermal cycle number on the reorientation of hydrides in cladding tube is shown to vary with hydrogen concentration in Fig. 5. A hoop stress of 160 MPa was applied on the cladding tube while thermal cycling was proceeding. The percentage of radial hydrides increased as the number of thermal cycles increased, until it reached a plateau value on the reorientation curves plotted in Fig. 5. More than 90% of hydride precipitates in the 200–300 wt ppm H specimens were reoriented into radial hydrides. For the specimen with a higher hydrogen content of 600 wt ppm, the applied stress of 160 MPa induced a maximum of about 20% radial hydrides after twelve cycles. Besides, a lower plateau value of approximately 78% radial hydrides was obtained for the 130 wt ppm H specimen. The fact that the extent of reorientation of hydrides in the cladding with 130 wt ppm hydrogen is lower than those of higher hydrogen content levels is believed to be related to the temperatures at which the hydrides begin to nucleate from the saturated matrix. According to the solubility data [11], a cladding material with hydrogen contents higher than 200 wt ppm would start to have hydrides precipitated when it was slowly cooled from the holding temperature of 400 °C, whereas precipitation in a 130 wt ppm H specimen did not occur until it was cooled to 357 °C. The diffusion rate of hydrogen atoms was smaller and the effect of the stress on the hydride reorientation was less significant in extent at lower temperatures, relative to those at 400 °C. Consequently, a lower plateau fraction value for radial hydrides was obtained on the cladding specimens with lower bulk hydrogen concentrations.

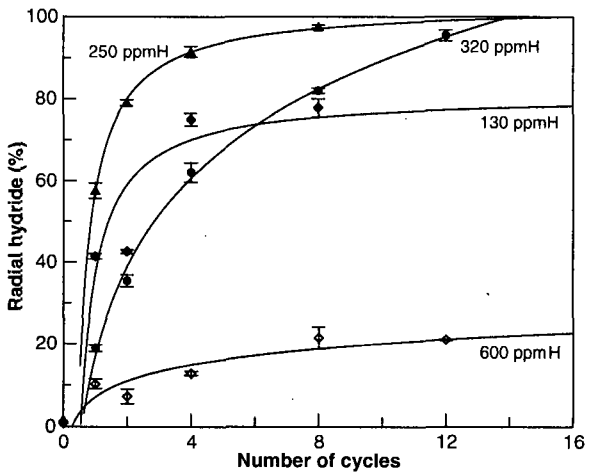

Fig. 5. Effect of the thermal cycle number on the hydride reorientation of cladding tubes with various hydrogen concentrations.

It is generally believed that stress reorientation takes place only on the hydrides which have dissolved and then re-precipitated under stress. Hence small proportions of hydrides in the 320 and 600 wt ppm H specimens aligned radially after the first cycle of heat treatment. A complete reorientation of hydrides was attainable on the 320 wt ppm H specimen after 12 cycles of thermal treatment, whereas there were still about 120 wt ppm of hydrides not dissolved at 400 °C during each cycle. Results obtained in this work imply that, under a proper combination of cladding temperature and hoop stress, a complete reorientation of all hydrides is possible with the aid of repeated heating and cooling even though hydrides are not fully dissolved in each thermal cycle.

3.2. Hydrided Zircaloy cladding under tension tests

3.2.1. General description

The uniaxial tension specimens were loaded in a plane stress state and the slotted arc tension specimens in a stress state approaching the plane strain loading condition. A comparison of the typical stress–strain curves for UTT and SAT tests on Zircaloy-4 cladding specimens was exemplified in Fig. 6. Except for the specimens containing radial hydrides, the SAT specimens sustain higher flow stress than the UTT specimens but much smaller ductility, which is similar to the observations of other researches on Zircaloy-2 [12,13]. The higher flow stress of SAT specimens is mostly attributed to the geometry of the plane strain tension specimen [14].

Fig. 7 shows the effect of hydrogen concentration on the mechanical properties of Zircaloy-4 fuel cladding tube tested under uniaxial and slotted

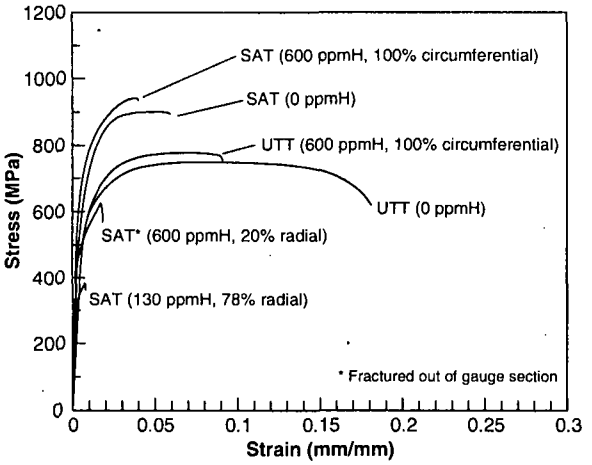

Fig. 6. Typical engineering stress–strain curves for uniaxial and slotted arc tension tests on Zircaloy-4 cladding specimens at room temperature.

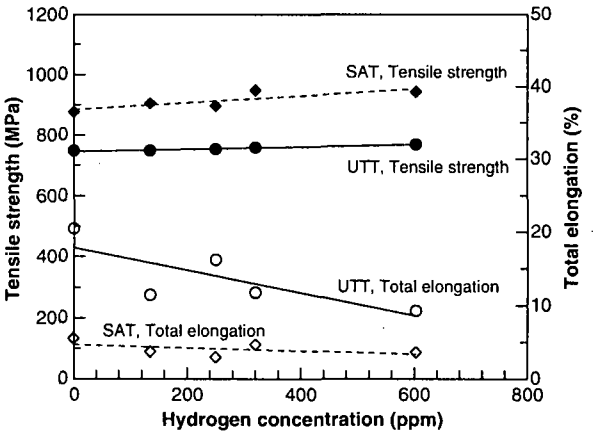

Fig. 7. Effect of hydrogen concentration on the mechanical properties of SRA fuel cladding specimens tested under uniaxial tension and slotted arc tension; all hydrides in specimens were circumferentially aligned.

arc tension at room temperature. All hydrides in this case were homogeneously distributed and completely oriented along the circumferential direction. The tensile strengths of both UTT and SAT fuel cladding specimens increased slightly with hydrogen content, their ductility values decreased as hydrogen concentration increased. These trends are in agreement with the observations by other investigators [2,3,15,16].

Some of the as-received tubes were treated under the same conditions as those for stress-reorientation experiments and tested at room temperature to verify the effect of thermal cycle itself on the deformation behavior of the material. Results of both UTT and SAT specimens showed little or no dependence on the number of thermal cycles.

3.2.2. Effect of radial hydride on uniaxial tension properties

The effects of radial hydrides on the uniaxial tensile properties of Zircaloy-4 cladding specimens, with hydrogen concentration levels ranging between 130 and 600 wt ppm, tested at room temperature are plotted in Fig. 8. The effect of radial hydrides on the axial ductility of the cladding tube was insignificant even with the case of 320 wt ppm specimens in which most of hydride platelets were reoriented into radial direction. This phenomenon could be ascribed to the fact that both the face normals of radial and circumferential hydride platelets were perpendicular to the applied stress. The effects of both circumferential and radial hydrides on the mechanical properties of cladding tube along the loading direction were similar.

On the other hand, when cladding tubes were subjected to tensile hoop stress, the radial hydrides with their platelet normals parallel to the stress direction and were susceptible to cracking along the hydride planes, a great loss in the circumferential ductility was expected. The effects of radial hydrides on the cladding hoop properties are discussed in the following section.

3.2.3. Effect of radial hydride on hoop tension properties

Fig. 9 shows the effects of radial hydrides on the hoop tensile properties of Zircaloy-4 cladding

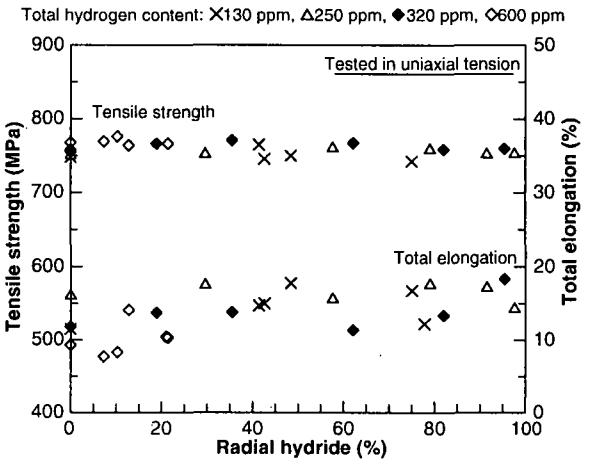

Fig. 8. Effect of radial hydrides on the mechanical properties of SRA fuel cladding specimens tested under uniaxial tension at room temperature.

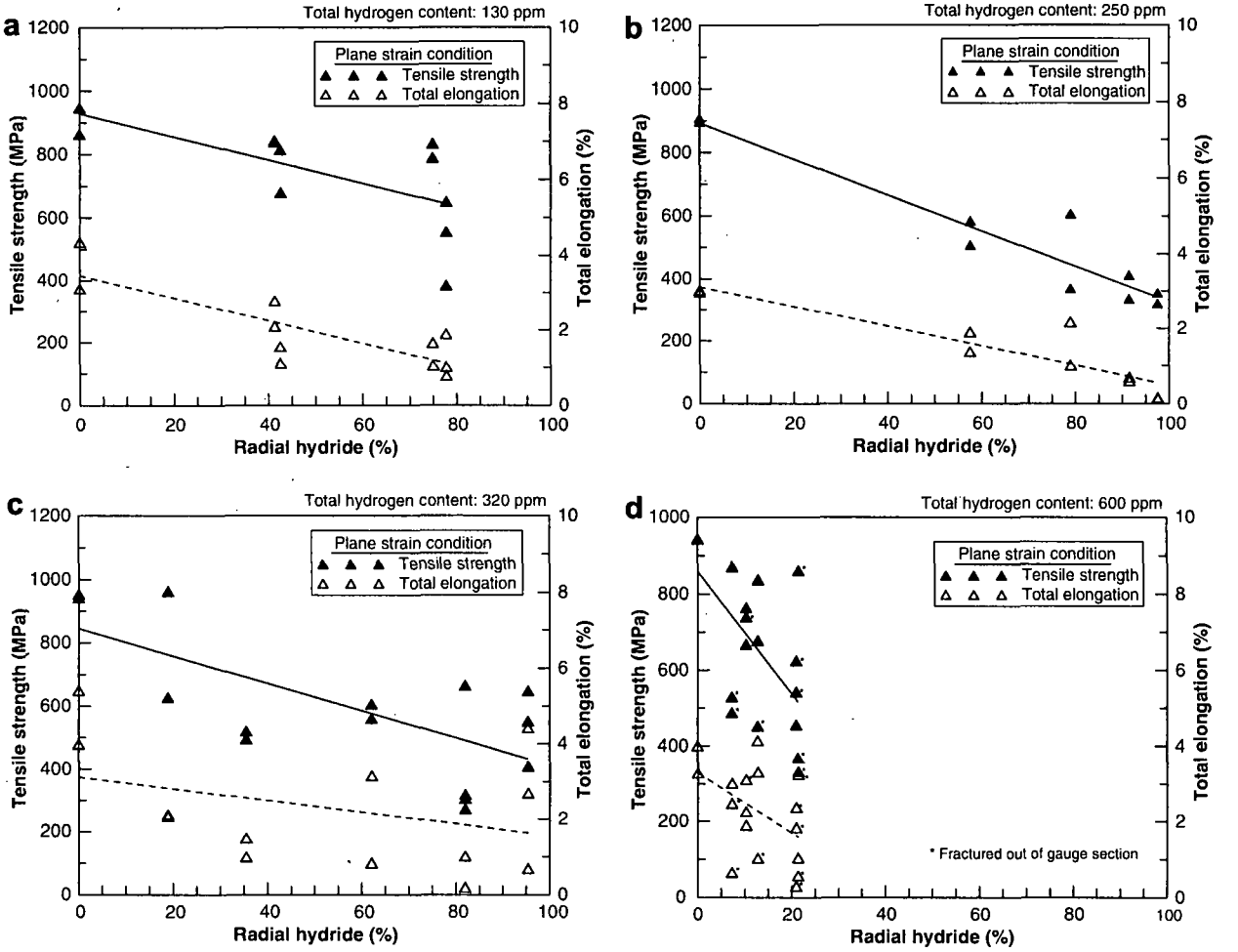

Fig. 9. Effect of radial hydrides on the mechanical properties of cladding specimens with various hydrogen content levels tested under slotted arc tension at room temperature: (a) 130 wt ppm, (b) 250 wt ppm, (c) 320 wt ppm, and (d) 600 wt ppm.

specimens, with hydrogen concentration levels ranging between 130 and 600 wt ppm, tested at room temperature. It was observed that if all hydrides in the cladding were 100% circumferentially oriented, the test results showed a good reproducibility. Once some of the circumferential hydrides transformed into radial, the hoop mechanical properties of cladding deteriorated and the data became scattered.

Fig. 9 also suggests that some specimens with significant amounts of radial hydrides apparently have sufficient ductility, but that they were very brittle and fractured at stresses lower than the yield strength. For example, the specimens with 600 wt ppm hydrogen failed when deformed in the elastic elongation range, but their stress–strain curves still showed nonlinear responses as if they underwent plastic deformation (Fig. 6). The contradictory observation could be ascribed to the formation of some small surface cracks from breaking of radial hydrides during testing. Because the strains were taken by measuring the distance between the two indentations on the gauge section (~0.7 mm), the formation of surface cracks caused an increment in this distance and thus higher strains were obtained. Choubey and Puls [17] have used acoustic emission (AE) to detect cracking of long radial hydrides in Zr–2.5Nb. They reported that cracking of hydrides was initiated in the low plastic region or slightly below the yield stress. And the small numbers of AE events generated in the early stage of deformation were not considered representative of hydride cracking because of unknown and uncontrolled stresses that might exist in the specimen. In this study, surface cracks appeared succes-

sively when specimens were gradually loaded up to ~300 MPa. Because of the slight bending effect during the initial stage of the test, most of the cracks tended to occur on the specimen inner surface to compensate the slightly different stress levels on both sides of the slotted area.

Fig. 10 illustrates the fractographic features of the specimens tested at room temperature. Normal dimples, ridges and round voids were the dominant features of the as-received specimens (Fig. 10(a)), the brittle features of microcracks, cleavages increased as hydrogen concentration increased (Fig. 10(b)). For the specimens having 100% circumferential hydrides, the number of microcracks on the fracture surface increased with increasing hydrogen concentration. As can be seen in Fig. 10(b) and (c) for specimens with the same hydrogen content levels, the number of secondary cracks decreased if some hydrides reoriented into radial direction.

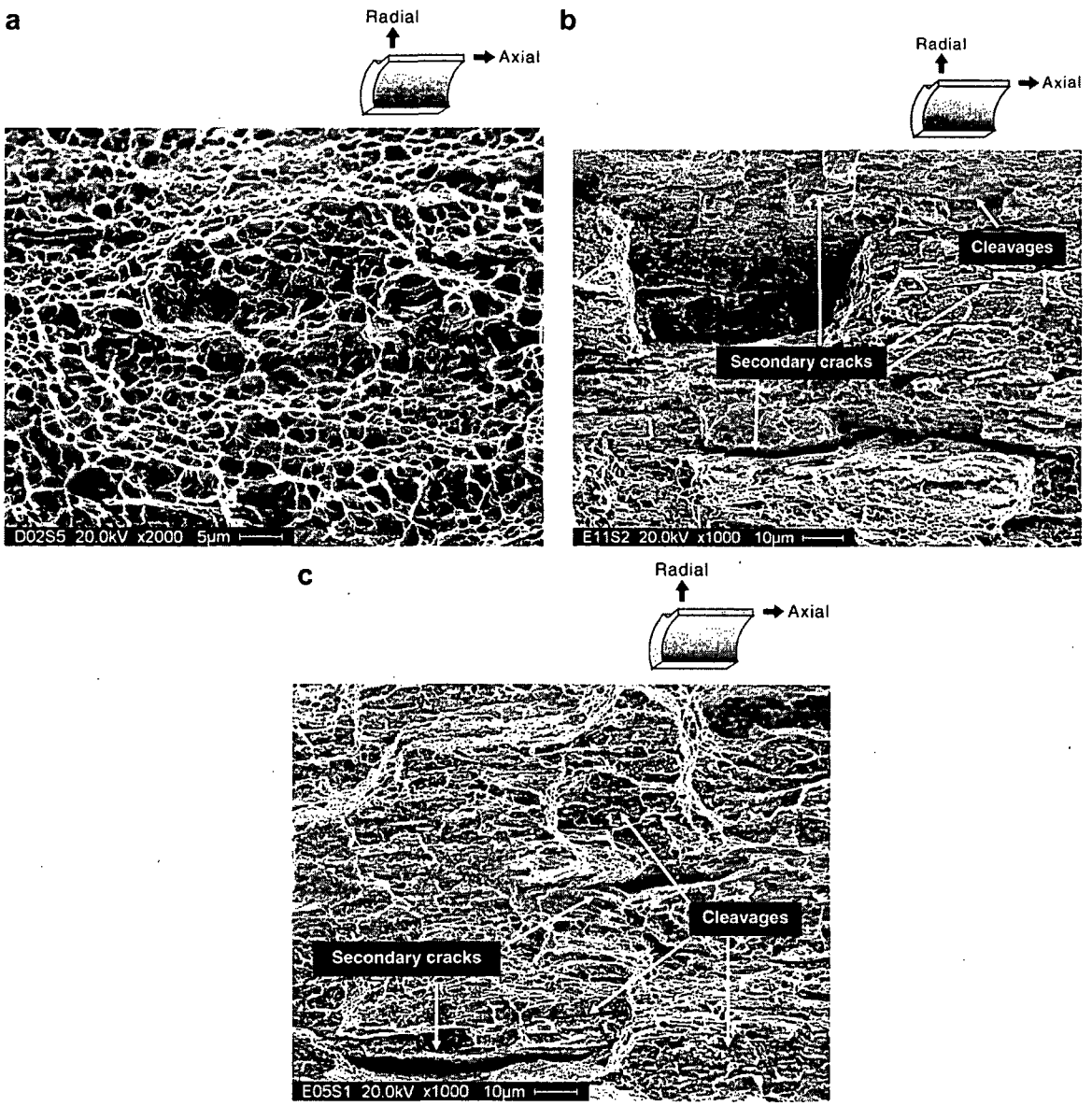

Fig. 10. SEM fractographs of SRA cladding specimens tested under slotted arc tension at room temperature: (a) SRA Zircaloy-4 with 7 wt ppm H (as-received), (b) 600 wt ppm H specimen with ~100% circumferential hydrides, and (c) 600 wt ppm H specimen with ~21% radial hydrides.

To better understand the cladding deformation behavior along the hoop direction, toughness was used to evaluate the effect of radial hydrides on the mechanical properties of cladding tube. The toughness was obtained by calculating the total area under the stress–strain curve [18]. It was an indicator which showed that the amount of work per unit volume could be done on a material prior to rupture. Unfortunately the concept of toughness could not give a clear trend of SAT test results. Since SAT test results were affected unpredictably by a tiny variation of hydride distribution along the cracking path, the worst-case data of each test batch were selected to assess the effect of radial hydride on the hoop mechanical properties of Zircaloy-4 cladding conservatively. The SAT test results were re-plotted in Fig. 11. The concentration of radial hydride in Fig. 11 was obtained by multiplying the percentage of radial hydride and the bulk hydrogen content of the specimen. A residual strain of 0.01 was commonly used as an acceptance criterion in evaluating the integrity of fuel cladding, so 1% total elongation was taken as a reference value in Fig. 11(a). It was found that cladding specimens failed to meet this criterion when radial hydride concentrations (reference concentrations) were higher than 74, 157, 106, and 37 wt ppm for the specimens with bulk hydrogen contents of 130, 250, 320 and 600 wt ppm, respectively. Because of the fact that the surface crack probably occurred during SAT testing, the reference concentration of radial hydrides determined by cladding ductility might not be conservative. As shown in Fig. 6, the yield strength of an intact Zircaloy-4 specimen (i.e. without surface crack) under plane strain condition was ~600 MPa. For this reason, a tensile strength level of 600 MPa was chosen as an alternative acceptance criterion to determine the reference concentrations conservatively. The reference radial hydride concentrations determined by 600 MPa for the specimen at each hydrogen level were 60, 100, 75, and 33 wt ppm, respectively (Fig. 11(b)). The results are summarized in Table 2. The reference radial hydride concentrations obtained in this work are comparable to those reported by Marshall and Louthan on the annealed Zircaloy-2 specimens with total hydrogen less than ~200 wt ppm [1,4]. They suggested that all specimens with radial hydrides containing more than 50 wt ppm H exhibited no macroscopic ductility. It should be noted that the engineering strain was less than 1% when the yield point was reached during a 'normal' SAT testing (a test with no surface crack occurring). The reference radial hydride concentrations determined by the cladding tensile strength were more conservative and reliable than those by the cladding ductility.

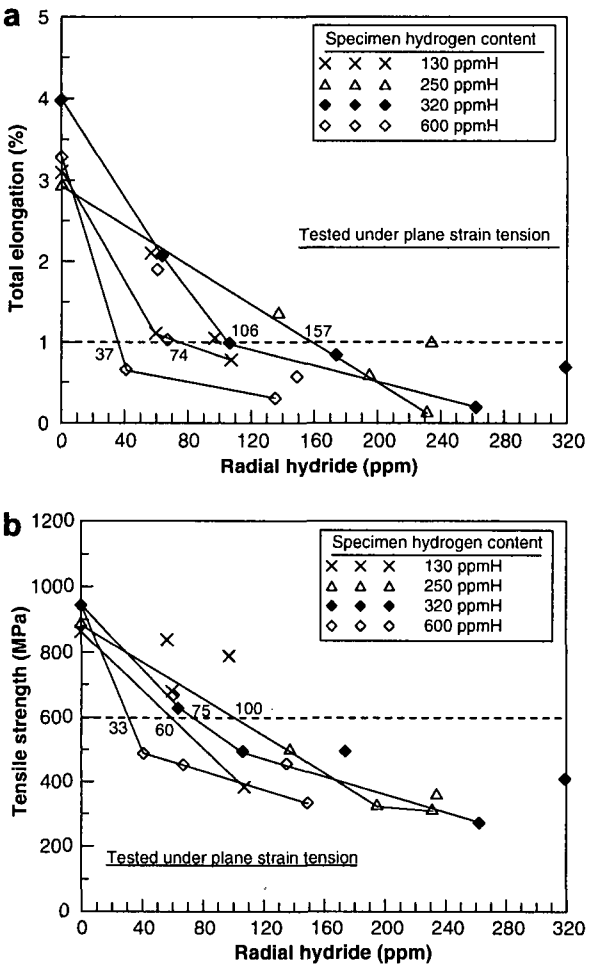

Fig. 11. Determination of the reference radial hydride concentration of Zircaloy-4 cladding material by the acceptance criteria of (a) 1% total strain and (b) tensile strength of 600 MPa.

Table 2
Reference concentrations of radial hydrides for brittle fracture of SRA Zircaloy-4 cladding with different hydrogen content levels tested under slotted arc tension

Specimen	Reference concentrations			
	Determined by 1% strain		Determined by 600 MPa stress	
	(wt ppm)	(%)	(wt ppm)	(%)
130 wt ppm H specimen	74	56.9	60	46.2
250 wt ppm H specimen	157	62.8	100	40.0
320 wt ppm H specimen	106	33.1	75	23.4
600 wt ppm H specimen	37	6.2	33	5.5

One factor that determines the mechanical properties of cladding specimens is the continuity of hydride precipitates. As reported by Arsene et al. [3], a ductile–brittle transition occurred when a critical inter-hydride spacing reached and the transition happened within a range of hydrogen contents (from 1500 to 2400 ppm). This work indicated, when parts of the circumferential hydrides became radial, the chance to form a continuous hydride network increased. However, the probability to reach the critical spacing between circumferential hydrides also decreased because some of hydrides were consumed as the reorientation process happened. It can be confirmed by comparing the hydride spacings in the specimens of the same hydrogen level but with different radial hydride contents. The continuity of hydrides and the inter-hydride spacing were the two factors interacting with each other in a complicated way to affect the deformation behavior of Zircaloy cladding under slotted arc tension, which was reflected in wide variations of SAT test results from specimen to specimen.

From the data shown in the last column of Table 2, the reference percentage of radial hydrides linearly decreased with increasing specimen hydrogen content. The reference hydrogen concentration increased with the specimen (bulk) hydrogen concentration to a maximum of ~90 wt ppm at the bulk concentration ~300 wt ppm H and then decreased towards higher concentrations, as plotted in Fig. 12. It could be accounted for by the hypothesis that a large percent of radial hydrides are needed to develop continuous cracking path due to the large inter-hydride spacings in the specimens of lower hydrogen contents, and that in the specimens of higher hydrogen contents, a reduction in hydride spacing would make it easier to link neighboring hydrides together with a demand for fewer radial hydrides to form a continuous network along the cracking (Fig. 13). Besides, circumferential hydrides would also work to exacerbate the brittle behavior when a cladding specimen had very high hydrogen contents. These results suggest that a small amount of radial hydrides can be extremely detrimental to

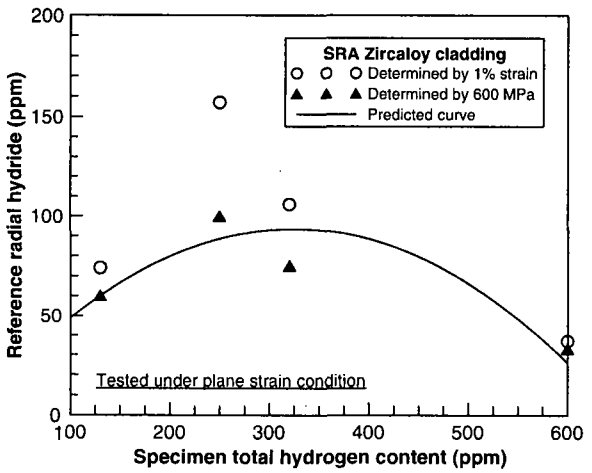

Fig. 12. Estimation of the reference radial hydride concentration as a function of specimen total hydrogen concentration.

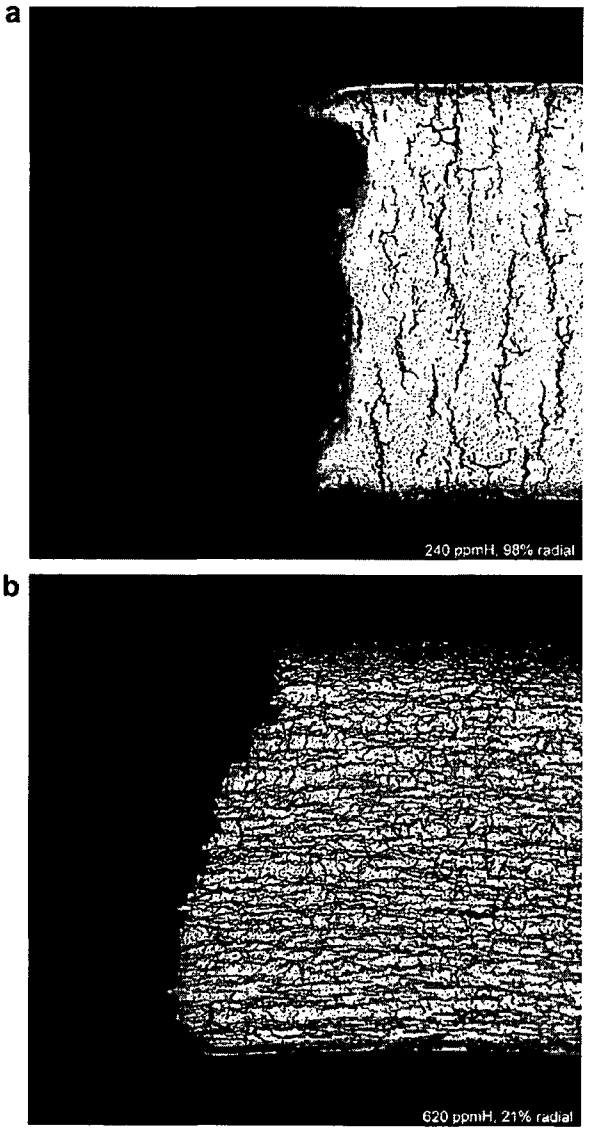

Fig. 13. Cross-sections of Zircaloy-4 cladding specimens tested under slotted arc tension at room temperature: (a) 240 wt ppm H specimen with 98% radial hydrides, and (b) 620 wt ppm H specimen with ~21% radial hydrides.

the integrity of cladding materials of higher hydrogen concentrations although they are difficult to be formed.

4. Conclusions

In this study, the hydride reorientation behavior and the effects of radial hydrides on the axial and hoop mechanical properties were investigated. Summarized below are the results:

1. Hydrided specimens with bulk hydrogen contents from 130 to 600 wt ppm were thermally cycled in an autoclave under a constant hoop stress. The percentage of radial hydrides increased as the number of thermal cycles increased until it reached a saturated value. More than 90% of hydride precipitates in the 200–300 wt ppm H specimens were reoriented into the radial direction after several thermal cycles.
2. The hydride-reoriented cladding specimens with bulk hydrogen contents from 130 to 600 wt ppm were tested in uniaxial tension at room temperature. The effect of radial hydrides on the axial ductility of cladding tube can be neglected.
3. The effects of radial hydrides on the hoop tensile properties of Zircaloy-4 cladding specimens with hydrogen concentration levels up to 600 wt ppm were tested at room temperature using slotted arc tensile specimens. Test results were scattered but indicated a trend that mechanical properties degraded with increasing percentage of radial hydrides.
4. The reference concentration of radial hydrides for brittle fracture of cladding material increased as the total hydrogen content increased to about 300 wt ppm and then decreased with increasing hydrogen concentration. The results in this study suggest that a small amount of radial hydrides can be extremely detrimental to the integrity of cladding materials of higher hydrogen concentrations although they are difficult to be formed.

References

[1] R.P. Marshall, M.R. Louthan Jr., Trans. ASM 56 (1963) 693.
[2] J. Bai, C. Prioul, D. Francois, Metall. Mater. Trans. A 25 A (1994) 1185.
[3] S. Arsene, J.B. Bai, P. Bompard, Metall. Mater. Trans. A 34A (2003) 579.
[4] M.R. Louthan Jr., R.P. Marshall, J. Nucl. Mater. 9 (1963) 170.
[5] C.E. Ells, J. Nucl. Mater. 35 (1970) 306.
[6] M. Leger, A. Donner, Can. Metall. Q. 24 (1985) 235.
[7] H.M. Chung, in: Proceedings of the International Meeting on LWR Fuel Performance, Orlando, FL, 19–22 September 2004.
[8] G. Domizzi, G. Vigna, S. Bermúdez, J. Ovejero-García, J. Nucl. Mater. 275 (1999) 255.
[9] S. Shimada, E. Etoh, H. Hayashi, Y. Tukuta, J. Nucl. Mater. 327 (2004) 97.
[10] E.W. Brach, Cladding considerations for the transportation and storage of spent fuel, Interim Staff Guidance-11, Revision 3, US NRC, Spent Fuel Project Office, 2003.
[11] J.J. Kearns, J. Nucl. Mater. 22 (1967) 292.
[12] D. Lee, R.B. Adamson, in: A.L. Lowe Jr., G.W. Parry (Eds.), Zirconium in Nuclear Industry, ASTM STP-633, American Society for Testing and Materials, 1977, p. 385.
[13] D. Lee, Trans. ASM 61 (1968) 742.
[14] D. Lee, W.A. Backofen, Trans. Met. Soc. AIME 236 (1966) 1077.
[15] R.C. Kuo et al., EPRI Report, TR-108753-P2, 2000.
[16] J.-H. Huang, S.-P. Huang, J. Nucl. Mater. 208 (1994) 166.
[17] R. Choubey, M.P. Puls, Metall. Mater. Trans. A 25A (1994) 993.
[18] G.E. Dieter, Mechanical Metallurgy, McGraw-Hill Book Company, London, 1988.

ELSEVIER

Journal of Nuclear Materials 248 (1997) 249–256

journal of nuclear materials

Fuel failure and fission gas release in high burnup PWR fuels under RIA conditions

Toyoshi Fuketa *, Hideo Sasajima, Yukihide Mori [1], Kiyomi Ishijima

Department of Reactor Safety Research, Japan Atomic Energy Research Institute, Tokai-mura, Ibaraki-ken 319-11, Japan

Abstract

To study the fuel behavior and to evaluate the fuel enthalpy threshold of fuel rod failure under reactivity initiated accident (RIA) conditions, a series of experiments using pulse irradiation capability of the Nuclear Safety Research Reactor (NSRR) has been performed. During the experiments with 50 MWd/kg U PWR fuel rods (HBO test series; an acronym for high burnup fuels irradiated in Ohi unit 1 reactor), significant cladding failure occurred. The energy deposition level at the instant of the fuel failure in the test is 60 cal/g fuel, and is considerably lower than those expected and pre-evaluated. The result suggests that mechanical interaction between the fuel pellets and the cladding tube with decreased integrity due to hydrogen embrittlement causes fuel failure at the low energy deposition level. After the pulse irradiation, the fuel pellets were found as fragmented debris in the coolant water, and most of these were finely fragmented. This paper describes several key observations in the NSRR experiments, which include cladding failure at the lower enthalpy level, possible post-failure events and large fission gas release. © 1997 Elsevier Science B.V.

1. Introduction

In order to achieve prudent utilization of natural resources and financial advantage with longer refueling cycles, the discharged burnup of commercial power-producing light water reactor (LWR) fuels has been increased in recent years. The burnup limit in Japan has been increased from 39 to 48 MWd/kg U for PWRs and 50 MWd/kg U for BWRs, and further increase of the limit to 55 MWd/kg U is in consideration. As for normal operating conditions, acceptable performance of the fuel has been shown in irradiation programs, operating experiences and analyses. However, extensive investigation for the behavior of the high burnup fuel during off-normal and accident conditions, in particular during reactivity initiated accident (RIA) conditions, is needed. Recent in-pile experiments performed in the Nuclear Safety Research Reactor (NSRR) of the Japan Atomic Energy Research Institute (JAERI) and in the CABRI test reactor of the Institut de Protection et de Sûreté Nucléaire (IPSN) show that the fuel failure may occur at a fuel enthalpy lower than expected.

Current Japanese safety evaluation guideline for reactivity initiated events defines an absolute limit of fuel enthalpy as 963 J/g fuel (230 cal/g fuel) to avoid mechanical forces generation. The guideline also defines an allowable limit of fuel enthalpy for fuel design as 272 to 712 J/g fuel (65 to 170 cal/g fuel), as a function of difference between rod internal and external pressures. When fuel rod internal pressure is lower than external pressure, as is in PWR, the limit is 712 J/g fuel. The guideline was established by the Nuclear Safety Commission of Japan in 1984 based mainly on the results of the NSRR experiments, but all of the NSRR data used were limited to those derived from the experiments with fresh, un-irradiated fuel rods. For this reason, the current guideline adopted the energy deposition at the cladding failure of 356 J/g fuel (85 cal/g fuel) in the SPERT 859 experiment as a provisional failure threshold of pre-irradiated fuel rod; and this failure threshold is used to evaluate the number of failed pre-irradiated fuel rods, and to assess the source term regarding fission gas release in a postulated RIA. For commercial LWR plants to be licensed, the

* Corresponding author. Tel.: +81-29 282 6386; fax: +81-29 282 6160; e-mail: toyo@nsrrsun1.tokai.jaeri.go.jp.

[1] Present address: Nuclear Development Corporation, Tokai-mura, Ibaraki-ken 319-11, Japan.

PII S0022-3115(97)00173-6

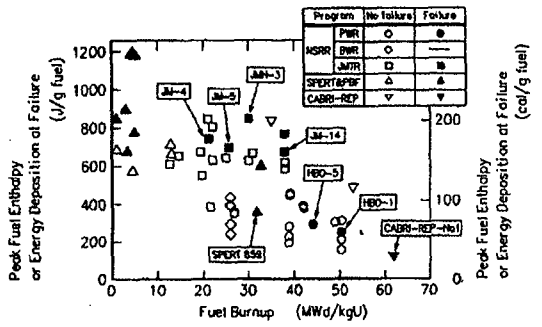

Fig. 1. Peak fuel enthalpy and energy deposition at fuel failure during transients in in-pile RIA experiments as a function of fuel burnup of subjected test fuels. Open symbols denote peak fuel enthalpy in an experiment resulting in no failure, and solid symbols denote energy deposition at failure in an experiment resulting in fuel failure.

safety evaluation must show that the events yield acceptable consequences.

In the HBO-1 test in the NSRR and the CABRI REP-Na 1 experiment an energy deposition appeared at a fuel failure of 250 J/g fuel (60 cal/g fuel) for 50 MWd/kg U PWR fuel and 125 J/g fuel (30 cal/g fuel) for 63 MWd/kg U fuel [1–4]. Fig. 1 summarizes the existing data of peak fuel enthalpy and energy deposition at fuel failure during transients in in-pile RIA experiments as a function of fuel burnup of subjected test fuels. The data points representing the data of the HBO-1 and CABRI REP-Na 1 tests suggest decreased failure threshold in the high burnup region. This paper describes the fuel failure, post-failure events and fission gas release observed in the NSRR experiments. The test fuel rods subjected to the pulse irradiation in the NSRR include segmented fuel rods refabricated from full size fuel rods of commercial power reactors and short fuel rods pre-irradiated in the Japan Materials Testing Reactor (JMTR) of JAERI. Fuel failure as observed in the HBO-1 test was reproduced in the recent HBO-5 test with 44 MWd/kg U PWR fuel. The cladding failure mode in the HBO-5 test is similar to that of the HBO-1 test, and the energy deposition at failure is a little higher in the HBO-5 test. The post-test evaluation and fuel examination for the HBO-5 test are not completed, so it is a little premature to describe the results from the HBO-5 test here.

2. Pulse irradiation in the NSRR

The NSRR is a modified TRIGA-ACPR (annular core pulse reactor) of which salient features are the large pulsing power capability and large (22 cm in diameter) dry irradiation space located in the center of the reactor core which can accommodate a sizable experiment. The shape of the NSRR power history depends on the inserted reactivity, and the smaller pulse becomes broader. While the full width at half maximum in a \$4.6 pulse is 4.4 ms, that in a \$3.0 pulse is 6.9 ms. The capsule used in the pulse irradiation experiment is a double-container system for the irradiated fuel rod test in the NSRR. The inner capsule is a sealed pressure vessel of 72 mm in inner diameter and 680 mm in height. The capsule contains an instrumented test fuel rod with stagnant coolant water at atmospheric pressure and ambient temperature. During a pulse irradiation experiment, cladding surface temperatures at three elevations, coolant water temperature and capsule internal pressure at the bottom of the inner capsule are measured. In some experiments, sensors for axial elongations of pellet stack and cladding tube are also instrumented.

In a series of the irradiated PWR fuel experiments, four different test fuels have been refabricated from full-size commercial reactor fuels, and subjected to the pulse irradiation in the NSRR. Fuel burnup and linear heat generation rate (LHGR) during the base-irradiation (the irradiation in each commercial reactor or the JMTR) are listed in Table 1. Preceding to the extension of PWR fuel burnup limit from 39 to 48 MWd/kg U, the lead use program of high burnup fuel had been performed in the Ohi unit #1 reactor. The HBO test fuel had been irradiated in this program, and the fuel burnup reached 50.4 MWd/kg U. It should be noted that the HBO fuel was not newly designed and manufactured for the high burnup application. The radial distance between the cladding inner surface and fuel pellet (P/C gap) listed in the table is obtained from metallography for arbitrary horizontal cross-section (round slice). As can be seen in this table, the P/C gap of the HBO test fuels is smaller than those of the other test fuels

Table 1
Test fuel rods subjected to the NSRR pulse irradiation experiments

Test fuel ID	Reactor	Initial enrichment (%)	Irradiation cycle	Fuel burnup (MWd/kg U)	LHGR at last cycle (kW/m)	Radial P/C gap (mm)
HBO	Ohi#1	3.2	4	50.4	15.4	< 0.01
OI	Ohi#2	3.2	2	39.2	20.5	0.02
MH	Mihama#2	2.6	4	38.9	19.3	0.02
GK	Genkai#1	3.4	3	42.1	19.8	0.02
JM	JMTR	10	15 to 25	12 to 40	about 25	0.085
JMH	JMTR	20	15 to 25	12 to 40	about 25	0.085

Table 2
Pulse irradiation conditions of irradiated PWR fuel experiments and selected JM and JMH experiments

Test ID	Fuel burnup (MWd/kg U)	Inserted reactivity ($)	Energy deposition (J/g fuel)	Peak fuel enthalpy (J/g fuel)	Remarks
HBO-1	50.4	4.6	390	305	large axial cracking
HBO-2	50.4	3.0	215	157	
HBO-3	50.4	4.6	397	310	
HBO-4	50.4	3.6	279	211	
OI-1	39.2	4.5	571	444	
OI-2	39.2	4.6	581	453	
MH-1	38.9	3.4	262	196	
MH-2	38.9	3.8	301	228	
MH-3	38.9	4.3	363	280	
GK-1	42.1	4.3	505	389	
GK-2	42.1	4.2	490	377	
JM-4	21.2	3.58	986	743	12 small defects
JM-5	25.7	3.37	934	697	23 small defects
JM-14	38	3.59	890	670	large axial cracking
JMH-3	30	3.47	1130	850	large axial cracking

since creep down of the cladding of the HBO test fuels exceeded that of the other test fuels. The information regarding the test fuel pre-irradiated in the JMTR is also listed in Table 1. Because of the limitation of the NSRR pulsing capability and the low residual fissile in the irradiated commercial reactor fuel, the maximum fuel enthalpy in the experiments with the irradiated commercial reactor fuels is restricted to 500 J/g fuel (120 cal/g fuel) or lower. On the other hand, the fuel rods subjected to the pre-irradiation in the JMTR, JM and JMH test fuels, contain the fuel initially enriched to 10% (JM) or 20% (JMH). This relatively high initial enrichment of the JM test fuel realizes the higher fuel enthalpy during the pulse irradiation in the NSRR. The P/C gap of the JM test fuel keeps almost the same value through the pre-irradiation, since the JM test fuel is irradiated in the capsule containing helium gas at atmospheric pressure. The details of the NSRR, the test scheme and the test fuel rods were previously reported in the documents [1,2,5,6]. The pulse-irradiation conditions including the energy deposition and peak fuel enthalpy are listed in Table 2. Because of high burnup and the small number of residual fissile in the HBO fuel, peak fuel enthalpy was restricted to 310 J/g fuel (74 cal/g fuel).

3. Results and discussion

3.1. Cladding failure

A total of forty two experiments, including nineteen commercial LWR fuel tests and twenty JMTR pre-irradiated fuel tests, were performed in the NSRR. Fuel failure occurred in eight of the forty two experiments. Cladding failure modes in these experiments can be categorized in the following manner: (a) vertical cracking over the full length of the fuel active length occurred in high burnup PWR fuel experiments, i.e., the HBO-1 [1,2] and HBO-5 tests; (b) generation of small wall-through defects in the vicinity of the pre-existing local hydride clusters in JM experiments, i.e., JM-4 [5] and JM-5 [6] tests and (c) vertical cracking originating from the local hydride spots observed in JM and JMH experiments, i.e., the JM-14 and JMH-3 tests. Fig. 2 shows the post-test appearance of the fuel rods in the HBO-1, JM-4 and JM-14 tests. The axial crack of the cladding in the HBO-1 test corresponds to the entire region of the fuel stack. The fracture in the experiment is similar to that which occurred by hydride-assisted PCMI (pellet/cladding mechanical interaction) in the SPERT 859 experiment. On the other hand, a number of small defects, twelve in total, were generated in the JM-4 test, and these wall-through defects were distributed over the active region. The long axial crack observed in the JM-14 test propagates through the axially local hydrided spots. Fig. 3 shows horizontal cross-sections in the vicinity of the cracking observed in the HBO-1, JM-4 and JM-14 tests. As for the HBO-1 test, significant hydride deposition below the oxide film in the cladding outer surface and many small cracks vertical to the surface can be seen in the picture. It can be thought that the wall-through crack in the HBO-1 tests originated from one of these crack tips. The crack shows a feature of brittle fracture in the outer region where a number of hydride clusters is deposited. On the other hand, the crack propagates diagonally to a radius in the inner region, and hence shows a typical feature of a ductile fracture. In the JM-4 and JM-14 tests, appearance of the cracks seems similar to that of the HBO-1 test. The cracks show brittle fracture in the outside and ductile in the inside. Although the state of pre-existing hydride deposition is different between the HBO and JM test fuels, as

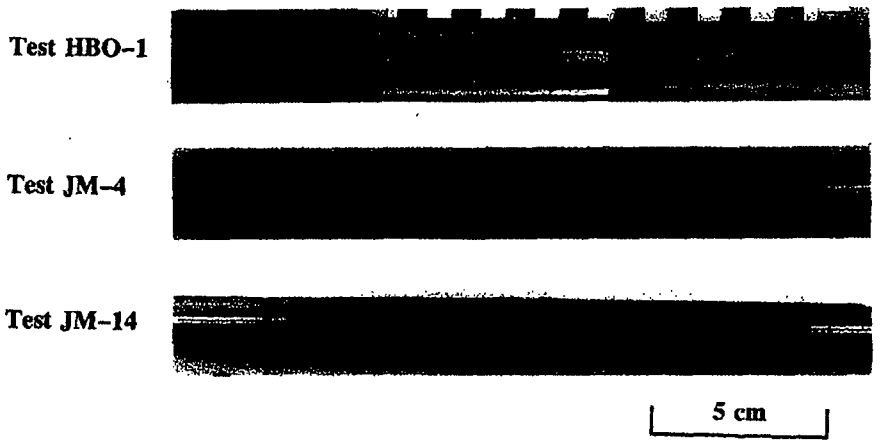

Fig. 2. Post test appearance of the test fuel rods in the tests HBO-1, JM-4 and JM-14. Large axial cracks generated in the tests HBO-1 and JM-14. A number of small wall-through defects appeared in the test JM-4.

shown in Fig. 4, appearance of the cracks suggests strong influence of the pre-existing hydride on the cladding failure in both the HBO and JM experiments. The hydride deposition in the JM test fuels is generated with residual air in the pre-irradiation capsule. In the several experiments, e.g., JM-4 and JM-5 tests, the cracks remain as small wall-through defects since the hydride deposition in the JM test fuel is localized not only radially but also axially and circumferentially. However, in the JM experiment with higher burnup or higher peak fuel enthalpy at pulse, e.g., JM-14 and JMH-3 tests, the crack propagates axially through several hydrided spots, and results in the large opening. Fig. 5 illustrates the interrelations of the elevations where the signals due to local hydride were detected during the eddy current test before the pulse; axial profile of the cladding outer diameter after the pulse; and locations where the wall-through defects were found after the pulse of the JM-4 test. The figure indicates that the occurrence of the cladding failure during the pulse irradiation is strongly influenced by the initially existing cladding hydride, since the location of the cladding defects generated during the pulse irradiation correlates well with the elevation where the signals corresponding to the pre-existing hydride were detected. At the elevation corresponding to the axial center of fuel pellet 'D' in the figure, hydride deposition was detected, and the cladding defect (#8) was

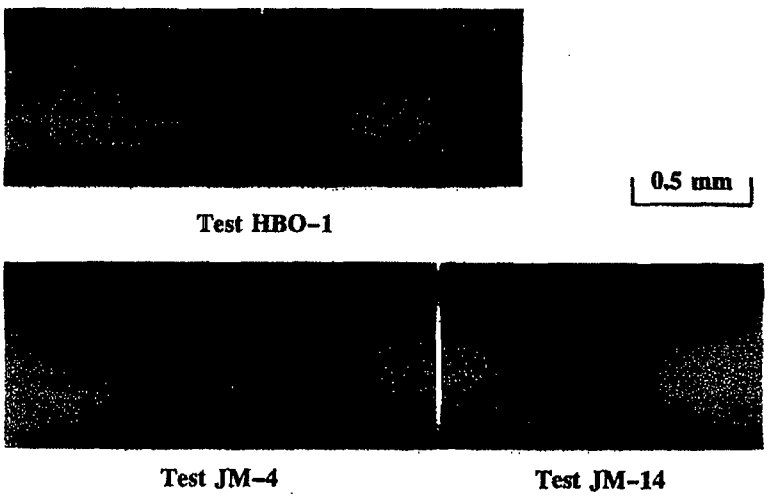

Fig. 3. Horizontal cross-sections in the vicinity of the cracks in the tests HBO-1, JM-4 and JM-14.

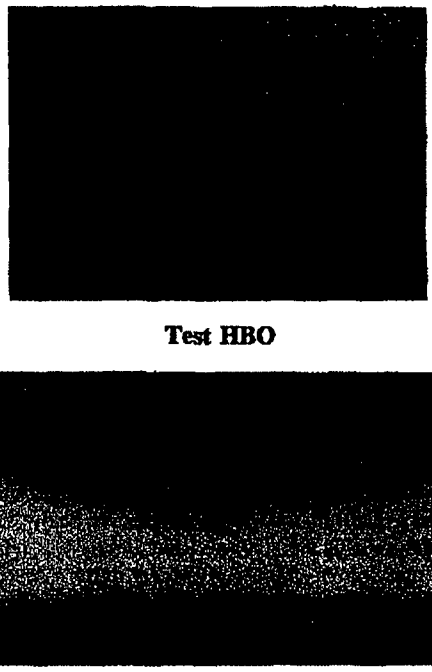

Fig. 4. Pre-existing hydride deposition in the HBO and JM test fuels.

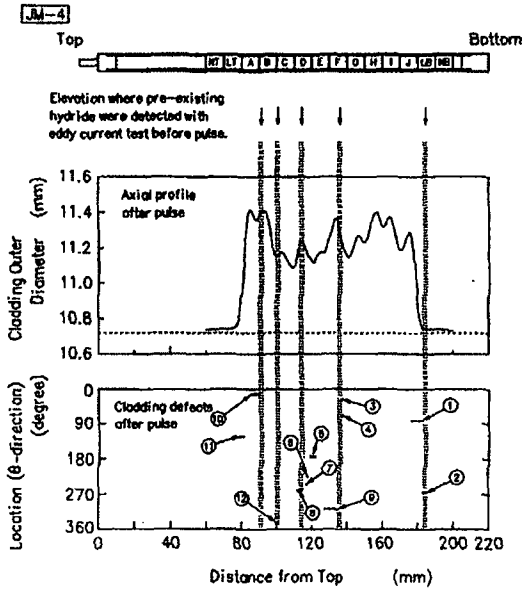

Fig. 5. Interrelations of pre-existing local hydride deposition, post-test cladding outer diameter and cladding defects generated at pulse irradiation in the test JM-4.

generated. At this elevation, the cladding outer diameter is less than 11.3 mm after the pulse. On the other hand, at the elevation of the axial center of pellet 'H' where hydride was not detected, the cladding outer diameter exceeds 11.4 mm, but cladding was not defected during the pulse. These facts indicate that the increase of cladding diameter reaches about 6% due to PCMI with large expansion of the fuel pellets, but the failure does not occur without the existence of the local hydrides.

During the experiments resulting in fuel failure, cladding failure was detected in transient records of capsule internal pressure and/or fuel rod internal pressure as pressure spikes. Transient records of the cladding surface temperature in each experiment show that the temperature remains relatively low at the instant of the cladding failure. As for the HBO-1 test, the cladding surface temperature at failure is about 320 K, and about 370 K in the JM-4 test. The cladding failure of the JM-4 test occurred before departure from nucleate boiling. Occurrence of these cladding failure in the relatively low cladding temperature suggests the failure mode of PCMI in the NSRR experiment.

The cladding failures in the NSRR, CABRI and SPERT programs with irradiated fuels are all believed to be caused by PCMI, assisted by embrittlement of the zircaloy cladding at regions with high local concentrations of hydrides [7]. Quantitative information, however, has not been obtained to define the influence of the hydride precipitation on the embrittlement, and on the cladding failure. Several organizations including JAERI and IPSN have initiated extensive separate-effect tests accordingly, including highly transient burst tests and ring tensile tests with newly developed method. These works will provide correlation between the hydride concentration and distribution, and cladding ductility loss under RIA conditions, including recovery of cladding ductility as a function of time and temperature.

3.2. Post-failure events

Fig. 6 shows transient histories of the capsule internal pressure in the JM-14 test. During the pulse operation, the

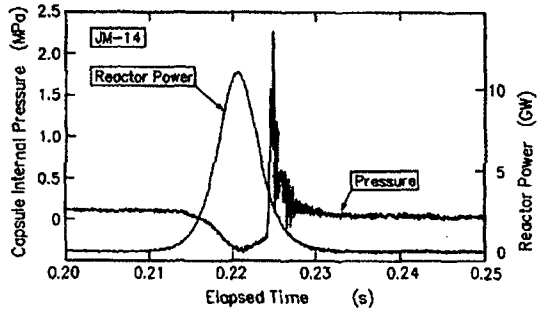

Fig. 6. Transient record of capsule internal pressure during the test JM-14. The pressure spike appeared at cladding failure.

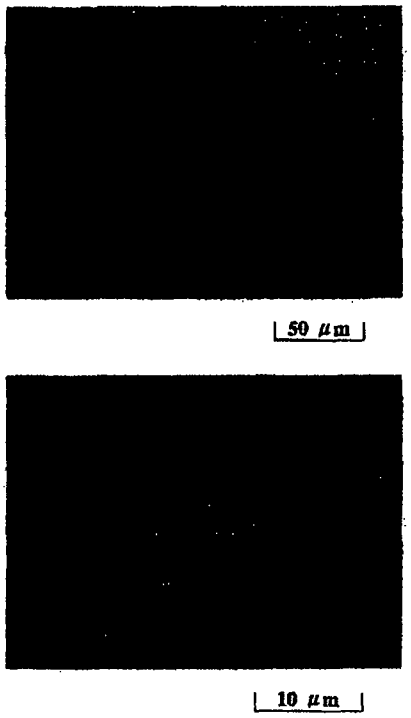

Fig. 7. Cross-sectional view of finely fragmented debris in the test HBO-1.

pressure signal gives a negative value as a noise due to neutron and gamma-ray irradiation. Pressure spikes can be seen in the history, and a peak reaches 2.3 MPa. In the JMH-3 test, the peak pressure of spikes reaches 4.8 MPa at maximum. The pressure spike generation is generally observed in the NSRR experiments resulting in cladding rupture [8]. The cladding failure in the irradiated fuel experiments is generated due to PCMI in the very beginning of the transient when the cladding surface temperature remained low. The pressure spikes caused with cladding rupture and subsequent release of fuel rod plenum gas become large when the cladding temperature remains low at failure.

In the HBO-1 test, all the fuel pellets were dispersed into the capsule water, and were found as fragmented debris [1,2]. Since the collected fuel pellets are finely fragmented, it can be thought that the fuel pellets are expelled from the fractured opening during the pulse. The particle size distribution of the debris shows an occurrence of intensive fragmentation. About 90% of the recovered particles are smaller than 500 μm, and a half or more is smaller than 50 μm. The appearance of the fragmented particles with optical and scanning electron microscopy (SEM) is shown in Fig. 7. During the PIE process, once-molten, spherical particles were not observed.

The predicted fuel temperature of the experiment is about 2600 K at maximum, which is well below the melting point, and hence the fuel pellets of the HBO-1 test have not melted during the experiment. Consequently, the possibility of mechanical energy generation due to violent molten fuel–coolant interaction, or steam explosion, can be neglected. However, fuel fragmentation as observed in the HBO-1 test may become a potential threat concerning fuel coolability, source term, plant contamination, etc. Prompt contact of fuel particles with coolant water may produce high pressure boiling bubbles and cause a pressure surge in PWRs, since the surface area of the finely fragmented fuel particles is considerably large. One of the indications regarding the pressure surge is observed in an NSRR fresh fuel experiment under high pressure and high temperature conditions [9], i.e., test #1206. This experiment was performed with stagnant water coolant at an initial pressure of 7.2 MPa and an initial temperature of 550 K and without gas plenum in the test section. Cladding failed at a relatively low energy deposition, below 800 J/g fuel, and most of the recovered fuel debris was relatively coarse and not once-molten. However, after a sharp pressure spike caused by cladding rupture, a pressure surge, 1.38 MPa increase, was observed in the experiment. In BWRs, such a pressure surge is hardly expected because of pre-existing voids. The pressure surge is not seen in most of the NSRR fresh fuel experiments resulting in vigorous fuel fragmentation, since a free interface exists between the coolant water and capsule plenum gas in the experimental system.

3.3. Fission gas release

Fission gas release to the fuel rod plenum region was destructively measured by rod puncture and gas analysis after the pulse irradiation experiments. The fission gas release during the pulse-irradiation is shown in Fig. 8 as a function of the peak fuel enthalpy. Fission gas release from the HBO fuel during base-irradiation was 0.49%. On the other hand, a significantly large fission gas release oc-

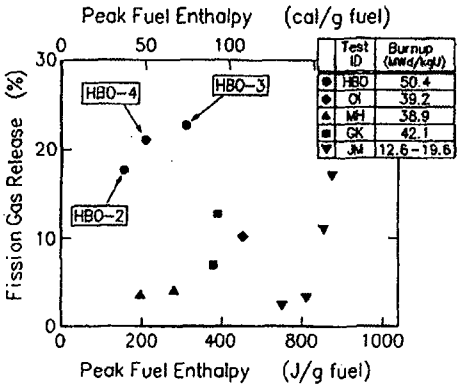

Fig. 8. Fission gas release as a function of peak fuel enthalpy.

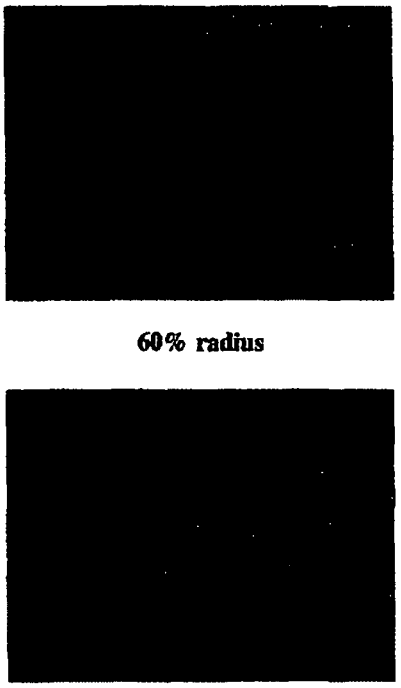

Fig. 9. SEM image of the post-test fuel pellet horizontal cross-section (test JM-4). Grain boundary separation can be seen.

curred in the pulse-irradiation of the HBO-2, -3 and -4 tests [1,2]. The fission gas release is 17.7% even in the HBO-2 test with the peak fuel enthalpy of 157 J/g fuel, and reaches 22.7% in the HBO-3 test. It should be noted that the fission gas release in the HBO-2 test is higher than the release in previous GK-1 experiments with a fuel burnup of 42 MWd/kg U and a peak fuel enthalpy of 389 J/g fuel. The results indicate that the fission gas release during the pulse irradiation depends mostly on the fuel burnup, and the higher fuel burnup correlates with the higher fission gas release.

Grain boundary separation was observed in the JM-4 test, and in the subsequent JM-5 experiment. As can been seen in Fig. 9, a secondary electron image of post-pulse fuel pellets shows the occurrence of significant grain boundary separation in an extensive area. Rapid pressurization of fission gas accumulated in the grain boundaries may cause weakening of the boundaries and subsequent separation, and then result in the expansion of the fuel pellets, fission gas release and fuel fragmentation. The results suggest that, at least, the whole amount of fission gas accumulated in the grain boundary may be released during the pulse irradiation. A preliminary calculation by using FRAPCON-2 code [10] with FASTGRASS module (version of the year 1983) [11] predicts that about 10% of the fission gas accumulates in the inter-granular region of the fuel subjected to the HBO test series. The peripheral 60 μm region of the HBO fuel pellet was characterized as rim region by loss of optically definable grain structure and high concentration of small porosity. The local burnup calculated with RODBURN code [12] reaches 82 MWd/kg U or higher in the rim region where local burnup is enhanced by plutonium production and fissioning. The RODBURN code predicts that about 6% of the fission gas is in the rim region. These preliminary calculations suggest that the total amount of fission gas in inter-granule and in rim regions is less than 16%. The fission gas release measured in the HBO-2, -3 and -4 tests is larger than the predicted value for fission gas in inter-granule and in rim regions. One can hardly expect the release of fission gas, including short-life fission products, from intra-granule during the rapid transient of the NSRR experiment. As stated previously, the calculations currently made are in preliminary stages. The analyses should be upgraded to provide an explanation for the significantly high fission gas release in the HBO experiments.

4. Conclusions

The NSRR experiments suggest possible reduction of failure threshold for high burnup fuels, and indicate that PCMI with expansion of the fuel pellets and decreased cladding integrity lead to the failure. Pre-existing hydride blister in the cladding played important roles in the failure of the rods. Rapid thermal expansion of accumulated fission gas could cause the expansion of fuel pellets and fission gas release, and subsequent fuel fragmentation to extremely small particles. The significantly large fission gas release and the fuel fragmentation producing extremely fine particles indicate that the grain boundary separation occurred almost instantaneously during the transients.

Acknowledgements

The authors would like to acknowledge and express their appreciation for the time and effort devoted by numerous engineers and technicians in the Reactivity Accident Research Laboratory, NSRR Operation Division, Department of Hot Laboratories and Department of JMTR Project, JAERI. They also acknowledge the support and help of individuals and other organizations too numerous to cite, whose contributions were critical to the success of the program. The tests HBO-1 through HBO-4 have been performed as a collaboration program between JAERI and Mitsubishi Heavy Industries, ltd. by using fuel rods transferred from Kansai Electric Power Company.

References

[1] T. Fuketa, K. Ishijima, Y. Mori, H. Sasajima, T. Fujishiro, Proc. 23rd Water Reactor Safety Information Meeting, Bethesda, MD, Oct. 23–25, 1995, NUREG/CP-0149, Vol. 1 (USNRC, 1996) p. 45.

[2] T. Fuketa, Y. Mori, H. Sasajima, K. Ishijima, T. Fujishiro, Behavior of High Burnup PWR Fuel Under a Simulated RIA Condition in the NSRR, Proc. CSNI Specialist Meeting on Transient Behavior of High Burnup Fuel, Cadarache, France, Sept. 12–14, 1995, NEA/CSNI/R(95)22 (OECD/NEA 1996) p. 59.

[3] F. Schmitz, J. Papin, M. Haessler, J.C. Nervi, P. Permezel, Investigation of the Behavior of High Burn-up PWR Fuel Under RIA Conditions in the CABRI Test Reactor, 22nd Water Reactor Safety Information Meeting, Bethesda, MD, Oct. 24–26, 1994.

[4] F. Schmitz, J. Papin, M. Haessler, N. Waeckel, Proc. 23rd Water Reactor Safety Information Meeting, Bethesda, MD, Oct. 23–25, 1995, NUREG/CP-0149, Vol.1 (USNRC 1996) p. 33.

[5] T. Fuketa, Y. Mori, H. Sasajima, K. Homma, S. Tanzawa, K. Ishijima, S. Kobayashi, T. Kikuchi, H. Sakai, Behavior of Pre-irradiated Fuel Under a Simulated RIA Condition [Results of NSRR Test JM-4], JAERI-Research 95-013, Japan Atomic Energy Research Institute, 1995.

[6] T. Fuketa, H. Sasajima, Y. Mori, K. Homma, S. Tanzawa, K. Ishijima, S. Kobayashi, T. Kamata, H. Sakai, Behavior of Pre-irradiated Fuel Under a Simulated RIA Condition [Results of NSRR Test JM-5], JAERI-Research 95-078, Japan Atomic Energy Research Institute, 1995.

[7] Ad hoc Group of the Principal Working Group on Coolant System Behavior (PWG-2), Transient Behavior of High Burnup Fuel, NEA/CSNI/R(96)23 (OECD/NEA 1996).

[8] T. Fuketa, T. Fujishiro, Nucl. Eng. Des. 146 (1994) 181.

[9] Reactivity Accident Research Laboratory and NSRR Operation Division, Annual Progress Report on the NSRR Experiment (15) (Jan. 1983 through Dec. 1983), Japan Atomic Energy Research Institute, 1984, p. 109 (in Japanese).

[10] G.A. Berna, M.P. Bohn, W.N. Rausch, R.E. Williford, D.D. Lanning, FRAPCON-2: A Computer Code for the Calculation of Steady State Thermal-Mechanical Behavior of Oxide Fuel Rods, NUREG/CR-1845 R3, 1981.

[11] J. Rest, Nucl. Technol. 61 (1983) 33.

[12] M. Uchida, H. Sato, RODBURN: A Code for Calculating Power Distribution in Fuel Rods, JAERI-M 93-108, Japan Atomic Energy Research Institute, 1993 (in Japanese).

ıand M. Garde[1]

ffects of Irradiation and Hydriding n the Mechanical Properties of ircaloy-4 at High Fluence

REFERENCE: Garde, A. M., **"Effects of Irradiation and Hydriding on the Mechanical Properties of Zircaloy-4 at High Fluence,"** *Zirconium in the Nuclear Industry: Eighth International Symposium, ASTM STP 1023,* L. F. P. Van Swam and C. M. Eucken, Eds., American Society for Testing and Materials, Philadelphia, 1989, pp. 548–569.

ABSTRACT: Tension and burst tests were conducted on irradiated Zircaloy-4 charged with hydrogen. The investigated ranges of experimental variables were deformation temperatures, 298 to 673 K; fluence levels, 7 to 12 × 10^{21} n/cm², $E > 0.821$ MeV; and hydrogen concentrations, 50 to 400 ppm. The data show a significant reduction in the elongation compared to the properties of Zircaloy-4 with lower levels of fluence and hydrogen concentration. Although the overall elongations of the specimens were low, the fracture surface examination showed evidence of ductility in the material and localized deformation bands were observed on the specimens deformed at higher temperatures. The inhomogeneous deformation bands, observed predominantly for deformation temperatures between 573 to 673 K, are consistent with the literature evidence of dislocation channeling in highly irradiated Zircaloy. Radiation anneal hardening was observed at the temperature interval of 573 to 623 K. Since the orientations of both the habit plane of hydrides in Zircaloy and the dislocation channels formed during deformation at ~600 K are close to the basal plane, hydrides appear to initiate fracture in the dislocation channels in highly irradiated Zircaloy containing quantities of hydrogen above the solubility limit. A failure mechanism involving hydride initiated fracture in dislocation channels is suggested for irradiated Zircaloy deformed at ~600 K. Mechanical property data on irradiated Zircaloy in recent literature appear to be consistent with the proposed failure mechanism. An alloy development program is suggested to enhance the ductility of highly irradiated Zircaloys.

KEY WORDS: Zircaloys, high fluence, mechanical properties, low ductility, hydrides, hydrogen uptake, dislocation channeling, radiation anneal hardening, niobium addition

n order to improve uranium utilization and reduce fuel cycle costs, a continuing U.S. lear industry objective has been to increase the discharge burnup of light water reactor VR) fuel. At the same time, the thermal efficiency of the newer LWR plants has been eased by utilizing higher coolant temperatures. To maintain a high reliability of these ended burnup fuels, it is necessary to evaluate the effects of longer in-reactor residence es under more demanding conditions on the properties of Zircaloy cladding and structural nponents. The important Zircaloy properties in this regard are in-reactor corrosion reance, as-irradiated mechanical properties, and irradiation growth. This paper deals with evaluation of the mechanical properties of highly irradiated Zircaloy-4.

Consulting engineer, Nuclear Fuel Product Development, Combustion Engineering, 1000 Prospect Rd., Windsor, CT 06095.

It is well known that the addition of hydrogen reduces the ductility of unirradiated Zircaloy. The extent of ductility reduction depends on the level of hydrogen concentration with respect to the solubility limit, the orientation of hydrides with respect to the direction of mechanical loading and the deformation temperature. The fabrication process, and thereby the texture of nuclear fuel cladding, is such that the majority of hydrides precipitate in the circumferential orientation in the tube cross section, and therefore, these hydrides are not significantly detrimental in the tube internal pressure loading mode. In a recent investigation [*1*], mechanical properties of hydrogen-charged fuel cladding were compared to the properties of as-received Zircaloy-4 with 15-ppm hydrogen. The addition of 700-ppm hydrogen had no effect on the uniform elongation but resulted in a 32% reduction of total elongation (from 19.9 to 13.6%) during tensile deformation at 616 K. Thus the presence of hydrides decreased the extent of localized (necking) deformation but did not affect the uniform (homogeneous) deformation. The fracture mode after the addition of 700 ppm hydrogen was completely ductile. In another investigation [*2*], Zircaloy-2 sheet specimens were charged with up to 615-ppm hydrogen and fractured at room temperature. Fractographic examination of these specimens showed that the fracture mode was ductile in all cases and consisted of void nucleation at the hydrides caused by fracturing of hydrides followed by void coalescence.

The major source of hydrogen for the fuel cladding is the waterside corrosion reaction occurring on the external surface of the cladding tube. There are conflicting indications in the literature regarding the extent of hydrogen uptake by Zircaloy at extended burnups (when the oxide layers are thick). On the basis of pressurized water reactor (PWR) data published by Kraftwerk Union (KWU) [*3*], the hydrogen uptake is shown to increase with increasing oxide thickness. On the other hand, the Oconee-1 data [*1*] seem to show a decreasing hydrogen uptake with increasing oxide thickness. One of the objectives of the current investigation is to evaluate the extent of hydrogen uptake by Zircaloy-4 at extended burnups.

Exposure to neutrons generates defects and results in damage to the Zircaloy microstructure. These effects also reduce the ductility of Zircaloy. Morize et al. [*4*] irradiated a capsule containing sodium potassium alloy (NaK) so that hydrogen uptake did not accompany the irradiation damage. For fluence levels up to 12 × 10^{21} n/cm², $E > 0.821$ MeV, there was a 60 to 85% loss of elongation during deformation at 293 K (compared to the properties of unirradiated Zircaloy-4) and a 20 to 60% loss of elongation at 588 K. Although the irradiated material had lower ductility than the unirradiated material, the failure mode still appeared to be ductile.

In a nuclear power reactor environment, hydrogen uptake and microstructural damage caused by neutron exposure are occurring simultaneously. Moreover, the hydrogen uptake may be accelerating at high burnups because of enhanced oxidation rates at high burnups [*3,5–7*]. The rate enhancement may be due to the thermal insulating effect of thick oxides. Mechanical property data from highly irradiated cladding from a commercial PWR would be useful to examine the synergistic effect, if any, of hydrogen uptake and neutron fluence on Zircaloy-4 ductility. Such data are essential to insure adequate performance of cladding at reactor operating conditions and safe handling of the discharged fuel assemblies. Mechanical property data of highly irradiated Zircaloy-4 have been collected by Combustion Engineering (C-E) in two programs and are discussed in this paper.

Under the joint sponsorship of the U.S. Department of Energy (DOE) and the C-E Utility Owners Group (CEOG), tube burst and axial tension tests were conducted [*8,9*] on four-, five- and six-cycle fuel rod cladding (Fluence range: 7 to 12 × 10^{21} n/cm², $E > 0.821$ MeV) irradiated in the Fort Calhoun Reactor operated by the Omaha Public Power District. Under the sponsorship of Electric Power Research Institute (EPRI, EPRI/C-E Fuel Performance

nducted on the guide tube material from a four-cycle assembly (fluence: 9×10^{21} n/cm², > 0.821 MeV) irradiated in the Calvert Cliffs Unit 1 Reactor operated by the Baltimore as and Electric Company. The coolant inlet and outlet temperatures for both of these WRs are 557 and 585 K, respectively. The results of these two investigations are presented id analyzed in this paper.

xperimental Procedure

Mechanical tests were conducted on irradiated Zircaloy-4. The cladding and guide tube aterial chemistry was consistent with ASTM Alloy Designation UNS R60804. The initial drogen concentration was typically less than 15 ppm. The fuel cladding was in a cold-orked and stress-relief-annealed condition, while the guide tubes were in a recrystallized-nealed condition. The textures of the fuel cladding and guide tube materials were similar. ie basal pole density distribution was concentrated in the plane containing the tube radii id tangent, with the density peaks at ±30° from the radial direction towards the tangential rection. Fuel assemblies were irradiated in the Fort Calhoun and Calvert Cliffs Unit 1 WRs. Fuel rods were examined nondestructively at the reactor poolside and destructively the Battelle Columbus Laboratories (BCL) hot cells [*8–9*]. In addition, the support ucture of a four-cycle assembly was examined in the same hot cell. This structure, referred as a "cage," consisted of grids welded to the guide tubes. As part of both of these vestigations, mechanical property tests were conducted on irradiated Zircaloy-4 specimens. etallographic examinations were conducted to determine hydride orientation in irradiated rcaloy-4. Hydrogen concentrations were either measured by an inert-gas-fusion technique estimated by comparison of the photomicrographs with visual standards. Fracture surfaces the irradiated guide tube specimens were examined by scanning electron microscope EM) for the ductile/brittle fracture mode features.

Cladding burst tests were performed at 588 K at a strain rate of 0.004 cm/cm · min. The nstant strain rate was achieved by controlling the rate of volume expansion by the feedback pressure and volume signals. The burst specimens were internally pressurized with a icone oil. A three-zone furnace was used to heat the specimen. A simulator tube with ermocouples spot welded over its length was used to adjust the furnace power inputs to ain a uniform temperature distribution along the length of the tube. The same procedure is subsequently used for the irradiated tubes. Burst specimens (length 20 cm) were tested thout defueling after confirming oil accessibility to the entire gage length with the fuel in ace. A system expansion curve (pressure versus volume) was generated for the specific lume expansion rate and temperature parameters using a heavy walled, nondeforming ecimen of approximately the same internal void volume as the test specimen. An expansion rve for the irradiated specimen was derived from the experimentally measured curve by btracting the system expansion. The burst fracture region was photographed, and the gion of maximum strain was sectioned and mounted as a transverse metallographic section determine the failure strain. The uniform plastic diametral strain was calculated using methodology described in Ref *10*. The failure stress was calculated using the formula a thin-walled cylinder and tube cross section excluding the oxide layer. The tube inside ameter was used to calculate the stress.

Cladding tension specimens with a total length of 12.5 cm were defueled. Grip support igs (length 3.8 cm) of snug fit were inserted at each end of the tube for the tension test. ie specimens were tested at room temperature, 473, 573, and 673 K. The specimen gage igth was 5 cm, and up to the maximum load point the specimen elongation was measured the extensometer separation. The testing machine crosshead speed was 0.0126 cm/min the initial 0.2% strain. The remaining

of 0.126 cm/min. Load elongation data were recorded on a strip chart. For stress calculations, the cross-sectional area without the oxide layer was used. The uniform elongation is the plastic strain associated with the maximum load point. The total elongation was measured from the combined length within the gage marks of the two fractured specimen pieces. Reduction in area was calculated from the micrometer measured values of the pre-test and post-test cross-sectional areas after subtracting the area covered by the oxide layer.

Dogbone tension specimens (covering part of the circumference of the guide tube and a gage length of 2.5 cm) and ring tension specimens (width 1.26 cm) were machined from guide tube sections from different axial locations of the irradiated cage. Tension tests were conducted using an Instron testing machine with a furnace. For the dogbone specimens, the same crosshead speeds were used as employed for cladding tension specimens. The ring tests were conducted at a constant crosshead velocity of 0.126 cm/min.

Results

Cladding Burst Properties

Cladding burst properties were measured at 588 K. The burst properties of irradiated Zircaloy-4 specimens taken from different axial locations of six-cycle fuel rods are given in Table 1. In two cases, hydrogen concentrations measured from tube pieces adjacent to the burst specimens are also given in Table 1. The hydrogen concentration values were a function of the axial elevation, being higher at the higher elevations. For all the remaining specimens in Table 1, the hydrogen concentrations are expected to be between 200 and 400 ppm. Compared to the mechanical properties of unirradiated cladding, the six-cycle cladding shows significant increase in the burst hoop stress and a significant decrease in the values of circumferential strain. Since the uniform strain values were less than 0.1%, 0.2% offset yield stress values could not be calculated. The total strain values are also low, ranging between 1 to 4%. It is estimated that at this low level of measured strain, the accuracy of the metallographic technique used to measure the strain is of the same order as the measured absolute values.

An examination of the fracture regions revealed that out of the eight burst specimens, six showed very narrow openings (maximum width less than 2 mm) that extended axially along the rod for a length (range 2 to 15 cm) equivalent to several uranium dioxide (UO_2) pellet lengths. For the specimen from Rod KJE051 (axial elevation 2.62 to 2.82 m from the rod bottom), the burst opening extended axially for approximately 14 pellet lengths (Fig. 1). The narrowness of the burst opening was consistent with the observed irradiation hardening and measured hydrogen level of the cladding material. The axial extension of the burst opening was consistent with the low value of retained ductility. Only two out of eight burst specimens exhibited a relatively broad burst opening (maximum width greater than 4 mm) showing a slight increase in cladding outside diameter at the burst location.

The burst properties of the six-cycle cladding can be compared to those of four- and five-cycle cladding irradiated in the same reactor (Table 2). The cladding hydrogen concentration for the four- and five-cycle rods was not measured. Instead it was estimated by comparison of the photomicrographs showing hydrides with visual standards [*11*]. Accordingly, the cladding hydrogen concentrations for the axial elevations noted in Table 2 for the four-cycle rod KKM098 and five-cycle rod KJE076 were estimated [*8*] to be ~100 and ~150 to 200 ppm, respectively. A comparison of the strain values listed in Tables 1 and 2 shows that at fluence values $<10^{22}$ n/cm² ($E > 0.821$ MeV) the uniform strain values were >1% and total strain values were >4%. For fluence levels $>10^{22}$ n/cm² ($E > 0.821$ MeV), there appears to be a significant reduction in

TABLE 1—*Burst properties of cladding irradiated in Fort Calhoun for six cycles and tested at 588 K (600 F).*

Rod Number	Local Hydrogen Concentration, ppm	Burst Specimen Location, m (in.)[a]	Local Burnup, GWd/MTU	Rod Average[b] Fluence, n/cm^2, $E > 0.821$ MeV	Ultimate[c,d] Hoop Stress, MPa (ksi)	Plastic Circumferential Strain, %	
						Uniform[d]	Total
KJD075	...	2.24 to 2.44 (88 to 96)	58.8 avg	11.6×10^{21}	843 (122)	0.10	2.70
KJD075	...	2.62 to 2.82 (103 to 111)	57.2 avg	11.6	823 (119)	0.10	1.20
KJE051	...	1.91 to 2.11 (75 to 83)	61.7–62.5	11.7	865 (126)	0.10	4.20
KJE051	330	2.62 to 2.82 (103 to 111)	61.7 avg	11.7	828 (120)	0.05	'
KJE089	...	1.78 to 1.98 (70 to 78)	59.5 avg	11.6	815 (118)	0.05	1.50
KJE089	400	2.62 to 2.82 (103 to 111)	54.7–59.5	11.6	793 (115)	0.05	2.15
KJD008	...	1.35 to 1.55 (53 to 61)	56.1 avg	11.2	848 (123)	0.10	4.05
KJD008	...	2.62 to 2.82 (103 to 111)	56.1 avg	11.2	704 (102)	0.05[f]	1.85[f]
Unirradiated	15	...	0	0	414 to 483 (60 to 70) nominal	...	15.00 to 20.00 nominal

[a] Measured from bottom of rod.
[b] Fluence normalized for total rod length.
[c] Wall thickness corrected for metal loss caused by in-reactor corrosion.
[d] Calculated from the maximum pressure value.
[e] Measurement unattainable because a piece was missing from the metallographic mount of the burst cross section.
[f] Data questionable because the specimen fractured at the bottom end fitting.

FIG. 1—*Burst opening region of specimen from Rod KJE051, 2.62 to 2.82 m (103 to 111 in.) from the rod bottom.*

Cladding Tube Tensile Properties

The measured tensile properties of the six-cycle fuel cladding are presented in Table 3. The hydrogen concentration and fluence levels in these specimens are estimated to be between 300 to 400 ppm and approximately 11.7×10^{21} n/cm², $E > 0.821$ MeV, respectively. At room temperature (298 K), the cladding exhibited limited ductility, uniform strain of 0.15%, and total strain of 1.1%. Consistent with the high values of the yield stress (YS) and ultimate tensile strength (UTS) at room temperature, the specimen fractured at room temperature did not show any evidence of necking near the fracture surfaces, and the fracture surfaces were perpendicular to the loading axis. As the deformation temperature was increased, the cladding ductility increased and regions of the specimen adjacent to the fracture

TABLE 2—*Burst properties of cladding irradiated in Fort Calhoun for four and five cycles and tested at 588 K (600°F).*

Rod Number	Burst Specimen Location, m (in.)[a]	Local Burnup, GWd/MTU	Rod Average[b] Fluence, n/cm^2, $E > 0.821$ MeV	Hoop Stress,[c] MPa(ksi)		Plastic Circumferential Strain, %	
				0.2% Yield	Ultimate[d]	Uniform[d]	Total
KKM098	1.91 to 2.11 (75 to 83)	41.6	6.9×10^{21}	775 (112)	811 (118)	1.1	6.9
KKM098	2.40 to 2.60 (94 to 102)	41.6	6.9	747 (108)	796 (116)	1.2	5.6
KJE076	1.91 to 2.11 (75 to 83)	53.2	9.1	676 (98)	823 (119)	1.8	4.5
KJE076	2.35 to 2.55 (93 to 101)	52.3	9.1	770 (112)	816 (118)	1.4	4.7

[a] Measured from bottom of rod.
[b] Fluence normalized for total rod length.
[c] Wall thickness corrected for metal loss caused by in-reactor corrosion at the burst location.
[d] Calculated from the maximum pressure point on the $P - \Delta V$ curve for the specimen.

TABLE 3—*Tensile properties of cladding irradiated for six cycles in Fort Calhoun.*

Rod Number	Section Elevation, Measured From Rod Bottom, m (in.)	Local Burnup, GWd/MTU	Test Temperature, K (F)	Yield Stress,[a] MPa (ksi)	UTS,[a] MPa (ksi)	Uniform Plastic Elongation,[b] %	Total Plastic Elongation,[c] %	Reduction in Area,[d] %
KJE089	2.39 to 2.51 (94 to 99)	59.0	298 (77)	879 (127)[e]	879 (127)[e]	0.15	1.1	~1.0
KJD008	2.29 to 2.41 (90 to 95)	57.6	473 (392)	661 (96)	811 (118)	0.70	5.2	>8.7
KJD015	2.41 to 2.54 (95 to 100)	57.6	573 (572)	677 (98)	763 (111)	0.80	9.1	>14.8
KJE051	2.39 to 2.51 (94 to 99)	63.3	673 (752)	519 (75)	636 (92)	0.75	6.2	>15.3
...	...	unirradiated	298 (77)	448 to 517 (65 to 75) nominal	620 to 689 (90 to 100) nominal	...	20.0 to 30.0 nominal	...
...	...	unirradiated	673 (752)	241 to 310 (35 to 45) nominal	354 to 414 (50 to 60) nominal	...	27.0 to 37.0 nominal	...

[a] Stress calculations based on the undeformed specimen area corrected for oxide layer.
[b] Based on the plastic extension at the maximum load and the extensometer gage length of 5 cm.
[c] Based on the combined length within gage marks of two fractured pieces of specimen and the length of unsupported region of the undeformed specimen.
[d] Estimated from the measurement of external diameter at fracture and assuming no wall thickness reduction. Since some wall thickness reduction did occur, the actual reduction in area will be greater than the estimated values.
[e] Maximum load occurred at a plastic strain of 0.15%, therefore both the yield stress and ultimate tensile strength were calculated from the load at 0.15% plastic strain.

area showed increasing evidence of necking. The fracture surfaces of the specimen deformed at 473 K were also perpendicular to the tensile axis. At the deformation temperatures of 573 and 673 K, inhomogeneous deformation bands were observed on the specimen surface at ~45° to the tube axis, and fracture occurred in one of the deformation bands.

Mechanical Properties of Guide Tube Material

The measured mechanical properties of the guide tube material are given in Table 4. Considering the texture of the as-fabricated guide tube material, basal poles were predominantly perpendicular to the tensile axis in the longitudinal (dogbone) specimen, which was not the case for the transverse ring specimens. At room temperature, the ring specimen showed higher strength and lower elongations than the dogbone specimen. The 573 K, strength and elongations for the dogbone and ring tension tests were similar. With increasing deformation temperature, the material ductility increased. All the fractured guide tube specimens (both the dogbone and ring specimens) showed deformation bands. An example is shown in Fig. 2. In addition, the dogbone specimen deformed at 673 K showed an extended neck spreading over about 7 mm of the specimen gage length. All specimens except the 673 K specimen had the fracture surface inclined at ~45° to the tensile axis.

Fracture surfaces of all the guide tube specimens were examined by SEM and showed evidence of predominantly ductile failure in every case. The fracture surfaces were covered with dimples; a typical example is shown in Fig. 3. The fracture surface appearance showed that although the absolute values of elongations for these guide tube specimens were low (<4% for deformation temperatures <623 K), the fracture mode was ductile.

Summary of Results

The temperature dependence of ductility of irradiated Zircaloy with different levels of fluence and hydrogen concentration is compared in Fig. 4. The low fluence, low hydrogen level curve is from Refs *12* and *13*. With increasing fluence and hydrogen uptake, the ductility of Zircaloy-4 is suppressed to higher deformation temperatures. Although the ductility (reduction in area) for highly irradiated Zircaloy (fluence $>9.0 \times 10^{21}$ n/cm^2, $E > 0.821$ MeV) is low for deformation temperatures lower than 623 K, the fracture mechanism for the two temperature regions, ~573 to 623 K, and temperatures less than 500 K, appears to be different. For deformation temperatures less than ~500 K, failure is associated with a limiting normal stress for homogeneous deformation, and fracture surfaces are perpendicular to the tensile axis. For the deformation temperature interval of 573 to 623 K, failure is associated with a localized shear (inhomogeneous deformation) band, and fracture surfaces are ~45° to the tensile axis.

The temperature dependence of the yield stress and ultimate tensile strength of irradiated Zircaloy-4 is shown in Fig. 5. Both the yield stress and ultimate tensile strength (UTS) generally decrease with increasing temperature. However, in the temperature interval 573 to 623 K, some strengthening is observed for both the cladding and guide tube materials, and this observation is an indication of radiation anneal hardening. The variation of uniform and total strain of irradiated Zircaloy-4 as a function of deformation temperature is shown in Fig. 6. Both the uniform and total strain of irradiated guide tube material show a ductility minimum at 573 K. This is probably another manifestation of radiation anneal hardening. Elongation minima are not apparent in the cladding data in Fig. 6. This may be due to some slip in the grips noted during the loading of 573 K cladding specimen and fewer data points. The fluence dependence of the uniform and total strain of irradiated Zircaloy-4 deformed

TABLE 4—*Guide-tube[a] tension test results.*

Temperature, K (°F)	Dogbone[b] (Longitudinal) Properties					Ring[c] (Transverse) Properties				
	Ultimate Tensile Strength, UTS, MPa (ksi)	0.2% Yield Strength, MPa (ksi)	Uniform Elongation, %	Total Elongation, %	Reduction in Area, %	Ultimate Tensile Strength, UTS, MPa (ksi)	0.2% Yield Strength, MPa (ksi)	Uniform Elongation, %	Total Elongation, %	Reduction in Area, %
298 (77)[d]	827 (120)	786 (114)	1.8	4.2	5.6	835 (121)	807 (117)	0.9	1.8	9.7
373 (212)	772 (112)	724 (105)	2.0	3.5	2.8	...	...	...	...	...
473 (392)	670 (97)	648 (94)	2.0	4.3	4.6	...	...	...	...	...
573 (572)	591 (86)	587 (85)	0.6	3.3	6.9	586 (85)	581 (84)	0.7	2.7	11.9
623 (662)	601 (87)	568 (82)	1.3	4.1	3.7	...	...	...	...	...
673 (752)	521 (76)	466 (68)	1.6	12.9	32.2	...	...	...	...	...

[a] Neutron fluence $9.0 \pm 0.2 \times 10^{21}$ n/cm^2 ($E > 0.821$ MeV); hydrogen concentration 50 to 60 ppm.
[b] Specimen gage length 2.5 cm; crosshead velocity 0.0125 cm/min past the yield point, then 0.125 cm/min to fracture.
[c] Constant crosshead velocity 0.125 cm/min to fracture.
[d] Nominal room temperature properties of Longitudinal unirradiated Zircaloy-4 material used to fabricate the guide tubes: UTS, 500 to 520 MPa (73 to 77 ksi); yield strength, 300 to 350 MPa (48 to 53 ksi); total elongation, 26 to 30%.

FIG. 2—*Visual appearance of a guide tube dogbone specimen fractured at 623 K (662°F).*

in the temperature interval of 573 to 588 K is shown in Fig. 7. It appears that for fluence values $>10^{22}$ n/cm^2 ($E > 0.821$ MeV), the uniform and total strains of irradiated Zircaloy-4 are below 1 and 4%, respectively.

The hydrogen uptake of Zircaloy-4 cladding as a function of oxide thickness for cladding exposed in PWRs is shown in Fig. 8. The three lines shown in this figure represent hydrogen uptake fraction values (that is, fractional amount of hydrogen absorbed by the cladding in relation to the hydrogen amount generated by the waterside corrosion of Zircaloy-4 cladding)

FIG. 3—*SEM fractograph of a guide tube ring specimen fractured at 298 K (77°F).*

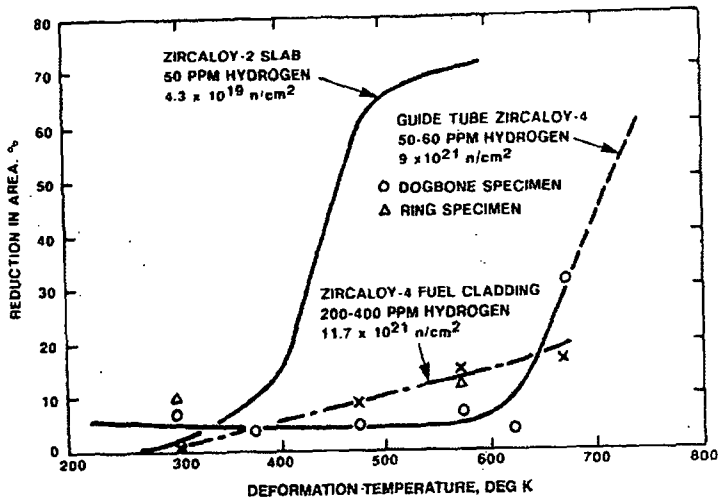

FIG. 4—*Reduction in area for fractured specimens as a function of deformation temperature.*

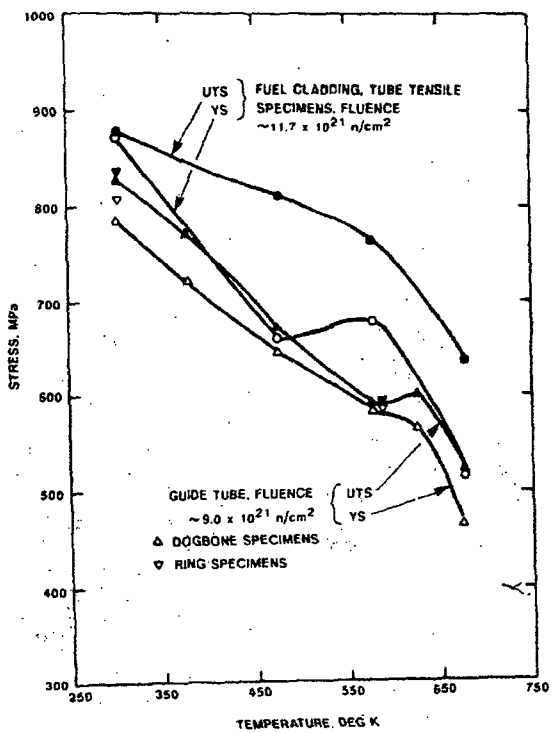

IG. 5—*Temperature dependence of the yield stress and ultimate tensile strength of irradiated aloy-4.*

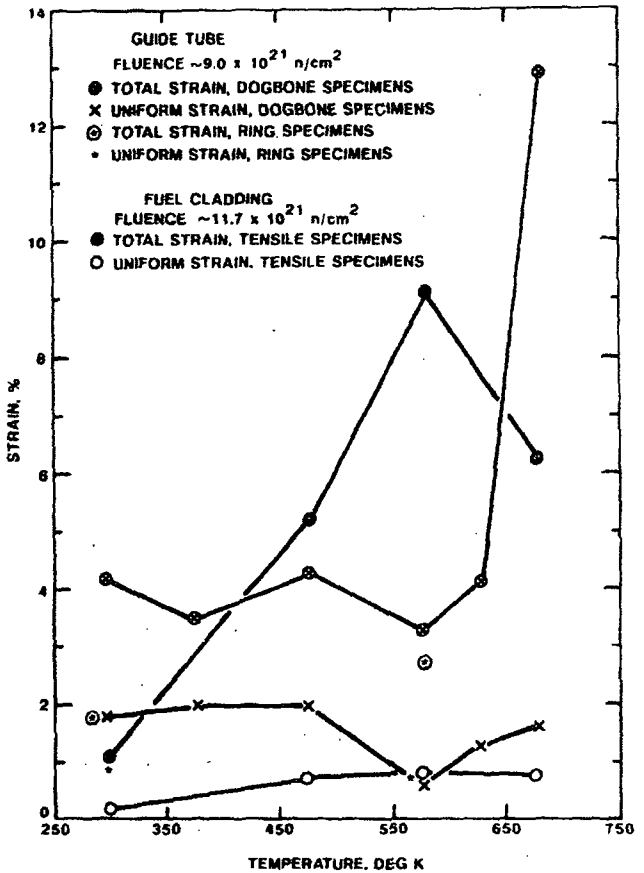

FIG. 6—*Temperature dependence of uniform and total strain of irradiated Zircaloy-4.*

of 1%, 18%, and 100%. For comparison, data obtained in the current program are plotted with data from KWU [3], Oconee-1 [1], Saxton [14,15], and Zion [16,17]. It appears that a pickup fraction of 18% provides a reasonable upperbound for the high burnup data, and the pickup fraction for the upperbound appears to be independent of the oxide thickness.

Discussion

Radiation Anneal Hardening (RAH) At 573 to 623 K

The evidence of radiation anneal hardening at ~600 K observed in the current investigation (Figs. 5 and 6) is consistent with literature data [10,18–20]. The effect is believed to be due to the interaction of oxygen interstitial atoms with either dislocations or irradiation induced defects or both [21]. The interaction may involve formation of interstitial atom-defect complexes. The interaction may take the form of radiation induced precipitation [22]. In unirradiated Zircaloy-2 [23] and Zircaloy-4 [24], the presence of yield point phenomenon, yield-

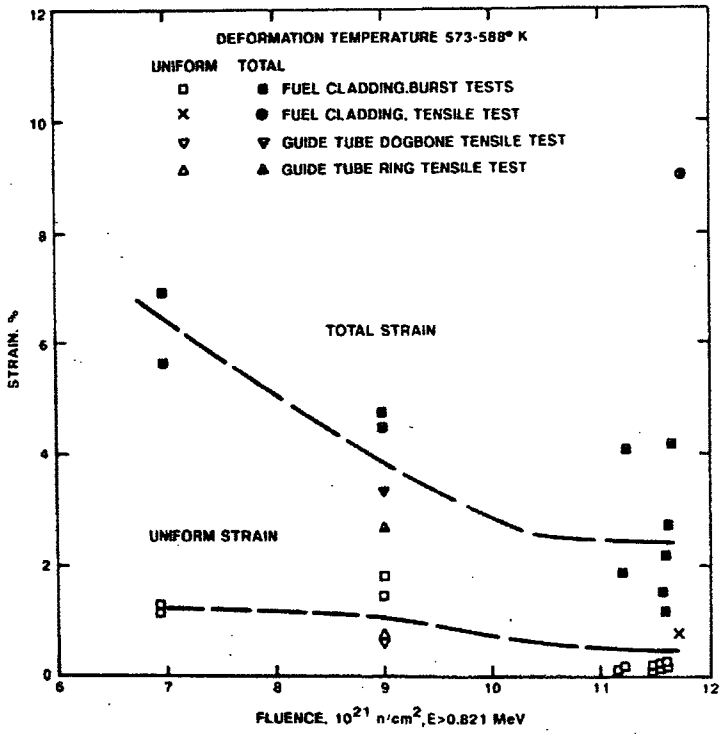

FIG. 7—*Fluence dependence of uniform and total strain of Zircaloy-4 deformed in the temperature interval 573 to 588 K.*

are attributed to the interaction between dislocations and oxygen atoms. In irradiated Zircaloy, oxygen atoms appear to interact with defects at the same deformation temperature interval resulting in the RAH effect. It is interesting to note that a similar RAH effect has been observed at 573 K [*25*] in irradiated pure iron and ferritic low-alloy steel, ASTM A533 Grade B, and is attributed to the formation of irradiation complex defects with nitrogen and nitrogen/carbon atoms, respectively. The RAH phenomenon is also observed in irradiated vanadium [*26*] in the temperature interval 473 to 773 K and is believed to be due to the migration of oxygen or carbon atoms, or both, to the defects generated by irradiation. The RAH effect in niobium is postulated to be due to precipitation of oxygen on defect aggregates believed to be dislocation loops [*27*].

As the deformation temperature is increased beyond ~623 K, the effectiveness of RAH in irradiated Zircaloy-4 decreases, and a softening mechanism of dislocation channeling becomes operative. At these higher temperatures, because of the higher rates of oxygen diffusion, the defect-oxygen complexes do not offer a strong resistance to the dislocation motion. In order to raise the temperature at which dislocation channeling first becomes operative, RAH effectiveness needs to be extended to higher temperatures. This can be achieved in Zircaloy by increasing the stability of the oxygen-atom-irradiation defect complexes by adding an alloying element, such as niobium. Niobium atoms are believed to interact with oxygen and inhibit the annealing out of the irradiation induced defects [*28*]. It is also reported that Zr-Nb alloys are more resistant to annealing of irradiation damage

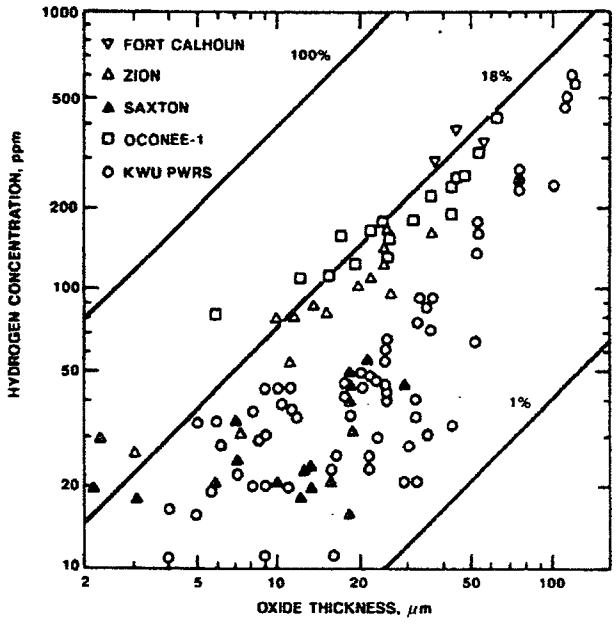

FIG. 8—*Hydrogen uptake as a function of oxide thickness for Zircaloy-4 cladding irradiated in PWRs.*

than Zircaloy-2 [*29*]. Well characterized mechanical property data are needed on Zr-Nb alloys at high fluences to examine the temperature range of effective RAH in these alloys. In a low-oxygen irradiated Zircaloy-2 specimen, stress-strain curve serrations have been observed [*21*], which are the manifestations of repeated dislocation channeling. By increasing the oxygen concentration, the strength of RAH can possibly be increased and thereby the channel formation retarded. Although higher oxygen may enhance effectiveness of RAH in Zircaloy and thereby delay plastic instability, higher oxygen will also increase the flow stress level for homogeneous plastic deformation that may be detrimental to the material ductility.

Dislocation Channeling at ~600 K

Localized surface deformation bands observed at the fracture locations of irradiated Zircaloy-4 specimens are a manifestation of dislocation channeling and have been reported by several other investigators [*10,16,17,20,30–36*]. In a highly irradiated Zircaloy structure, the radiation induced defect density is high, and a large stress is needed to initiate the deformation. At deformation temperatures above ~600 K, the effect of radiation anneal hardening is weakened. Because of the high flow stress requirements, homogeneous deformation is difficult at this temperature. Under these high flow stress conditions one dislocation moves, and during its motion, radiation induced defects on a slip plane are annihilated [*31,37*]. Subsequent motion of dislocations on this defect-denuded plane is easy, leading to a concentrated deformation band called a dislocation channel. Dislocation channeling was observed both under uniaxial and biaxial loading conditions [*38*]. Using transmission electron microscopy (TEM) [*38*], the orientation of dislocation channels were observed to be $\{10\bar{1}0\}$ and {0001}. It has been reported in another investigation [*36*] that for Zircaloy deformed at

K, the dislocation channels are almost perpendicular to the *c* axis, that is, the channel ntation is close to the basal plane orientation. Formation of dislocation channels, by lf, does not reduce the ductility of Zircaloy as is shown by Morize et al. [*4*]. In the ab-ce of hydrogen pickup, even after a fluence of 12 × 10^{21} n/cm², (E > 0.821 MeV), form and total elongations are reasonable (0.55 to 1.4 and 7.2 to 8.5%, respectively) at eformation temperature of 588 K. At this fluence level, in the absence of hydride pre-itates at the deformation temperature, material within a dislocation channel work hardens l a new channel is formed [*31*]. It appears that the low elongations observed in the current estigation, with similar fluence levels and deformation temperatures are a direct result a higher hydrogen concentration (300 to 400 ppm). In Zircaloy material containing a nificant quantity of hydride precipitates at the deformation temperature, once the dis-ation channel is formed, the hydride precipitates induce failure in the channel before nificant repetitive slip in the channel. This explanation seems justifiable since the habit ne for hydride precipitation in Zircaloy-2 and Zircaloy-4 is {10$\bar{1}$7} [*39,40*], that is, a plane h orientation close to that of the basal plane. Since the habit plane of hydrides and the ne of dislocation channel formation have similar orientations, hydrides may be instru-ntal in initiation and propagation of fracture in a dislocation channel at low strains. A nificant number of these hydride precipitates, however, needs to be present at the de-mation temperature for fracture initiation. Therefore, hydrogen concentration in excess he solubility limit at the deformation temperature is necessary for this effect. To verify s hypothesis, more mechanical property data are needed on highly irradiated Zircaloy h variations of hydrogen level. In this regard, it is interesting to note that hydride cipitation has been observed in irradiated Zircaloy after deformation at 598 K at dislo-ion channels [*34*]. The predominantly ductile appearance of the fracture surface of highly adiated Zircaloy, despite the low overall total strain values, is consistent with the proposed chanism of hydride assisted failure in a dislocation channel. It seems that for this failure chanism to operate, both the fluence level and the hydrogen concentration need to be ve certain critical values. The fluence needs to be >10^{22} n/cm² (E > 0.821 MeV) to erate enough defects to promote dislocation channeling leading to highly localized de-mation bands; and, to precipitate the hydrides, the hydrogen concentration needs to be 0 ppm, the approximate solubility limit at 593 K [*41*]. The solubility limit defines the er limit of hydrogen amount needed to see the effect. The actual amount needed may end on the hydride orientation factor, which is the fraction of hydrides oriented within iven angle from the radial direction in the cladding wall cross section. Higher values of orientation factor imply more radial hydrides, and the lower values indicate more cir-nferential hydrides. With a lower value of the hydride orientation factor, hydrogen con-tration well in excess of the solubility limit may be necessary to observe the hydride uced failure in a dislocation channel. With a high value of hydride orientation factor, lrogen concentration slightly above the solubility limit may be sufficient to initiate hydride uced failure in a dislocation channel. The mechanical property data of highly irradiated caloy deformed at temperatures between 561 and 623 K are compared in Table 5. For specimens with a fluence >10^{22} n/cm² (E > 0.821 MeV), the hydrogen concentrations ater than the solubility limit, failures with low strains (uniform strain <1% and total in <4%) are generally observed [*9,17*].

ect of Decreased Cladding Ductility on the Extended Burnup Capability of LWR Fuels

ow ductility values of highly irradiated (fluence >10^{22} n/cm², E > 0.821 MeV) and lrogen-charged (concentration >100 ppm) Zircaloy-4, such as those observed in Fort

Calhoun cladding, imply degradation of material ductility under these conditions. A signif-icant decrease of cladding ductility was also observed in Oconee fuel [*1*] and Zion fuel [*17*] during the fifth irradiation cycle. Whether such a ductility degradation will pose a limitation on extending the batch burnup capability of the current LWR fuels significantly beyond 55 giga-watts day/metric ton of uranium (GWd/MTU) needs to be evaluated by comparing the loading conditions actually experienced by the cladding and those used to obtain the mechanical property data. It appears that the bend loading is more relevant to the fuel rod in-reactor mechanical loading and subsequent post-irradiation handling. The uniaxial tension and biaxial burst testing used to gather the mechanical property data may be more severe types of loading compared to the bend loading. For the bend loading conditions, because of the stress gradient and reversal of stress, dislocation channeling may be less favored as compared to the uniaxial tension and biaxial burst test conditions. Therefore, the material may exhibit more ductility in a bend test compared to a uniaxial tension or biaxial burst test. Therefore, bend test data are needed on highly irradiated Zircaloy to evaluate the burnup limitation, if it exists. Although the mechanical property data for burnups >50 GWd/MTU are limited at present, available information suggests the following possible approaches for increasing the ductility of irradiated Zircaloy:

1. Develop advanced claddings with superior corrosion resistance, that is, decrease the amount of hydrogen generated by reducing the amount of corrosion.
2. Develop cladding alloys with lower hydrogen absorption characteristics, that is, decrease cladding hydrogen uptake. For example, it has been reported [*45*] that Zr-2.5%Nb has a lower hydrogen uptake than both Zircaloy-2 and Zircaloy-4. Lower hydrogen concentration in the irradiated cladding is expected to delay failure initiation and propagation in a dislocation channel.
3. Evaluate the effect of higher concentration levels of current or new alloying elements in Zircaloy on the effective temperature range and strength of RAH. Higher alloying element concentrations may delay the initiation of dislocation channeling to higher temperatures. The ductility of highly irradiated Zircaloy may thereby be enhanced by promoting homogenous deformation instead of a concentration of deformation in a localized deformation band leading to early failure in the band. It may be necessary to add a new alloying element in Zircaloy that would stabilize the oxygen-irradiation defect complexes to higher temperature (that is, greater than ~600 K) compared to the behavior of the base Zircaloy. The effective temperature range of RAH may thereby be increased and dislocation channeling will initiate at higher temperatures.
4. Consider ways to increase the work hardening characteristics of highly irradiated Zircaloy so that when dislocation channeling initiates, work hardening occurs on the slip plane of the first channel and thereby early failure in the first channel is avoided. Subsequent deformation will initiate additional channels. Material in each succeeding channel will work harden and the material will exhibit significant macroscopic deformation before the failure.

Considering all the factors listed above, the most promising alloying element addition to Zircaloys appears to be niobium. As stated earlier, the addition of niobium will reduce hydrogen uptake [*45*], stabilize oxygen-irradiation defect complexes [*28*], and make the alloy more resistant to annealing of irradiation damage [*29*]. Niobium will also enhance work hardenability of irradiated Zircaloy [*28*]. Addition of up to 1% Niobium would probably be sufficient to achieve optimum mechanical properties. The addition of niobium above the 1% level would not result in additional benefit in the mechanical properties [*28*]. In another investigation [*46*], it was concluded that irradiated Zr-Nb alloys should undergo more uni-

TABLE 5—*Comparison of high-fluence mechanical property data for Zircaloy irradiated in commercial power reactors.*

Reactor, Component, Reference	Type of Test, Deformation Temperature	Fluence, n/cm², $E > 0.821$ MeV	Hydrogen Concentration in Specimen, ppm	Solubility Limit for Hydrogen at the Deformation Temperature, ppm [40]	Measured Strains in Deformed Specimen, % U = Uniform T = Total	Comment, Probable Reason for the Measured High or Low Value of Strain after Deformation
Fort Calhoun Zircaloy-4 fuel cladding [9]	tube burst, 588 K	11 to 12 × 10^{21}	300 to 400	80	$U < 0.1$, $T < 4.0$	low ductility caused by hydride precipitation in dislocation channels
" "	" " "	9.1	150 to 200	80	$U \sim 1.5$, $T \sim 4.5$	radiation damage not sufficient to induce strong localization of strain
" "	" " "	7.0	100	80	$U \sim 1.1$, $T \sim 6.2$	" " and number of hydride precipitates may be insufficient
" "	tube tensile, 573 K	11 to 12	300 to 400	~65	$U \sim 0.80$, $T \sim 9.1$	the uniform elongation is consistent and total elongation is not consistent with the proposed failure mechanism
Calvert Cliffs Zircaloy-4, guide tubes	dogbone tensile, 573 K	9.0	50 to 60	~65	$U \sim 0.6$, $T \sim 3.3$	Because of high value of hydride orientation factor, hydrogen concentration barely above the solubility limit may be sufficient to cause low ductility
" "	" " 623 K	9.0	50 to 60	~125	$U \sim 1.3$, $T \sim 4.1$	radiation damage not sufficient & all hydrogen in solution at deformation temperature
" "	ring tensile, 573 K	9.0	50 to 60	~65	$U \sim 0.7$, $T \sim 2.7$	Because of high value of hydride orientation factor, hydrogen concentration barely above the solubility limit may be sufficient to cause low ductility
Oconee 1 Zircaloy 4, fuel cladding [1]	tube tensile, 616 K	11.2	150 to 325	~115	$U \sim 1.3$, $T = 6$ to 15	the number of hydride precipitates is probably not sufficient so ductility values are reasonable
" "	ring tensile, 616 K	11.2	~150 to 325	~115	$U = 2$ to 3, $T =$ 4 to 8	" "
Zion Zircaloy-4, fuel cladding [16]	tube burst, 588 K	9.5 to 11.3	45 to 95	80	$T = 3$ to 3.5	low ductility in specimens with the higher hydrogen concentration
" " [17]	" "	15.1 to 16.2	120 to 170	80	$T = 0.8$ to 2.7	" "
Monticello Zircaloy-2, fuel cladding water rods [42]	tube burst, 605 K	6 to 10	20 to 30	~100	$T = 14$ to 29	hydride precipitates not present so ductility is high
" "	face notch tensile, 605 K	4 to 10	20 to 30	~100	$U = 4$ to 10, $T =$ 11 to 18	" "
" "	dogbone tensile, 605 K	9.5 to 10.2	20 to 30	~100	$U = 0.9$ to 1.4, T = 3.8 to 9.0	" "
Zircaloy-4, spacers [43]	strip tensile, 561 K	9.5 to 10.4	<15	~55	$U = 1.3$ to 2.2, T = 4.4 to 8.1	" "
Zircaloy-4, spacers [44]	" "	8.2 to 13.4	55 to 74	~55	$U = 1.7$ to 2.2, T = 5.7 to 8.5	the number of hydride precipitates probably not sufficient to initiate an early failure in the dislocation channel

m circumferential strain before onset of plastic instability compared to Zircaloy-4 or caloy-2. Tensile properties of irradiated Zr-Nb alloys with different levels of niobium re measured at 575 K in both longitudinal and transverse directions. Considering the asured uniform elongation values, especially in the transverse direction, Zr-0.6% Nb oy was superior [46] to Zr-Nb alloys containing 0.14, 2.35, and 2.5% Nb. It appears that niobium atoms homogeneously distributed in solution within the alpha phase zirconium Zr-0.6% Nb alloy are instrumental in enhancing ductility of irradiated Zr-0.6% Nb alloy. ldition of niobium beyond 0.6 wt% results in the precipitation of beta-niobium, and these cipitates do not appear to enhance ductility of irradiated Zr-Nb alloys. These results gest that a 0.6 wt% niobium addition to Zircaloy may result in enhancing the ductility Zircaloys in the irradiated condition. The in-reactor corrosion rate after up to 1% niobium dition is expected to be comparable to or superior than that of Zircaloy. Niobium additions up to 1% to Zircaloy-4 have shown beneficial influence on the corrosion resistance of caloy-4 in high-temperature autoclave water [47]. It is interesting to note that for a 1% Sn-1% Nb-0.5% Fe alloy, it has been shown [48] that the PCI resistance and ductility he irradiated condition were superior than those for Zircaloy-2. On the basis of measured chanical properties of irradiated zirconium-niobium alloys, the Russian investigators [49] e also concluded that the Zr-1% Sn-1% Nb-0.5% Fe alloy is superior to other Zr-Nb ys. It has been concluded [50] that under power cycling conditions, the performance of r-1% Nb alloy would be superior to that of Zircaloy.

nclusions

. Highly irradiated Zircaloy-4 (fluence $>10^{22}$ n/cm^2, $E > 0.821$ MeV) charged with nificant amounts of hydrogen ($\geq$100 ppm) exhibits limited ductility (uniform plastic elonions $\leq$1.0% and total plastic elongations $\leq$4.0%) for deformation temperatures below roximately 650 K. There is a synergistic effect of radiation damage and hydrogen uptake the decrease in ductility.

. Although the elongation values are low for deformation temperatures below 650 K, tographic results reveal the presence of dimples on the fracture surface indicating a tile fracture.

. The observation of localized deformation bands on the fractured specimens of the hly irradiated Zircaloy-4 specimens deformed at 573 to 623 K implies that the failure is ciated with dislocation channels. The presence of a significant quantity of hydrides bably enhances failure initiation and propagation within a dislocation channel.

. Radiation anneal hardening is observed in irradiated Zircaloy in the temperature inal 573 to 623 K and is probably associated with the formation of irradiation defect plexes with oxygen atoms.

. The hydrogen absorption in highly irradiated Zircaloy-4 may be bounded by an uptake tion of about 18% and appears to be independent of the oxide thickness.

. Limited available mechanical property data on highly irradiated and hydrogen charged caloy-4 suggest a possible degredation of Zircaloy ductility for fluence levels $>10^{22}$ m^2, $E > 0.821$ MeV and hydrogen concentrations >100 ppm. The influence of this tility degredation on the in-reactor performance and handling capabilities of current eration LWR fuel exposed to batch average burnups significantly greater than 55 GWd/ U needs to be evaluated with respect to the different loading conditions. More mechanical perty data are needed for highly irradiated Zircaloy containing hydrogen levels signifitly above the solubility limit.

. It may be necessary to develop new cladding materials with improved ductility in the irradiated condition. An addition of less than 1% niobium to Zircaloy appears to be promising in this regard.

Acknowledgments

Sponsorship of the hot-cell work on the Fort Calhoun fuel rods by the U.S. Department of Energy and C-E Owners Group Utilities is gratefully acknowledged. The hot-cell examination of the Calvert Cliffs-1 fuel assembly cage was sponsored by the Electric Power Research Institute. The author would like to thank R. Kohli of BCL and G. P. Smith of C-E for their efforts in the hot-cell experimental work.

References

[1] Newman, L. W., "The Hot-Cell Examination of Oconee 1 Fuel Rods after Five Cycles of Irradiation," Babcock and Wilcox Report BAW-1874, DOE/ET/34212-50, Oct. 1986.

[2] Yunchang, F. and Koss, D. A., "The Influence of Multiaxial States of Stress on the Hydrogen Embrittlement of Zirconium Alloy Sheet," *Metallurgical Transactions A*, Vol. 16A, April 1985, pp. 675–681.

[3] Garzarolli, F. and Stehle, H., "Behavior of the Core Structural Materials in Light Water Cooled Power Reactors," IAEA-SM-288/24, *Proceedings of the IAEA Symposium on Improvements in Water Reactor Fuel Technology and Utilization*, Stockholm, Sweden, Sept. 1986, International Atomic Energy Agency, Vienna, 1987, pp. 387–407.

[4] Morize, P., Baicry, J., and Mardon, J. P., "Effects of Irradiation at 588 K on Mechanical Properties and Deformation Behavior of Zirconium Alloy Strip," *Zirconium in the Nuclear Industry: Seventh International Symposium, STP 939*, R. B. Adamson and L. F. P. Van Swam, Eds., American Society for Testing and Materials, Philadelphia, 1987, pp. 101–119.

[5] Knaab, H. and von Jan, R., "Fuel Performance Evaluation and Improved Fuel Utilization by Pool-Site Fuel Services," *Proceedings of the ANS Topical Meeting on Light Water Reactor Fuel Performance*, DOE/NE/34130-1, Orlando, FL, April 1985, pp. 1–35 to 1–51.

[6] Matheson, J. E., Newman, L. W., McInteer, W. A., and Bain, G. M., "Recent Operating Experience with B&W Fuel with the Emphasis on Extended Burnup," *Proceedings of the ANS Topics Meeting on Light Water Reactor Fuel Performance*, DOE/NE/34130-1, Orlando, FL, April 1985, pp. 2–47 to 2–62.

[7] Garzarolli, F., Bodmer, R. P., Stehle, H., and Trapp-Pritsching, S., "Progress in Understanding PWR Fuel Rod Waterside Corrosion," *Proceedings of the ANS Topical Meeting on Light Water Reactor Fuel Performance*, DOE/NE/34130-1, Orlando, FL, April 1985, pp. 3–55 to 3–72.

[8] Smith, G. P., "The Evaluation and Demonstration of Methods for Improved Fuel Utilization: End-of-Cycles 6 and 7 Fuel Examinations," Combustion Engineering Report CEND-414, DOE/ET/34010-10, Oct. 1983.

[9] Garde, A. M., "Hot-Cell Examination of Extended Burnup Fuel from Fort Calhoun," Combustion Engineering Report CEND-427, DOE/ET/34030-11, Sept. 1986.

[10] Lowry, L. M., Markworth, A. J., Perrin, J. S., and Landow, M. P., "Evaluating Strength and Ductility of Irradiated Zircaloy Task 5," *Experimental Data*, Final Report, NUREG/CR-1729, BMI-2066, Vol. 1, May 1981.

[11] Hyatt, B. Z., "Metallographic Standards for Estimating Hydrogen Content of Zircaloy-4 Tubing," WAPD-TM-1431, Feb. 1982.

[12] Cox, B., "Effect of Hydrogen Injection on Hydrogen Uptake by BWR Fuel Cladding," EPRI-NP-3146, Project 1930-5, Final Report, June 1983.

[13] Evans, W. and Parry, G. W., "The Deformation Behavior of Zircaloy-2 Containing Directionally Oriented Zirconium Hydride Precipitates," *Electrochemical Technology*, Vol. 4, May-June 1966, pp. 225–231.

[14] Smalley, W. R., "Saxton Core II, Fuel Performance Evaluation, Part 1: Materials," Westinghouse Electric Corporation Report, WCAP-3385-56, Part I, Sept. 1971.

[15] Smalley, W. R., "Evaluation of Saxton Core III, Fuel Materials Performance," Westinghouse Electric Corporation Report, WCAP-3385-57, July 1974.

[16] Belfour, M. G., Smalley, W. R., Kuszyk, J. A., and Pritchett, P. A., "Hot Cell Examination of Zion Fuel-Cycles 1 Through 4," Research Report EP80-16, Empire State Electric Energy Research Corporation, Final Report, April 1985.

Nayak, U. P., Kunishi, H., and Smalley, W. R., "Hot Cell Examination of Zion Fuel Cycle 5," Research Report EP80-16, Empire State Electric Energy Research Corporation, final report, June 1985.

Snowden, K. U. and Veevers, K., "Radiation Hardening in Zircaloy-2," *Radiation Effects*, Vol. 20, 1973, pp. 169–174.

Onchi, T., Kayano, H., and Higashiguchi, Y., "The Inhomogeneous Deformation Behavior of Neutron Irradiated Zircaloy-2," *Journal of Nuclear Materials*, Vol. 88, 1980, pp. 226–235.

Onchi, T., Kayano, H., and Higashiguchi, Y., "Inhomogeneous Plastic Deformation and its Relevance to Iodine Stress Corrosion Cracking Susceptibility in Irradiated Zircaloy-2 Tubing," *Journal of Nuclear Materials*, Vol. 116, 1983, pp. 211–218.

Adamson, R. B. and Bell, W. L., "Effects of Neutron Irradiation and Oxygen Content on The Microstructure and Mechanical Properties of Zircaloy," *Microstructure and Mechanical Behavior of Materials*, Vol. 1, Proceedings of the International Symposium at X'ian, Republic of China, 21–24 Oct. 1985, Engineering Materials Advisory Services Ltd., Warley, United Kingdom, pp. 237–246.

Chung, H. M., Yaggee, F. L., and Kassner, T. F., "Fracture Behavior and Microstructural Characteristics of Irradiated Zircaloy Cladding," *Zirconium in the Nuclear Industry: Seventh International Symposium, STP 939*, R. B. Adamson and L. F. P. Van Swam, Eds., American Society for Testing and Materials, Philadelphia, 1987, pp. 775–801.

Nakatsuka, M., Imahashi, H., and Nagai, M., "Effect of Oxygen Content on Tensile Properties of Low Oxygen Zircaloy-2," *Journal of Nuclear Science and Technology*, Vol. 22, No. 3, March 1985, pp. 239–241.

Hong, S. I., Ryu, W. S., and Rim, C. S., "Elongation Minimum and Strain Rate Sensitivity Minimum in Zircaloy-4," *Journal of Nuclear Materials*, Vol. 116, 1983, pp. 314–316.

Takaku, H. and Kayano, H., "Combined Effects of Neutron Irradiation and Hydrogen Absorption on Tensile Properties and Fracture Mode of Steels for Nuclear Pressure Vessels," *Journal of Nuclear Materials*, Vol. 110, 1982, pp. 286–295.

Smidt, F. A., Jr., "Correlation of Microstructure and Strength during Stage III Annealing of Irradiated Vanadium," *Radiation Effects*, Vol. 10, 1971, pp. 205–214.

Tucker, R. P., Ohr, S. M., and Wechsler, M. S., "Radiation Damage in Reactor Materials," *Proceedings of the International Atomic Energy Agency*, Vol. 1, 1969, p. 215.

Ells, C. E., "Deformation of Irradiated Zirconium-Niobium Alloys," *Zirconium in Nuclear Applications, STP 551*, American Society for Testing and Materials, Philadelphia, 1974, pp. 311–327.

Carpenter, G. J. C. and Watters, J. F., "Irradiation Damage Recovery in Some Zirconium Alloys," *Zirconium in Nuclear Applications, STP 551*, American Society for Testing and Materials, Philadelphia, 1974, pp. 400–415.

Rieger, G. F. and Lee, D., "Strength and Ductility of Neutron Irradiated and Textured Zircaloy-2," *Zirconium in Nuclear Applications, STP 551*, American Society for Testing and Materials, Philadelphia, 1974, pp. 355–369.

Lee, D. and Adamson, R. B., "Modeling of Localized Deformation in Neutron Irradiated Zircaloy-2," *Zirconium in the Nuclear Industry, STP 633*, A. L. Lowe, Jr. and G. W. Parry, Eds., American Society for Testing and Materials, Philadelphia, 1977, pp. 385–401.

Yasuda, T., Nakatsuka, M., and Yamashita, K., "Deformation and Fracture Properties of Neutron Irradiated Recrystallized Zircaloy-2 Cladding Under Uniaxial Tension," *Zirconium in the Nuclear Industry: Seventh International Symposium, STP 939*, R. B. Adamson and L. F. P. Van Swam, Eds., American Society for Testing and Materials, Philadelphia, 1987, pp. 734–747.

Bell, W. L., "Determination and Microscopic Study of Incipient Defects in Irradiated Power Reactor Fuel Rods," EPRI NP-812, Project 829, final report, July 1978, pp. 3–159 and 4–18.

Chung, H. M., Materials Science Division Light-Water-Reactor Safety Research Program: Quarterly Progress Report, Jan.-March, 1982, Argonne National Laboratory, NUREG/CR-2970, Vol. 1, ANL-82-41, Vol. 1, p. 86.

Bauer, A. A. and Lowry, L. M., "Tensile Properties and Annealing Characteristics of H. B. Robinson Spent Fuel Cladding," *Nuclear Technology*, Vol. 41, Mid-December 1978, pp. 359–372.

Petterson, K., "Evidence for Basal or Near-Basal Slip in Irradiated Zircaloy," *Journal of Nuclear Materials*, Vol. 105, 1982, pp. 341–344.

Olander, D. R., *Fundamental Aspects of Nuclear Reactor Fuel Elements*, ERDA Publication TID-26711-P1, National Technical Information Service, Springfield, VA, April 1976, pp. 442–443.

Adamson, R. B., Wisner, S. B., Tucker, R. P., and Rand, R. A., "Failure Strain for Irradiated Zircaloy Based on Subsized Specimen Testing and Analysis," *Use of Small-Scale Specimens for Testing Irradiated Material, STP 888*, W. R. Corwin and G. E. Lucas, Eds., American Society for Testing and Materials, Philadelphia, 1986, pp. 171–185.

[39] Ells, C. E., "Hydride Precipitates in Zirconium Alloys," *Journal of Nuclear Materials*, Vol. 28, 1968, pp. 129–151.

[40] Westlake, D. G., "The Habit Planes of Zirconium Hydride in Zirconium and Zircaloy," *Journal of Nuclear Materials*, Vol. 26, 1968, pp. 208–216.

[41] Douglass, D. L., *The Metallurgy of Zirconium*, Atomic Energy Review, IAEA Supplement 1971, International Atomic Energy Agency, Vienna, Austria, 1971, p. 160.

[42] Baumgartner, J. A., "BWR Fuel Bundle Extended Burnup Program Technical Progress Report, January 1982—December 1982," General Electric Report GEAP-30268, DOE/ET/34031-15, Sept. 1983.

[43] Baumgartner, J. A., "BWR Fuel Bundle Extended Burnup Program Technical Progress Report, January 1981—December 1981," General Electric Report GEAP-30083, DOE/ET/34031-12, July 1983.

[44] Baumgartner, J. A., "BWR Fuel Bundle Extended Burnup Program Technical Progress Report, January 1983—December 1983," General Electric Report GEAP-30643, DOE/ET/34031-17, May 1984.

[45] Urbanic, V. F., Cox, B., and Fields, G. J., "Long-Term Corrosion and Deuterium Uptake in CANDU-PHW Pressure Tubes," *Zirconium in the Nuclear Industry: Seventh International Symposium, STP 939*, R. B. Adamson and L. F. P. Van Swam, Eds., American Society for Testing and Materials, Philadelphia, 1987, pp. 189–205.

[46] Cheadle, B. A., Ells, C. E., and van der Kuur, J., "Plastic Instability in Irradiated Zr-Sn and Zr-Nb Alloys," *Zirconium in Nuclear Applications, STP 551*, American Society for Testing and Materials, Philadelphia, 1974, pp. 370–384.

[47] Sabol, G. P. and McDonald, S. G., "The Effect of Niobium Additions on the Corrosion Behavior of Zircaloy-4," *Nuclear Science and Engineering*, Vol. 63, 1977, pp. 83–90.

[48] Castaldelli, L., Fizzotti, C., and Lunde, L., "Long-Term Test Results of Promising New Zirconium Alloys," *Zirconium in the Nuclear Industry: Fifth Conference, STP 754*, D. G. Franklin, Ed., American Society for Testing and Materials, Philadelphia, 1982, pp. 105–126.

[49] Tsykanov, V. A., Finko, A. G., Samsonov, B. V., and Pokrovskii, A. S., "Hardening and Embrittlement of Zirconium Cladding Alloys under Neutron Irradiation," NIIAR-44 (403), V. I. Lenin's Scientific Research Institute of Atomic Reactors (NIIAR), Dimitrovgrad, USSR, 1979.

[50] Krett, V., Novak, J., and Pazdera, F., "Research Carried out on LWR Fuel and Cladding Alloys under Operational and Accident Conditions," IAEA-SM-288/21, *Proceedings of the IAEA Symposium on Improvements in Water Reactor Fuel Technology and Utilization*, Stockholm, September 1986, International Atomic Energy Agency, Vienna, Austria, 1987, pp. 419–434.

Journal of NUCLEAR SCIENCE and TECHNOLOGY, Vol. 37, No. 8, p. 670–675 (August 2000)

Influence of Precipitated Hydride on the Fracture Behavior of Zircaloy Fuel Cladding Tube

Masatoshi KURODA[*1,†], Kunihiko YOSHIOKA[*1], Shinsuke YAMANAKA[*1], Hiroyuki ANADA[*2], Fumihisa NAGASE[*3] and Hiroshi UETSUKA[*3]

[*1] *Department of Nuclear Engineering, Graduate School of Engineering, Osaka University*
[*2] *Sumitomo Metal Industries, Ltd.*
[*3] *Department of Reactor Safety Research, Japan Atomic Energy Research Institute*

(Received December 27, 1999)

In order to clarify the influence of precipitated hydride on the fracture behavior of Zircaloy cladding tubes, the stress-strain distribution of the cladding was estimated by finite element method (FEM) analysis. The mechanical properties of α-phase of zirconium and zirconium hydride required for the analysis were examined by means of an ultrasonic pulse-echo method and a tensile test. It was found from the analysis that the non-hydrided cladding has the highest equivalent plastic strain at the inner surface of the cladding, suggesting that the fracture initiated at the inner surface of the cladding. Since the hydride accumulated layer located in the outer surface of the hydrided cladding fails at a lower internal pressure, the crack appears to initiate at the outer surface of the cladding. The fracture behavior estimated from the stress states of the hydrided cladding was in good agreement with the experimental results obtained by pulse irradiation tests of the Nuclear Safety Research Reactor (NSRR) and high-pressurization-rate burst tests in the Japan Atomic Energy Research Institute (JAERI).

KEYWORDS: ***high burnup, reactivity initiated accident, fuel cladding tube, Zircaloy, zirconium alloys, zirconium hydride, hydrogen embrittlement, finite element method, mechanical properties, fractures***

I. Introduction

In recent years, many efforts have been paid to study the fracture behavior of high burnup LWR rods during reactivity initiated accident (RIA) conditions. In Japan and France, the experimental programs with regards to high burnup fuel are in progress[1]. The program in Japan has been conducted in the Nuclear Safety Research Reactor (NSRR) of the Japan Atomic Energy Research Institute (JAERI). It was found from the results of a pulse irradiation test in the NSRR that the pre-existing hydride strongly affected the cladding failures[2]. Although the failure results from pellet-clad mechanical interaction (PCMI) accompanied by hydrogen embrittlement, quantitative analysis has not been carried out for the influence of the precipitated hydride on the cladding failure. Thus, high-pressurization-rate burst tests have been performed in the JAERI to simulate the fracture behavior of the cladding tube observed in the NSRR[3][4]. In these tests, pressure was exerted from the inside of the cladding tubes with hydraulic power to simulate the PCMI in the NSRR. The following types of claddings were studied in the burst tests:

(Type-I): As received claddings without hydrogenation,
(Type-II): Hydrided claddings with zirconium hydride accumulated locally beneath the outer surface of the cladding,
(Type-III): Hydrided claddings with zirconium hydride distributed uniformly and oriented to circumferential direction of the cladding.

The authors employed the Type-II and Type-III as a typical model to clarify the influence of the distribution and location of the hydride on the burst pressure. It was revealed that such hydride accumulation as the Type-II was mainly caused by the temperature gradient in the cladding and could be expected commonly for the high burnup fuel cladding[5]. The failure morphology of the fuel cladding rods post-irradiated in the NSRR was close to the Type-II rather than the Type-III. In order to elucidate the fracture behavior of the fuel cladding tube, it is necessary to examine the stress states of the claddings in detail. In the present study, finite element method (FEM) analysis was performed to estimate the stress-strain distribution of the claddings. The mechanical properties of zirconium hydride required for the analysis were measured by means of an ultrasonic pulse-echo method and a tensile test. On the basis of the FEM analysis, the experimental results of the burst test in the JAERI were discussed.

[*1] *Yamadaoka, Suita-shi, Osaka 565-0871.*
[*2] *Fuso-cho, Amagasaki-shi, Hyogo 660-0891.*
[*3] *Tokai-mura, Naka-gun, Ibaraki 319-1195.*
[†] Corresponding author, Tel. +81-6-6879-7905, Fax. +81-6-6879-7889, E-mail: mkuroda@nucl.eng.osaka-u.ac.jp

II. Experimental

The zirconium hydride specimen in the form of pellet was directly fabricated from zirconium metal with 99.9% purity in a modified Ultra High Vacuum (UHV) Sieverts apparatus. The hydrogen content of the bulk specimen ranged from about 1.5 to 1.7 H/Zr. Microstructure of the hydride specimen consisted of many platelets inside large grains without any microcrack or pore, showing a Widmanstatten characteristic.

Sound velocities were measured by an ultrasonic pulse-echo method. From the ratio of the longitudinal sound velocities (V_l) to shear sound velocities (V_s), all the hydride specimens appear to be isotropic. For isotropic media, the Young's modulus (E) and Poisson's ratio (ν) can be written in terms of the V_l and the V_s by

$$E = \rho V_s^2 \left(\frac{3V_l^2 - 4V_s^2}{V_l^2 - V_s^2} \right), \quad (1)$$

$$\nu = \frac{V_l^2 - 2V_s^2}{2(V_l^2 - V_s^2)}, \quad (2)$$

where ρ is the density of the specimen.

The stress-strain diagrams of the α-phase of zirconium (αZr) and the δ-phase of $ZrH_{1.73}$ ($\delta ZrH_{1.73}$) were obtained by tensile tests at room temperature for sheet-type specimens with gauge length of 5 mm using a strain gauge attached on the center position of the specimen. Strain rate of the tests was 3.3×10^{-3}/s. In order to examine the fracture mechanism of the zirconium hydride, the fracture surface of the $\delta ZrH_{1.73}$ was observed by scanning electron microscopy (SEM).

III. Analytical

Figure 1(a) shows the schematic diagram of the burst test apparatus in the JAERI. Hydraulic internal pressure was applied to Zircaloy-4 cladding tubes with inner and outer diameters of 8.36 mm and 9.50 mm, respectively, and the length of 160 mm. In this test, deformation to the axial direction was restricted at the lower end of the tube, while the upper end was without restriction. This type of test corresponds to a closed-end burst test. The stress states of the cladding in the closed-end burst test are close to the cladding under the plane strain condition where axial strain is null ($\varepsilon_z = 0$) rather than the plane stress condition where axial stress is null ($\sigma_z = 0$). Therefore, the axial total deformation was ignored and the plane strain condition was assumed as shown in **Fig. 1**(b) in the present study. Taking account of the symmetry, a cladding tube was modeled as **Fig. 1**(c) to reduce the number of elements.

In the present analysis, the matrix and the zirconium hydride were considered as αZr and $\delta ZrH_{1.73}$, respectively. All hydrogen absorbed in the αZr was assumed

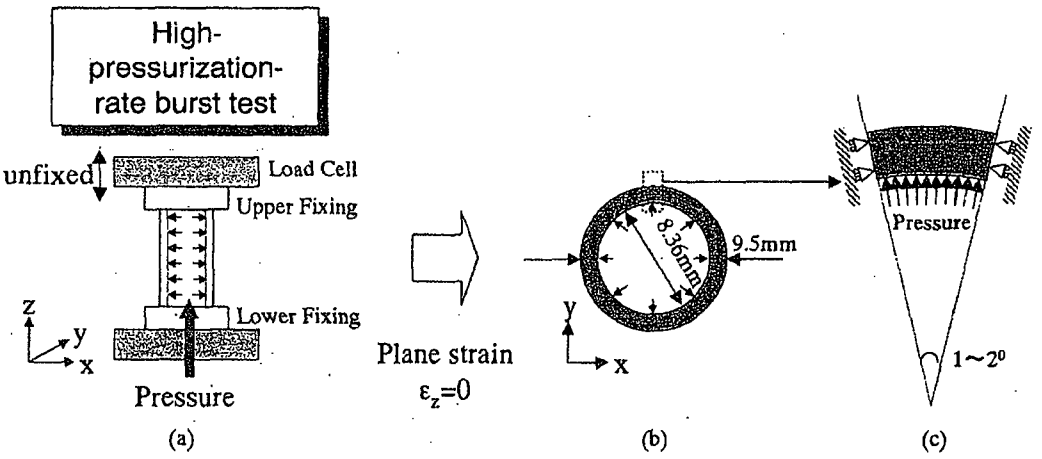

Fig. 1 Modeling procedures of the burst test

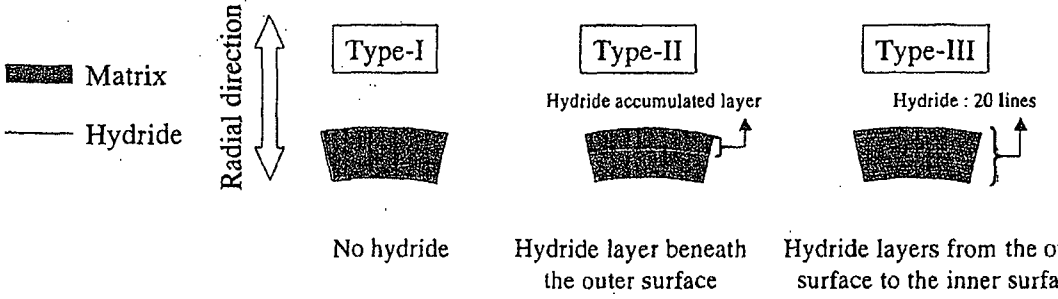

Fig. 2 Schematic illustration of the distribution of hydride

to precipitate the hydride. In the case that the average hydrogen concentration is 1,000 wtppm, the volume ratio of the $\delta ZrH_{1.73}$ to the αZr is about 5%. The Type-II and Type-III modelings with the two types of the distribution of hydride in the claddings are illustrated in **Fig. 2**: In Type-II, the hydride exists only beneath the outer surface of the cladding, and in Type-III, the hydride is located on the cladding with 20 lines of the plate-shaped hydride arraying to the circumferential direction of the cladding from the outer surface to the inner surface.

The FEM analysis was carried out to estimate the stress-strain distribution of the three types of claddings by a general-purpose program of "MARC". No dynamic effect was considered in the present analysis.

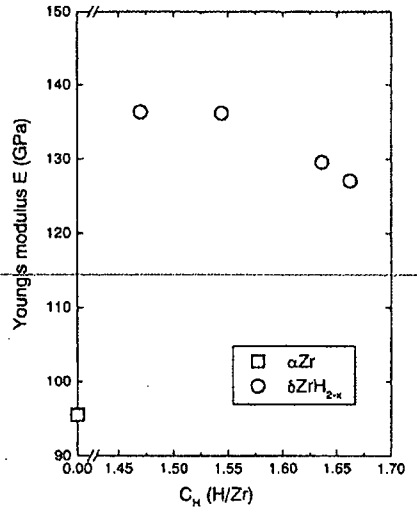

Fig. 3 Change in the Young's modulus E of δZrH_{2-x} with the hydrogen content C_H

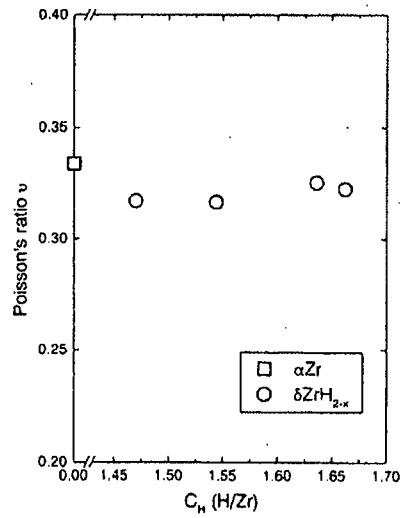

Fig. 4 Change in the Poisson's ratio ν of δZrH_{2-x} with the hydrogen content C_H

IV. Results and Discussion

1. Mechanical Properties of αZr and Zirconium Hydride

(1) Ultrasonic Pulse-echo Measurement

As a result of ultrasonic pulse-echo measurement, it is found that the Young's modulus of δ zirconium hydride is larger than that of zirconium metal, and slightly decreases with increasing hydrogen content as shown in **Fig. 3**. **Figure 4** shows that the Poisson's ratio of the hydride can be estimated to be about 0.32 regardless of hydrogen content, and no marked difference was observed between zirconium metal and hydride.

(2) Tensile Test of αZr Specimen

The stress-strain relation of the αZr was measured by a tensile test. The Young's modulus and yield stress were about 105GPa and 350 MPa, respectively. The Young's modulus makes little difference between the tensile test and the former ultrasonic pulse-echo measurement. The stress-plastic strain diagram obtained by the test was shown in **Fig. 5**.

(3) Tensile Test of Hydride Specimen

Figure 6 shows the stress-strain diagram of $\delta ZrH_{1.73}$

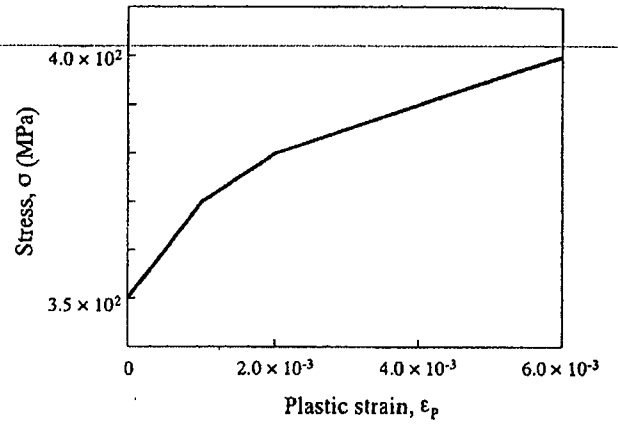

Fig. 5 Stress-plastic strain diagram of αZr

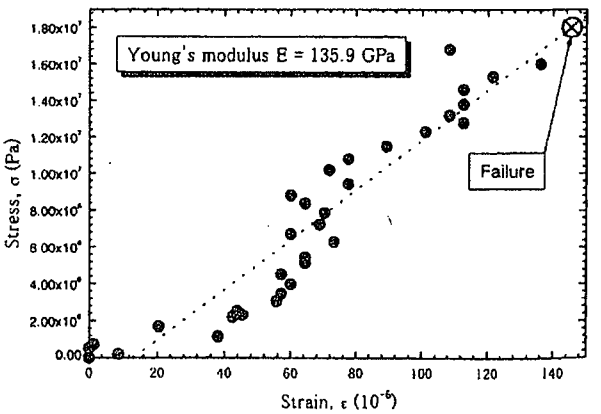

Fig. 6 Stress-strain diagram of $\delta ZrH_{1.73}$

obtained by a tensile test. The Young's modulus was estimated to be approximately 135.9 GPa, and agreed with the results obtained by means of the ultrasonic pulse-echo method. The hydride specimen failed before yielding begins, and the failure occurred at an extremely low applied stress of approximately 18 MPa. **Photograph 1** indicates the presence of river patterns within cleavage facets by microscopic observation of the fracture surface. The formation of the river patterns is caused by cleavage fracture. Therefore, it is reasonable that the fracture surface of the hydride is oriented perpendicular to the direction of the applied uniaxial stress as shown in **Photo. 2**.

A critical stress for describing hydride fracture has been used by several authors[6]-[10]. However, there were no data that directly give the fracture stress of the zirconium hydride in the literature, which is associated with difficulty in preparing suitable solid hydride specimens[6][7]. Barraclough *et al.*[8] measured the fracture stress based on uniaxial compression tests, and showed that the stress may be in the range of 100 to 200 MPa in the temperature range between 22 and 453°C for $\delta ZrH_{1.66}$ bulk specimens. Shi *et al.*[6][7] considered the possibility of the assumption that the fracture strength of a brittle material such as zirconium hydride is related to the bond strength, which is reflected in the magnitude of Young's modulus. The failure stress of hydride is expressed in terms of the Young's modulus as follows[6][7]:

$$\sigma = 7.357 \times 10^3 E, \tag{3}$$

where E should be the Young's modulus of hydride. In the present study, the failure stress estimated through Eq. (3) is about 1.00 GPa, which is definitely higher value than the experimental results of 18 MPa. It suggests that the theoretical failure stress derived from the atomic bond strength was estimated too highly to apply to the present analysis. In the following analysis, the experimental data of 18 MPa was employed as the failure stress of the hydride.

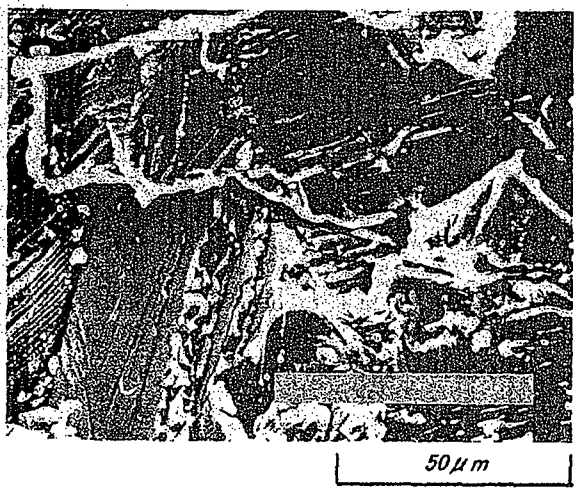

Photo. 1 SEM observation of the fracture surface of $\delta ZrH_{1.73}$

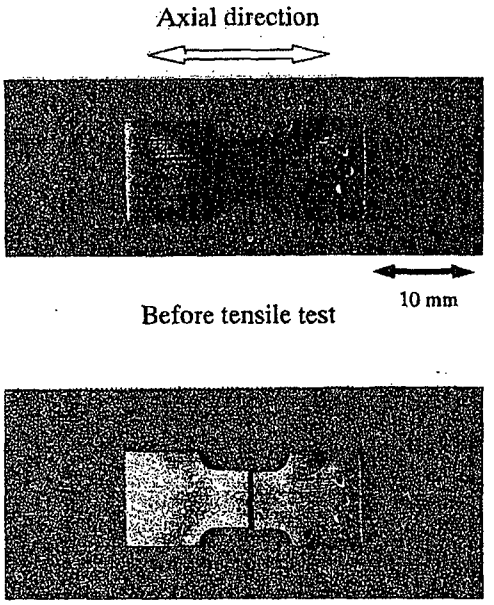

Photo. 2 Fracture morphology of $\delta ZrH_{1.73}$

2. FEM Analysis

Figure 7 shows the stress and plastic strain distribution of the non-hydrided Type-I cladding at internal pressure of 50 MPa. It is found from Fig. 7(a) that plane stress condition is made at the outer surface of the cladding since radial stress is null. On the other hand, the equivalent plastic strain is the highest at the inner surface of the cladding as shown in Fig. 7(b). The stress distribution of the hydrided claddings, Type-II and Type-III, is revealed in **Fig. 8** with the failure stress of hydride 18 MPa. From these diagrams, the outer surface of the claddings was also found to be under plane stress. The circumferential component of the stress almost attains to the failure stress of hydride at an internal pressure 2 MPa. Hence the hydride phase existing in both the claddings is fractured at a lower internal pressure than the yield point of the matrix.

3. Consideration on the Fracture Behavior

(1) Crack Initiation Site of the Claddings

Figure 9 shows the fracture morphology of the Type-I and Type-II claddings obtained by the burst tests[3]. Since the crack initiation site could not be determined only by the experiment, it is discussed on the basis of the FEM analysis in the present study.

The Type-I cladding was found to have the highest equivalent plastic strain at the inner surface of the cladding as described in the former section. This suggests that the fracture initiated at inner surface of the

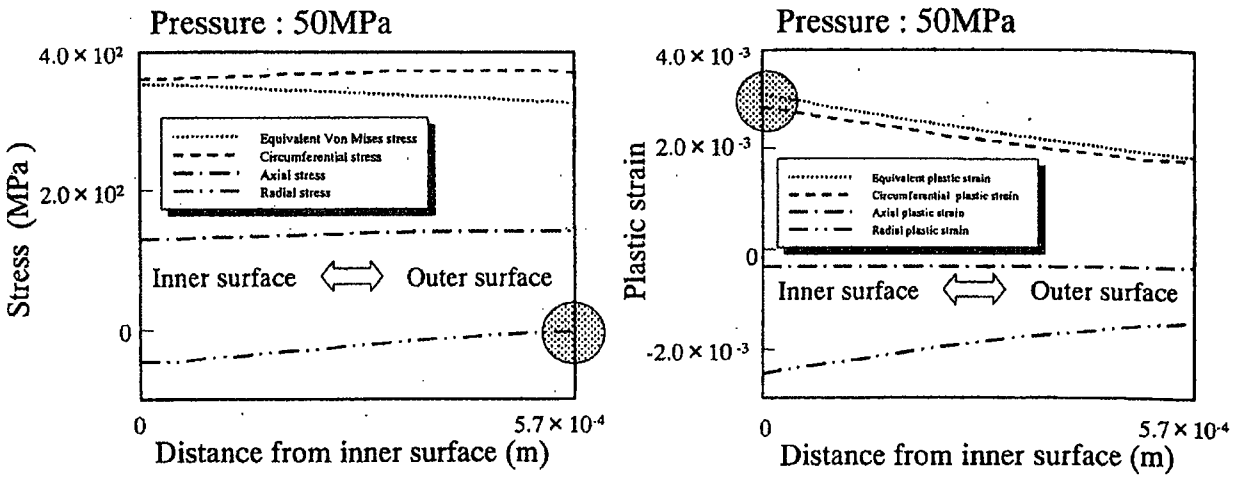

(a) Stress distribution (b) Plastic strain distribution

Fig. 7 Stress and plastic strain distribution of the Type-I cladding

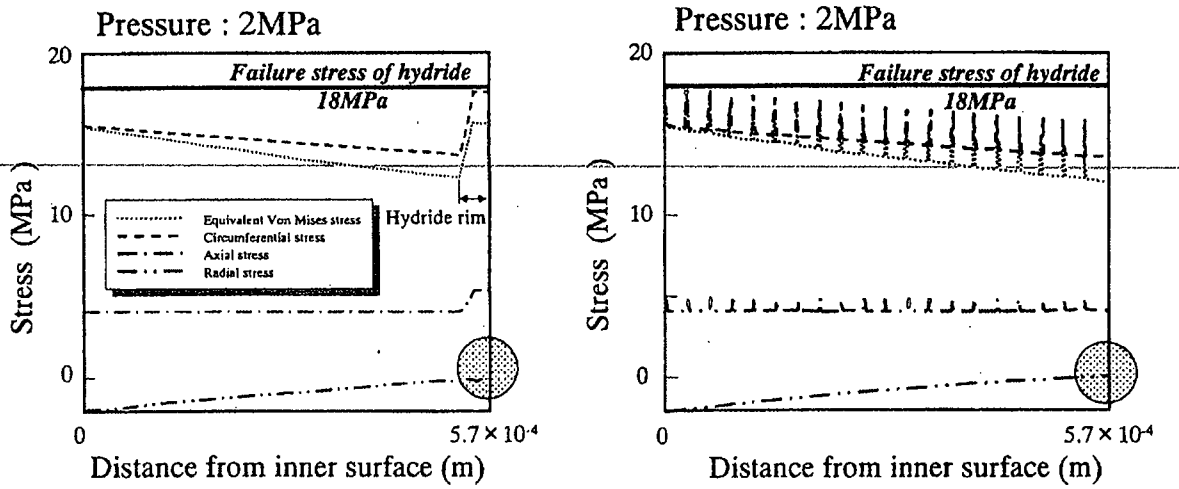

(a) Type-II cladding (b) Type-III cladding

Fig. 8 Stress distribution of the hydrided claddings

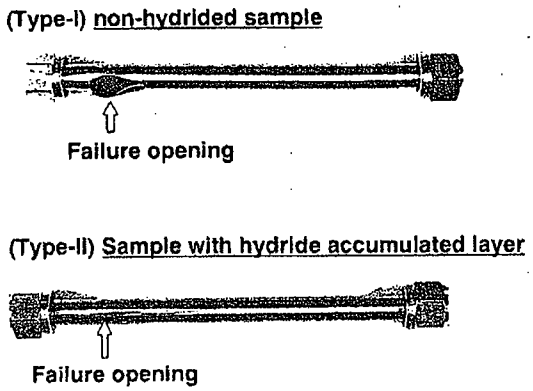

Fig. 9 Fracture behavior of the claddings by the high-pressurization-rate burst test[3]

cladding. Since the hydride accumulated layer in the Type-II appears to fail at an extremely low internal pressure as shown in Fig. 8(a), the crack initiation is supposed to occur at the outer surface of the cladding.

(2) Failure Morphology of the Type-II Cladding

Figure 10 shows the cross section of the fracture surface in the Type-II cladding[3]. It is found from Figs. 9 and 10 that the crack propagated perpendicularly to the circumferential direction at the hydride accumulated layer, and the crack extended towards 45° to the circumferential direction in the matrix. On the basis of the stress states of the cladding, this phenomenon can be analyzed as follows.

The hydride accumulated layer of the Type-II cladding caused cleavage fracture by SEM observation[3]. The cleavage fracture occurs when the tensile component of

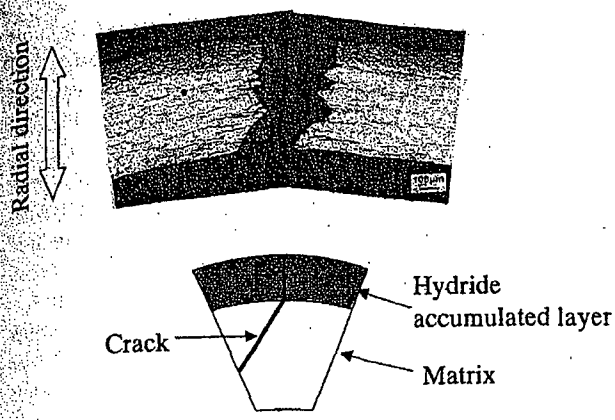

Fig. 10 Cross section of the fracture surface (Type-II cladding)[3]

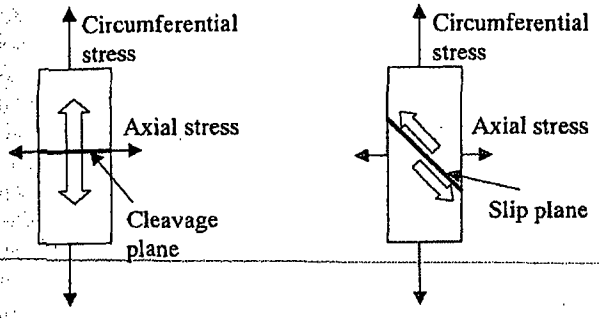

(a) Cleavage fracture (b) Shear fracture

Fig. 11 Schematic diagram of the fracture behavior under plane stress condition

the external applied stress is beyond the bond strength. Since the plane stress condition is attained at the crack initiation site of the Type-II as shown in **Fig. 11**(a), the maximum component of the tensile stress is circumferential. Consequently, the fracture surface appears to be normal to the circumferential direction at the hydride accumulated layer. On the other hand, the shear fracture appears to occur at the matrix. Plastic deformation tends to be confined to the slip planes, which have a low resistance to shear. The slip plane inclined at 45° to the circumferential direction has the maximum shear stress under the plane stress condition at the outer surface of the Type-II cladding as shown in **Fig. 11**(b). Therefore, the 45° slant fracture will be formed in the matrix. The results for the present analysis are consistent with the experimental results in the JAERI[3][4].

V. Conclusion

The stress-strain distribution of the cladding was estimated by finite element method (FEM) analysis to clarify the influence of precipitated hydride on the fracture behavior of Zircaloy fuel cladding tubes. The measurement for the mechanical properties of zirconium hydride required for the FEM analysis was carried out by an ultrasonic pulse-echo method and a tensile test. The hydride specimen of $\delta ZrH_{1.73}$ failed before yielding of matrix begins, and the failure stress was estimated to be about 18 MPa. Non-hydrided Type-I cladding was found to have the highest equivalent plastic strain at the inner surface of the cladding, suggesting that the fracture initiated at the inner surface of the cladding. Since the zirconium hydride fails at a lower internal pressure for Type-II cladding with hydride accumulated locally beneath the outer surface of the cladding, the crack appears to initiate at the outer surface. Based on the stress states of the Type-II cladding, the crack appears to propagate perpendicularly to the circumferential direction at the hydride accumulated layer, and the crack extends towards 45° to the circumferential direction in the matrix. These considerations agreed well with the experimental results obtained by pulse irradiation tests of the Nuclear Safety Research Reactor (NSRR) and high-pressurization-rate burst tests in the Japan Atomic Energy Research Institute (JAERI).

Acknowledgments

This work was supported by the Japan Atomic Energy Research Institute (JAERI).

—References—

(1) Lemoine, F.: *J. Nucl. Mater.*, **248**, 238 (1997).
(2) Fuketa, T., Sasajima, H., Mori, Y., Ishijima, K.: *J. Nucl. Mater.*, **248**, 249 (1997).
(3) Nagase, F., Otomo, T., Uetsuka, H.: *JAERI-Research* 98-064, (1998), [in Japanese].
(4) Fuketa, T., Nagase, F., Nakamura, T., Uetsuka, H., Ishijima, K.: 26th Water Reactor Safety Information Mtg., Bethesda, Maryland, *NUREG/CP*-0166, Vol. 3, p. 223 (1998).
(5) Nagase, F., Uetsuka, H.: *Int. Topical Mtg. LWR Fuel Performance*, Portland, Oregon, p. 677 (1997).
(6) Shi, S. Q., Puls, M. P.: *J. Nucl. Mater.*, **208**, 232 (1994).
(7) Shi, S. Q., Puls, M. P., Sagat, S.: *J. Nucl. Mater.*, **208**, 243 (1994).
(8) Barraclough, K. G., Beevers, C. J.: *J. Mater. Sci.*, 4, 518 (1969).
(9) Smith, E.: *Int. J. Pressure Vessel Piping*, **60**, 159 (1994).
(10) Smith, E.: *Int. J. Pressure Vessel Piping*, **61**, 1 (1995).